TAMPEREEN TEKNILLINEN YLIOPISTO
TAMPERE UNIVERSITY OF TECHNOLOGY

Lauri Anttila

Digital Front-End Signal Processing with Widely-Linear Signal Models in Radio Devices

Julkaisu 985 • Publication 985

Tampere 2011

Tampereen teknillinen yliopisto. Julkaisu 985
Tampere University of Technology. Publication 985

Lauri Anttila

Digital Front-End Signal Processing with Widely-Linear Signal Models in Radio Devices

Thesis for the degree of Doctor of Science in Technology to be presented with due permission for public examination and criticism in Tietotalo Building, Auditorium TB109, at Tampere University of Technology, on the 14th of October 2011, at 12 noon.

Tampereen teknillinen yliopisto - Tampere University of Technology
Tampere 2011

ISBN 978-952-15-2651-0 (printed)
ISBN 978-952-15-2978-8 (PDF)
ISSN 1459-2045

Abstract

Necessitated by the demand for ever higher data rates, modern communications waveforms have increasingly wider bandwidths and higher signal dynamics. Furthermore, radio devices are expected to transmit and receive a growing number of different waveforms from cellular networks, wireless local area networks, wireless personal area networks, positioning and navigation systems, as well as broadcast systems. On the other hand, commercial wireless devices are expected to be cheap, be relatively small in size, and have a long battery life.

The demands for flexibility and higher data rates on one hand, and the constraints on production cost, device size, and energy efficiency on the other, pose difficult challenges on the design and implementation of future radio transceivers. Under these diametric constraints, in order to keep the overall implementation cost and size feasible, the use of simplified radio architectures and relatively low-cost radio electronics are necessary. This notion is even more relevant for multiple antenna systems, where each antenna has a dedicated radio front-end. The combination of simplified radio front-ends and low-cost electronics implies that various nonidealities in the remaining analog radio frequency (RF) modules, stemming from unavoidable physical limitations and material variations of the used electronics, are expected to play a critical role in these devices. Instead of tightening the specifications and tolerances of the analog circuits themselves, a more cost-effective solution in many cases is to compensate for these nonidealities in the *digital domain*. This line of research has been gaining increasing interest in the last 10-15 years, and is also the main topic area of this work.

The direct-conversion radio principle is the current and future choice for building low-cost but flexible, multi-standard radio transmitters and receivers. The direct-conversion radio, while simple in structure and integrable on a single chip, suffers from several performance degrading circuit impairments, which have historically prevented its use in wideband, high-rate, and multi-user systems. In the last 15 years, with advances in integrated circuit technologies and digital signal processing, the direct-conversion principle has started gaining popularity. Still, however, much work is needed to fully realize the potential of the direct-conversion principle.

This thesis deals with the analysis and digital mitigation of the implementation nonidealities of direct-conversion transmitters and receivers. The contributions can be divided into three parts. First, techniques are proposed for the joint estimation and predistortion of in-phase/quadrature-phase (I/Q) imbalance, power amplifier (PA) nonlinearity, and local oscillator (LO) leakage in wideband direct-conversion transmitters. Second, methods are

developed for estimation and compensation of I/Q imbalance in wideband direct-conversion receivers, based on second-order statistics of the received communication waveforms. Third, these second-order statistics are analyzed for second-order stationary and cyclostationary signals under several other system impairments related to circuit implementation and the radio channel. This analysis brings new insights on I/Q imbalances and their compensation using the proposed algorithms. The proposed algorithms utilize complex-valued signal processing throughout, and naturally assume a *widely-linear* form, where both the signal and its complex-conjugate are filtered and then summed. The compensation processing is situated in the *digital front-end* of the transceiver, as the last step before digital-to-analog conversion in transmitters, or in receivers, as the first step after analog-to-digital conversion.

The compensation techniques proposed herein have several common, unique, attributes: they are designed for the compensation of frequency-dependent impairments, which is seen critical for future wideband systems; they require no dedicated training data for learning; the estimators are computationally efficient, relying on simple signal models, gradient-like learning rules, and solving sets of linear equations; they can be applied in any transceiver type that utilizes the direct-conversion principle, whether single-user or multi-user, or single-carrier or multi-carrier; they are modulation, waveform, and standard independent; they can also be applied in multi-antenna transceivers to each antenna subsystem separately. Therefore, the proposed techniques provide practical and effective solutions to real-life circuit implementation problems of modern communications transceivers. Altogether, considering the algorithm developments with the extensive experimental results performed to verify their functionality, this thesis builds strong confidence that low-complexity digital compensation of analog circuit impairments is indeed applicable and efficient.

Preface

The work for this thesis was carried out over the years 2005-2011 at the Department of Communications Engineering (DCE), Tampere University of Technology, Tampere, Finland. Several individuals and organizations have contributed to the thesis process and final outcome, and deserve a special mention.

First and foremost, I would like to express my gratitude to my boss and thesis supervisor, Prof. Mikko Valkama for his support, advice and encouragement, and for being an outstanding role-model not just for me but for everyone in our research group. I also wish to extend my sincere thanks to Prof. Markku Renfors, co-author and the previous head of the department, for the guidance and support during my years at the DCE. Prof. Valkama and Prof. Renfors are jointly responsible for having created such a fantastic working environment that no one wants to leave! It has truly been a pleasure and a privilege to work and study under their guidance. I also wish to express my gratitude to Prof. Peter Händel of KTH, Stockholm, Sweden, for initiating the fruitful cooperation that culminated in two journal articles.

I am grateful to the thesis pre-examiners, Prof. Håkan Johansson and Dr. Tech. Kari Kalliojärvi for their valuable time and careful reviews. I also wish to thank Prof. Thomas Eriksson for agreeing to act as the opponent at my defense.

I gratefully acknowledge the financial support of the following organizations and funds: the Graduate School in Electronics, Telecommunications, and Automation (GETA), the Academy of Finland (under the projects “Understanding and Mitigation of Analog RF Impairments in Multi-Antenna Transmission Systems” and “Digitally-Enhanced RF for Cognitive Radio Devices”), the Finnish Funding Agency for Technology and Innovation (Tekes; under the projects “Advanced Techniques for RF Impairment Mitigation in Future Wireless Radio Systems” and “Enabling Methods for Dynamic Spectrum Access and Cognitive Radio”), the Technology Industries of Finland Centennial Foundation, the Austrian Center of Competence in Mechatronics, Nokia Siemens Networks, the Nokia Foundation, and the Finnish Foundation for Technology Promotion (TES). I also wish to thank Marja Leppäharju, the coordinator of GETA, for the excellent work she does.

I am also indebted to my colleagues in the RF-DSP group, as well as all other co-workers at the department, for the great cooperation, discussions, and general atmosphere. I especially wish to thank my roommates Tero, whom I have known from day one of my studies and who has been a dear friend ever since, and Vesa for his friendship, technical insights, and entertainment. I am grateful to Ali Shahed for the peer support and all the interesting

discussions on technology, music, politics, family, the Finnish health care system, etc. Furthermore, I wish to thank the following current and former colleagues at DCE, without the intention of forgetting anyone: Yaning Zou, Adnan Kiayani, Olli Mylläri, Tuomo Kuusisto, Ari Asp, Ahmet Gökceoglu, Ville Syrjälä, Jaakko Marttila, Markus Allen, Tobias Hidalgo Stitz, Ari Viholainen, Toni Huovinen, Tero Isotalo, and Toni Levanen. I am also grateful to our administrative personnel Tarja Erälaukko, Sari Kinnari, Kirsi Viitanen, and Daria Ilina, as well as computer and network administrator Jani Tuomisto (and his predecessors) for helping me with numerous practical matters over the years.

I wish to express my warmest gratitude to my mother Maija and father Arto for supporting me all the way, in every way. Finally, I want to thank, from the bottom of my heart, my dear wife Sari for her love, support, and patience over the years, and my lovely children Eevi and Alvari for reminding me of what is truly important in life.

Tampere, August 2011,

Lauri Anttila

Contents

List of Publications

This thesis consists of an introduction part and the following eight articles:

[P1] L. Anttila, M. Valkama, M. Renfors, "Frequency-Selective I/Q Mismatch Calibration of Wideband Direct-Conversion Transmitters," *IEEE Transactions on Circuits and Systems II, Express Briefs,* vol. 55, no. 4, April 2008, pp. 359-363.

[P2] L. Anttila, M. Valkama, M. Renfors, "Circularity-Based I/Q Imbalance Compensation in Wideband Direct-Conversion Receivers," *IEEE Transactions on Vehicular Technology*, vol. 57, no. 3, July 2008, pp. 2099-2113.

[P3] L. Anttila, P. Händel, M. Valkama, "Joint Mitigation of Power Amplifier and I/Q Modulator Impairments in Broadband Direct-Conversion Transmitters," *IEEE Transactions on Microwave Theory and Techniques*, vol. 58, April 2010, pp. 730-739.

[P4] L. Anttila, P. Händel, O. Mylläri, M. Valkama, "Recursive Learning-Based Joint Digital Predistortion for Power Amplifier and I/Q Modulator Impairments," *International Journal of Microwave and Wireless Technologies*, July 2010, pp. 173-182.

[P5] L. Anttila, M. Valkama, M. Renfors, "Blind Moment Estimation Techniques for I/Q Imbalance Compensation in Quadrature Receivers," in *Proc. 17th Annual IEEE International Symposium on Personal, Indoor and Mobile Radio Communications (PIMRC '06)*, Helsinki, Finland, September 2006.

[P6] L. Anttila, M. Valkama, M. Renfors, "Blind Compensation of Frequency-Selective I/Q Imbalances in Quadrature Receivers: Circularity –Based Approach," in *Proc. IEEE International Conference on Acoustics, Speech, and Signal Processing (ICASSP '07)*, Hawaii, HI, USA, April 2007.

[P7] L. Anttila, M. Valkama, M. Renfors, "Gradient-Based Blind Iterative Techniques for I/Q Imbalance Compensation in Digital Radio Receivers," in *Proc. IEEE 8th Workshop on Signal Processing Advances in Wireless Communications (SPAWC '07)*, Helsinki, Finland, June 2007.

[P8] L. Anttila and M. Valkama, "On Circularity of Receiver Front-End Signals Under RF Impairments," in *Proc. 17th European Wireless Conference*, Vienna, Austria, April 2011.

List of Acronyms

3GPP	Third Generation Partnership Project
A/D	analog-to-digital
ACPR	adjacent channel power ratio
ADC	analog-to-digital converter/conversion
AFE	analog front-end
AGC	automatic gain control
AIC	adaptive interference cancellation
ASIC	application-specific integrated circuit
BER	bit error rate
BPF	bandpass filter
BPSK	binary phase shift keying
BSS	blind source separation
CDMA	code division multiple access
CE	constant envelope
CFO	carrier frequency offset
CMOS	complementary metal-oxide-semiconductor
DAC	digital-to-analog converter/conversion
DC	direct current
DCR	direct-conversion receiver
DCT	direct-conversion transmitter
DFE	digital front-end
DSP	digital signal processing/processor
EVM	error vector magnitude
FDMA	frequency division multiple access
FPGA	field-programmable gate array
FT	Fourier transform
I/Q	in-phase/quadrature-phase
IC	integrated circuit

IEEE	Institute of Electrical and Electronics Engineers
IF	intermediate frequency
IFT	inverse Fourier transform
ILR	image leakage ratio
IRR	image rejection ratio
LNA	low noise amplifier
LO	local oscillator
LPF	lowpass filter
LS	least squares
LTE	Long Term Evolution
MFI	mirror-frequency interference
ML	maximum likelihood
MSE	mean-square error
NCE	non-constant envelope
NMSE	normalized mean square error
OFDM	orthogonal frequency division multiplexing
OFDMA	orthogonal frequency division multiple access
PA	power amplifier
PAPR	peak-to-average power ratio
pdf	probability density function
PEP	peak envelope power
PSK	phase shift keying
QAM	quadrature amplitude modulation
QPSK	quadrature phase shift keying
RF	radio frequency
RLS	recursive least squares
RMS	root mean square
SC-FDMA	single-carrier frequency division multiple access
SDR	software-defined radio
SER	symbol error rate
SIR	signal-to-interference ratio
SNR	signal-to-noise ratio
UMTS	Universal Mobile Telecommunications System
WCDMA	wideband code division multiple access
WL	widely-linear

Chapter 1

Introduction

1.1 Background and Motivation

The world has witnessed an unprecedented growth of wireless communications during the past 20 years, accompanied by big economical, technological, social, and even societal changes. The number of wireless devices has exploded and keeps on growing, and the Wireless World Research Forum (WWRF) projects that by 2020, 7 milliard ($7 \cdot 10^9$) wireless devices will be serving the global population [28]. The data transfer capacity per wireless device has also been growing constantly, being motivated by wideband multimedia applications such as video and music, as well as increased online gaming and internet browsing in general. The International Telecommunication Union's Radiocommunication Sector (ITU-R) has specified the so-called IMT-Advanced requirements for fourth generation (4G) cellular wireless standards, calling for device peak data rates between 100 Mbit/s and 1 Gbit/s, depending on mobility [61]. From technology point of view, the increased data rates are being fueled (among other factors) by advances in integrated circuit (IC) technology and communication theory, most notably through the development of multiple antenna techniques and iterative receiver structures [49]. In spite of the many technological advances of the past 20 years, there are still many challenges ahead before technology catches up with these aspirations.

An important characteristic of modern wireless devices is *multi-standard operation*, i.e., the ability to receive and transmit a wide variety of different waveforms over different carrier frequencies, from cellular networks (GSM, UMTS, LTE), wireless metropolitan, local and personal area networks (IEEE 802.16, 802.11, and 802.15 –series, respectively), positioning and navigation (GPS and Galileo), as well as broadcast networks (DVB-T/H, DAB, FM radio) [75]. The *reconfigurability* or *flexibility* of transceivers, in line with the software defined radio (SDR) principle, will enable adoption of new standards and waveforms through software updates only, without hardware changes [141]. The SDR is also the platform of cognitive radio (CR) devices [91], which are expected to bring big improvements in spectral efficiency through opportunistic spectrum usage.

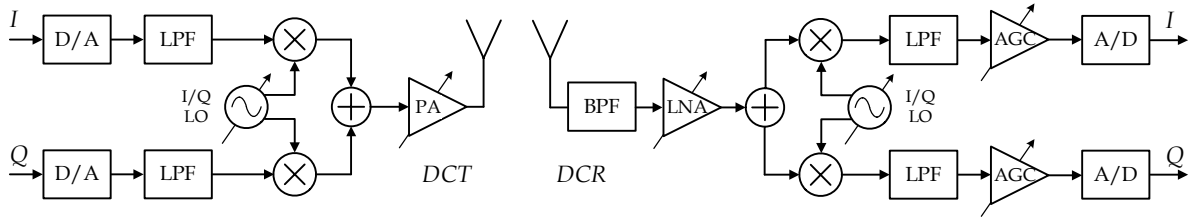

***Figure 1-1**: Conceptual radio transmitter (left) and radio receiver (right) block-diagrams using quadrature (I/Q) mixing. In plain direct-conversion radio, the I and Q signal are baseband signals while in the low-IF radio, the I and Q signals are intermediate frequency signals.*

On the other hand, there is an overriding trend in consumer electronics of *ever-falling prices*. This has been driven by improvements in manufacturing efficiency and automation, lower labor costs by moving manufacturing facilities to lower-income countries, and increased miniaturization, which is a direct result of advances in integrated circuit (IC) technologies and the adoption of simpler transceiver structures such as the direct-conversion architecture. These observations apply to non-consumer electronics as well, such as cellular basestation radios, although the cost-per-device is not as important in these lower volume markets. An important additional constraint for battery-powered devices is *power consumption*, which should be optimized for longer battery life without sacrificing too much performance.

The demands for multi-standard operation, flexibility, and higher data rates on one hand, and the constraints on production cost, device size, and energy efficiency on the other, pose difficult challenges on the design and implementation of future radio transceivers [15], [88], [90]. Under these diametric constraints, in order to keep the overall implementation costs and size feasible, the use of simplified radio architectures and low-cost radio electronics are necessary. The *direct-conversion radio architecture* (or zero-IF or homodyne architecture) is considered as one of the most promising radio structures for building flexible multi-standard radios at a low cost [3], [5], [10], [15], [27], [75], [84], [88], [90], [110], [141]. The direct-conversion transmitter and receiver (DCT and DCR) are depicted in Figure 1-1. Here, the signal is converted directly from radio frequencies (RF) to baseband (in a DCR), or from baseband to RF (in a DCT), without any intermediate frequency (IF) stages. Thus, compared to the traditional superheterodyne principle, the IF stages, which are typically off-chip components, are replaced by baseband stages. Furthermore, the RF image rejection (IR) filter becomes unnecessary. Instead, image rejection is provided by the coherent complex mixing with quadrature (90-degree phase difference) local oscillator (LO) signals, which theoretically gives infinite image rejection. Removal of the off-chip IF stages and IR filter allows for the whole receiver or transmitter (with the exception of the power amplifier) to be integrated on a single chip, using cheap IC technology such as CMOS [5], [15], [75], [84], [88], [111].

The use of direct-conversion principle in combination with low cost radio electronics gives rise to certain implementation-related problems, stemming from the physical limitations

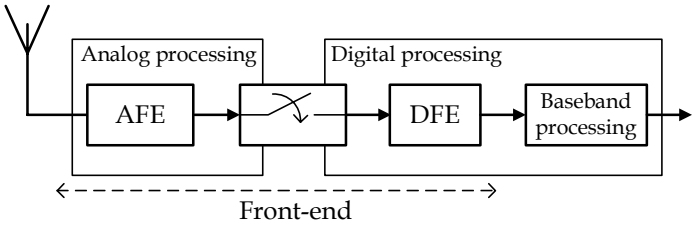

Figure 1-2: *Digital receiver where functionalities of the traditional radio front-end are shared between the analog front-end (AFE) and the digital front-end (DFE). Adapted from [52].*

and component variations of the used electronics [3], [110]. Nonideal gain and phase matching of the two signal branches creates the so-called *I/Q imbalance* or *I/Q mismatch* problem, which compromises the image rejection capabilities of DCR's and DCT's [90], [110], [144], [P1], [P2], [P5]-[P8]. Signal leakages between LO ports and other components create *DC offsets* in DCR's, and *LO leakage* in DCT's [3], [35] [90], [111], [127]. Even-order intermodulation products and flicker noise are other inherent problems in DCR's [3], [110]. In DCT's, power amplifier nonlinearity, I/Q imbalance, and LO leakage interact in a way that the created problems are greater than the sum of the parts [22], [34], [P3], [P4].

Instead of tightening specifications and tolerances of the radio front-ends themselves, a more cost-effective solution in many cases is to handle the consequences of these nonidealities in the digital domain, using sophisticated digital signal processing (DSP) [37]. This line of research, sometimes called "dirty RF" signal processing (due to Fettweis et al. [37]), has gained increasing interest in the past 10-15 years, and it is also the general topic area of this thesis.

The general idea of shifting functionalities that have traditionally been implemented with analog techniques to the digital domain is at the core of the software-defined radio (SDR) paradigm [52], [88], [89], [141]. The objective of SDR is to provide a flexible, reconfigurable radio platform that is capable of accommodating both current and future communication standards, thus operating over a wide variety of carrier frequencies, bandwidths, and waveforms. SDR implies that the A/D interface be as close to the antenna as possible. However, RF sampling (digitization at RF frequencies) is not attainable in the near future with sufficient dynamic range, low power consumption, and low cost. The direct-conversion principle represents an appealing alternative for implementing SDR's, minimizing the needed analog components as well as offering a good tradeoff between flexibility, performance, and implementation cost.

Moving the A/D interface closer to the antenna also implies that functionalities of the traditional radio front-end such as channel selection filtering and synchronization need to be split between the analog front-end (AFE) and digital front-end (DFE) [52], [88], [89]. In addition to channelization and synchronization, the DFE also performs sample-rate conversion, as well as most of the dirty RF signal processing, such as I/Q imbalance

compensation in DCR's and DCT's, and PA digital predistortion. Figure 1-2 depicts a conceptual digital receiver housing a digital front-end.

1.2 Thesis Objectives

The ultimate objective of this thesis is to facilitate the implementation of cheaper, smaller, and more energy efficient radio front-ends for wideband, multi-standard, and multi-user radio systems, through the application of sophisticated DSP techniques. To this end, the goal is to develop novel algorithms for estimating and compensating for the performance-degrading impairments in direct-conversion transmitters and receivers, and to test them in realistic scenarios with extensive computer simulations and laboratory RF measurements.

1.3 Thesis Contributions and Structure

The main outcomes of this thesis are: developing several novel algorithms for compensating I/Q mismatches in wideband, multi-standard, multi-user DCRs [P2], [P5]-[P7] (reviewed in Chapter 4 of this manuscript); analyzing the second-order statistics of DCR front-end signals under impairments related to the circuit implementation and the radio channel [P2], [P8] (in Chapter 3); establishing the concept of *time-average properness*, which is essential for analyzing and understanding the second-order statistics of cyclostationary signals under I/Q imbalances (in Chapter 3); developing an algorithm for the estimation and predistortion of frequency-selective I/Q mismatch in DCTs [P1] (in Chapter 5); developing the first ever predistortion structure for the joint compensation of frequency-selective power amplifier nonlinearity, I/Q mismatch, and LO leakage in DCTs [P3] (in Chapter 5); deriving estimation algorithms and procedures for training the previous predistorter structure [P3], [P4] (in Chapter 5).

All the results outlined above, and all the techniques introduced in this thesis, are in principle applicable to almost *any* type of communication signals, whether they are single or multi-carrier signals, single or multi-user signals, or sums of such signals, independent of modulation format. Furthermore, they can be applied in multi-antenna systems to each antenna subsystem separately. They are thus very generally applicable, and waveform and standard independent. Due to their nature, the techniques can find application in basestation as well as mobile transceivers in cellular networks, broadcast transmitters, as well as future software-defined, flexible, radio terminals targeted for cognitive radio.

Several supplementary articles related to the thesis scope, including two book chapters and six conference articles, have also been published by the Author together with his supervisors and colleagues. These are: book chapters related to I/Q imbalance modeling and compensation in [8], and to joint predistortion of PA nonlinearity, I/Q imbalance, and LO leakage in [150]; the conference publications dealing with the effects and mitigation of

receiver I/Q imbalance with specific modulation formats (WCDMA, SC-FDMA, and OFDM, respectively) in [132], [6], and [7]; the overview of radio implementation challenges in 3G-LTE context in [146]; the measurement-based studies on digital transmitter I/Q imbalance calibration in [59] and [90].

The thesis is organized such, that Chapters 2 and 3 introduce the needed background theory, while Chapters 4 and 5 present the main contributions of the thesis (although some novel results are presented already in Chapter 3). Chapter 2 introduces the essentials of digital front-end signal processing in radio transceivers, including complex (I/Q) baseband representation of bandpass signals; modeling, implications, and compensation structures for I/Q imbalances and PA nonlinearity. In Chapter 3, the second-order statistics of I/Q signals are presented. Definition of time-average properness and its spectral interpretation in Subsection 3.4 are new results, while Subsection 3.5, which deals with the effects of RF and circuit impairments on properness, presents results from [P8] and [P2]. The main results of the receiver signal processing studies of [P2], [P5]-[P7] are recapped in Chapter 4, while Chapter 5 reviews the results of the transmitter calibration studies, originally published in [P1], [P3], [P4]. Finally, Chapter 6 concludes the thesis with a summary and some prospects for future research.

1.4 Author's Contribution to the Publications

The research topics of receiver and transmitter I/Q imbalance compensation were proposed by Prof. Valkama, originally in the framework of a Tekes-funded project with Nokia Networks. Prof. Valkama's article [148] was the inspiration for the development of the circularity-based algorithms for receivers in [P2], [P5]-[P7], all of which were developed by the author. The concept and algorithms for transmitter I/Q imbalance compensation in [P1] were developed by the author. The analysis in all these publications was done by the author, except for subsections III B. and III C. in [P2], which were done by Prof. Valkama. The writing of [P2] and [P7] were joint efforts between the author and Prof. Valkama (in proportions of about 80%/20%, respectively), while [P1], [P5], [P6] were written mostly by the author. The idea, analysis, simulations, and writing in [P8] were done solely by the author. Prof. Valkama has naturally contributed to the final appearance of all these publications.

The studies on joint predistortion of PA nonlinearity, I/Q mismatch and LO leakage were initiated by Prof. Händel of KTH, Stockholm, Sweden, who visited our lab in the fall of 2008. Prof. Händel provided the first version of the joint predistorter structure, which the Author then developed to the final structure introduced in [P3]. The recursive implementation and its training procedures in [P4] were developed by the author. The analysis and writing in [P3], [P4] was performed by the author, but Prof. Händel and Prof. Valkama both contributed to the final structure and appearance of the papers.

1.5 Mathematical Notations and Definitions

Time-domain signals and systems are written in italic lower case ($x(t)$ or $x(n)$), while the corresponding frequency-domain expressions or transfer functions are in italic upper case ($X(f)$, $X(z)$, or $X(e^{j\omega})$). Vectors are in bold lower case ($\mathbf{x}$), and the corresponding italic lower case letter with subscript *i* (x_i) refers to the *i*th entry of $\mathbf{x}$. Bold upper case letters are used to denote matrices ($\mathbf{X}$), and the corresponding italic lower case letter with subscript kl (x_{kl}) refers to the (k,l) entry of $\mathbf{X}$. The notation $\mathbf{X}(k,l)$ may also be used when appropriate. Vectors are in bold lower case ($\mathbf{x}$), and the corresponding italic letter with subscript *k* (x_k) refers to the *k*th entry of $\mathbf{x}$. Transpose, conjugate transpose, conjugate, matrix inverse, and matrix pseudo-inverse are indicated by superscripts $(\cdot)^{\mathrm{T}}$, $(\cdot)^{\mathrm{H}}$, $(\cdot)^{*}$, $(\cdot)^{-1}$, and $(\cdot)^{+}$, respectively.

The expected value of a random variable *X* with probability density function (pdf) $p(x)$ is defined by

$$\mathrm{E}[X] \triangleq \int_{-\infty}^{\infty} x\, p(x)\, dx\,, \tag{1.1}$$

whereas the expected valued of the function $Y = g(X)$ of the random variable *X* is [126]

$$\mathrm{E}[Y] \triangleq \int_{-\infty}^{\infty} g(x) p(x)\, dx\,. \tag{1.2}$$

The Fourier transform (FT) of a deterministic, continuous-time, complex-valued signal $x(t)$ is defined as

$$X(f) = \mathcal{F}\{x(t)\} \triangleq \int_{-\infty}^{\infty} x(t) e^{-j2\pi ft} dt\,. \tag{1.3}$$

The corresponding inverse Fourier transform (IFT) is

$$x(t) = \mathcal{F}^{-1}\{X(f)\} \triangleq \frac{1}{2\pi} \int_{-\infty}^{\infty} X(f) e^{j2\pi ft} df\,. \tag{1.4}$$

The *discrete-time Fourier transform* (DTFT) and inverse DTFT of a complex-valued discrete-time signal $x(n)$, with sample interval *T* and frequency variable $\omega = 2\pi fT$, are defined as

$$X(e^{j\omega}) = \mathcal{F}\{x(n)\} \triangleq \sum_{n=-\infty}^{\infty} x(n) e^{-j\omega n}\,. \tag{1.5}$$

$$x(n) = \mathcal{F}^{-1}\{X(e^{j\omega})\} \triangleq \frac{1}{2\pi} \int_{-\pi}^{\pi} X(e^{j\omega}) e^{j\omega n} d\omega\,. \tag{1.6}$$

A Fourier transform pair is denoted by

$$x(t) \leftrightarrow X(f) \text{ or } x(n) \leftrightarrow X(e^{j\omega})\,. \tag{1.7}$$

We denote the *convolution* of a signal $x(t)$ and the impulse response $h(t)$ of a linear time-invariant (LTI) system as

$$h(t) \star x(t) \triangleq \int_{-\infty}^{\infty} x(\lambda)h(t-\lambda)d\lambda\,. \tag{1.8}$$

For discrete-time signal $x(n)$ and impulse response $h(n)$, the *discrete convolution* is

$$h(n) \star x(n) \triangleq \sum_{m=-\infty}^{\infty} x(m)h(n-m)\,. \tag{1.9}$$

Chapter 2

Transceiver Signal Processing Essentials

Complex-valued (I/Q) signal processing is an important ingredient in today's radio communication systems. Analog I/Q processing is used for frequency translations and image rejection, while digital I/Q processing is necessary for any baseband processing of a bandpass communication signal, from synchronization to channel equalization and detection [19], [87], [89], [90], [102]. In this Chapter, the fundamentals of complex-valued signal processing for communications are briefly introduced. Widely linear filtering is defined. Some of the inherent circuit implementation problems of direct-conversion radios are addressed, with the focus on frequency-selective I/Q mismatches and PA nonlinear distortion, and their interactions.

In this Chapter, we concentrate on deterministic signal models, because of their simple and well-defined relations between the time and frequency domains, through the Fourier and inverse Fourier transforms (FT and IFT, respectively). Similar relations hold for random signals also, but the frequency-domain equivalent of a random process is a *spectral process*, which is a more laborious mathematical construct compared to the FT (see [80] for details). Complex-valued random signals will be described through their second-order statistical properties in Chapter 3.

A complex-valued continuous-time signal is defined as

$$x(t) = u(t) + j \cdot v(t)\,, \tag{2.1}$$

where $u(t)$ and $v(t)$ are real-valued continuous-time signals, and $j^2 = -1$ defines the imaginary unit. Even though a complex signal is simply a pair of real-valued signals, complex notation gives certain insights that are not evident with real-valued signal models, and it also leads to more economical mathematical notations and derivations [85], [87], [120].

With complex notations, unidirectional frequency translation of a signal $s(t)$ by frequency ω_0 is expressed compactly as

$$s_0(t) = \exp(j\omega_0 t)s(t)\,. \tag{2.2}$$

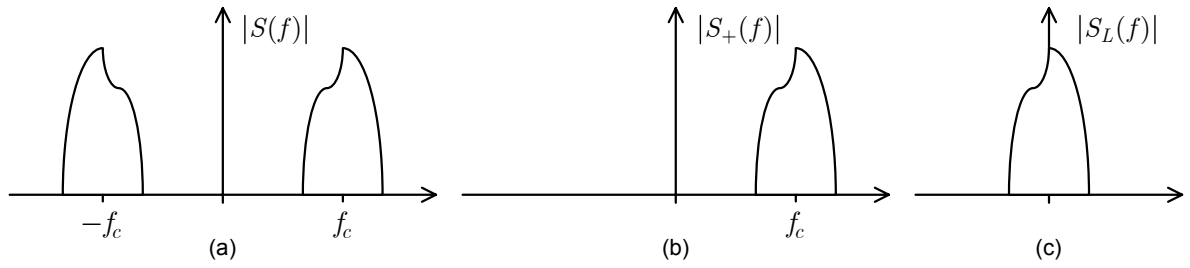

Figure 2-1: *Amplitude spectra of (a) a real-valued bandpass signal, (b) its analytic signal, and (c) its complex envelope.*

The operation is called complex mixing. Denoting $s(t) = u(t) + jv(t)$ and making use of Euler's identity $\exp(\pm j\phi) = \cos\phi \pm j\sin\phi$, we can rewrite (2.2) as

$$s_0(t) = \cos(w_0 t)u(t) - \sin(w_0 t)v(t) + j[\sin(w_0 t)u(t) + \cos(w_0 t)v(t)]. \tag{2.3}$$

Complex mixing thus entails *four* real-valued mixing operations. More generally, multiplication of two complex-valued numbers corresponds to four real-valued multiplications.

Another example of the insights brought on by complex signal models is the *spectrum* of a complex-valued signal $x(t) = u(t) + j \cdot v(t)$. Denote the FT of the signal as $X(f) = \mathcal{F}\{x(t)\} = U(f) + jV(f)$, where $U(f) = \mathcal{F}\{u(t)\} = \mathrm{Re}\{U(f)\} + j\,\mathrm{Im}\{U(f)\}$ and $V(f) = \mathcal{F}\{v(t)\} = \mathrm{Re}\{V(f)\} + j\,\mathrm{Im}\{V(f)\}$. The amplitude spectrum $|X(f)|$ has the form

$$|X(f)| = \sqrt{(\mathrm{Re}\{U(f)\} - \mathrm{Im}\{V(f)\})^2 + (\mathrm{Re}\{V(f)\} + \mathrm{Im}\{U(f)\})^2}, \tag{2.4}$$

while the amplitude spectra of the real and imaginary parts reads

$$\begin{aligned} |U(f)| &= \sqrt{\mathrm{Re}\{U(f)\}^2 + \mathrm{Im}\{U(f)\}^2} \\ |V(f)| &= \sqrt{\mathrm{Re}\{V(f)\}^2 + \mathrm{Im}\{V(f)\}^2} \end{aligned} \tag{2.5}$$

The amplitude spectra of the real-valued signals, $|U(f)|$ and $|V(f)|$, are *symmetric*. The amplitude spectrum of the complex-valued signal $|X(f)|$, however, does *not* exhibit any symmetry in general [102]. Thus, simply viewing the FTs of the real and imaginary parts of $x(t)$, one can not immediately visualize its actual spectral content. A related benefit, from signal processing point of view, is that complex signals allow processing the positive and negative parts of the spectrum separately.

2.1 Bandpass and Complex I/Q Signals and Systems

A real-valued bandpass signal $s(t)$ is defined as a signal having frequency content only in a narrow band of frequencies around a center frequency f_c, as shown in Figure 2-1 (a). The

Fourier transform of $s(t)$ is $S(f)$. The *analytic signal* of $s(t)$ is obtained by retaining only the positive frequencies of $S(f)$, that is

$$S_+(f) = 2u(f)S(f) \tag{2.6}$$

where $u(f)$ is the unit step function. This is illustrated in Figure 2-1 (b). The time domain representation of (2.6) is [102]

$$\begin{aligned} s_+(t) &= \mathcal{F}^{-1}(S_+(f)) \\ &= \left(\delta(t) + j\frac{1}{\pi t}\right) \star s(t) \\ &= s(t) + j\frac{1}{\pi t} \star s(t) \end{aligned} \tag{2.7}$$

where

$$s_{HT}(t) \triangleq \frac{1}{\pi t} \star s(t) \tag{2.8}$$

is called the *Hilbert transform* of $s(t)$, and the filter

$$h(t) \triangleq \frac{1}{\pi t} \tag{2.9}$$

is known as the *Hilbert transformer* or *Hilbert filter* (see [89], [102] for more details).

An *equivalent lowpass representation* of the analytic bandpass signal $S_+(f)$ can be obtained by simple frequency translation, as $S_L(f) \triangleq S_+(f + f_c)$, depicted in Figure 2-1 (c), or in time-domain as

$$\begin{aligned} s_L(t) &= s_+(t)e^{-j2\pi f_c t} \\ &= (s(t) + js_{HT}(t))e^{-j2\pi f_c t} \end{aligned} \tag{2.10}$$

The (generally complex-valued) lowpass signal $s_L(t) \triangleq s_I(t) + js_Q(t)$ is usually called the *complex envelope* of $s(t)$, or simply the *baseband equivalent* of $s(t)$.

Another way of generating the complex envelope, which is equivalent to (2.10) for the relatively narrow signal band of interest, can be obtained as follows. First, replace the filter $\delta(t) + j/\pi t$ in (2.7) with an *analytic bandpass filter* $h'(t) \leftrightarrow H'(f)$, which has been obtained from a *real-valued lowpass filter* $h_L(t) \leftrightarrow H_L(f)$ through frequency translation, i.e., $H'(f) \triangleq H_L(f - f_c)$. $H'(f)$ passes the signal on the positive frequency axis unchanged, but suppresses the copy on the negative frequency axis. The analytic signal, in frequency domain, is $S'_+(f) = H'(f)S(f)$. Frequency translation yields the baseband equivalent

$$\begin{aligned} S_L(f) &= S'_+(f+f_c) \\ &= H'(f+f_c)S(f+f_c) \\ &= H_L(f)S(f+f_c) \end{aligned} \tag{2.11}$$

where the order of filtering and downconversion has now been exchanged, by replacing the bandpass filter with the real-valued lowpass filter $h_L(t)$ [89]. Going back to the time domain, and applying the Euler identity $\exp(\pm j\phi) = \cos\phi \pm j\sin\phi$, we obtain

$$\begin{aligned} s_L(t) &= h_L(t) \star (s(t)e^{-j2\pi f_c t}) \\ &= h_L(t) \star (s(t)\cos 2\pi f_c t) - jh_L(t) \star (s(t)\sin 2\pi f_c t) \end{aligned} \tag{2.12}$$

Equation (2.12) can be seen to correspond almost exactly to the *direct-conversion receiver* in Figure 1-1, and represents a simple and practical way of extracting the complex envelope of a real-valued bandpass signal $s(t)$.

Frequency translation of (2.10) into the opposite direction yields

$$s(t) + js_{HT}(t) = s_L(t)e^{j2\pi f_c t}. \tag{2.13}$$

If we substitute $s_L(t) = s_I(t) + js_Q(t)$ into (2.13), apply the Euler identity, and match the real parts of the left and right hand sides, we obtain

$$\begin{aligned} s(t) &= \mathrm{Re}\{s_L(t)e^{j2\pi f_c t}\} \\ &= \frac{1}{2}\left(s_L(t)e^{j2\pi f_c t} + s_L^*(t)e^{-j2\pi f_c t}\right) \\ &= s_I(t)\cos 2\pi f_c t - s_Q(t)\sin 2\pi f_c t \end{aligned} \tag{2.14}$$

The last form of (2.14) is known as the *quadrature carrier representation* of the bandpass signal $s(t)$, and $s_I(t)$ and $s_Q(t)$ are called the *in-phase* (I) and *quadrature-phase* (Q) *components* of $s(t)$. The lowpass signals $s_I(t)$ and $s_Q(t)$ can be viewed as amplitude modulating the cosine and sine carriers. The terminology stems from the carriers being in *phase quadrature*, i.e., 90 degrees apart.

The quadrature carrier representation is useful from modulation point of view, since it reveals the possibility of transmitting *two independent real-valued signals* $s_I(t)$ and $s_Q(t)$ (or, equivalently, a single complex-valued signal $s_L(t)$) on the same frequency band, a technique known as *I/Q modulation*. The *direct-conversion transmitter*, for example, uses this modulation principle for upconverting the baseband signals to RF, as was seen in Figure 1-1. Compared to traditional AM or DSB modulations, I/Q modulation doubles the spectral efficiency. I/Q modulation is used extensively in almost all current and emerging radio system standards.

A third possible representation of a bandpass signal can be obtained by first writing the complex envelope in polar form as $s_L(t) = a(t)e^{j\theta(t)}$, where $a(t) = |s_L(t)| = \sqrt{s_I^2(t) + s_Q^2(t)}$

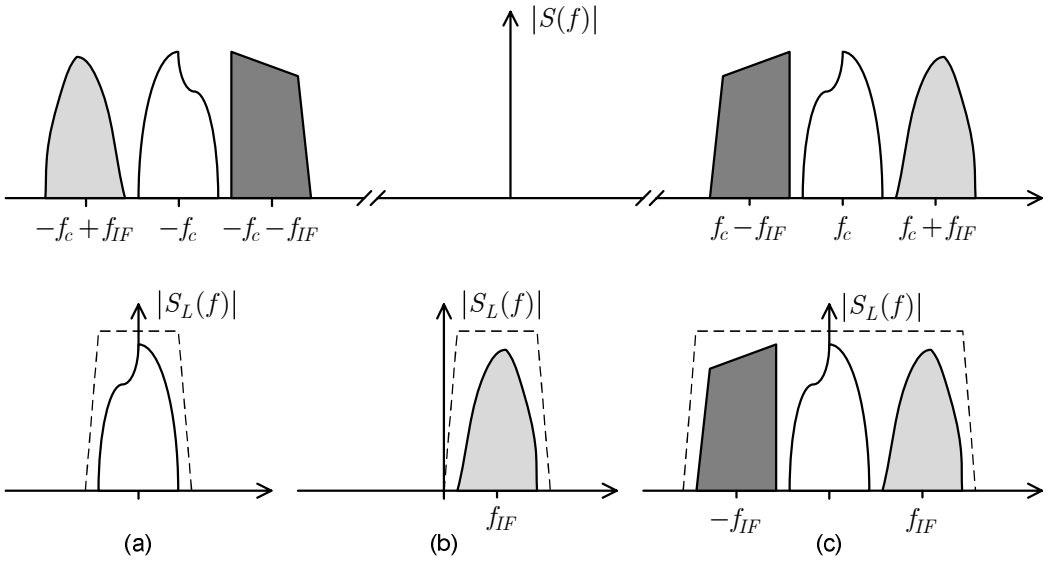

Figure 2-2: *Direct-conversion receiver variants: (a) single-channel DCR, (b) low-IF receiver, and (c) multi-channel or multi-carrier DCR. The dashed lines represent the baseband channel-selection filters.*

and $\theta(t) = \tan^{-1}[s_Q(t)/s_I(t)]$ are the *envelope* and *phase*, respectively, of $s_L(t)$. Then, the polar representation of the bandpass signal becomes

$$s(t) = a(t)\cos[2\pi f_c t + \theta(t)]. \tag{2.15}$$

The spectral representation of $s(t)$, in terms of the complex envelope $s_L(t)$, is [102]

$$\begin{aligned} S(f) &= \mathcal{F}\{s(t)\} \\ &= \tfrac{1}{2}[S_L(f - f_c) + S_L^*(-f - f_c)] \end{aligned} \tag{2.16}$$

where $S_L(f)$ is the Fourier transform of $s_L(t)$.

Up to now, the description of the complex envelope has been very general. It is useful to notice that the complex envelope need not be a single signal, but can basically represent a sum of any number of bandlimited signals. From signal reception point of view, it could represent, for example, a group of signals on adjacent, non-overlapping frequency channels, corrupted by additive noise, as seen for example in 3GPP Long-Term Evolution (LTE) uplink, which utilizes single-carrier frequency-division multiple access (SC-FDMA). Figure 2-2 illustrates different variants of a DCR, depending on how the desired signal is located in the received signal band. If the desired signal is sitting symmetrically around f_c, the receiver (transmitter) is called a *single-channel DCR* (DCT). If the signal is located around $f_c + f_{IF}$, where f_{IF} is a small intermediate frequency (usually slightly greater than half the signal bandwidth), we speak of a *low-IF receiver* (transmitter). If the received signal band consists of multiple signals, any (or many) of which could be the desired signal(s), the RX (TX) is called *multi-channel DCR* (DCT). The 3GPP LTE uplink signal and FDMA signals in general fall in this category.

2.2 Widely Linear Systems

Widely-linear time-invariant filtering is defined as [16], [100], [120]

$$\begin{aligned} y(t) &= \int_{-\infty}^{\infty} [\, h_1(t-\tau)x(\tau) + h_2(t-\tau)x^*(\tau)\,]\, d\tau \\ &= h_1(t) \star x(t) + h_2(t) \star x^*(t) \end{aligned} \tag{2.17}$$

where $x(t) = x_I(t) + jx_Q(t)$, $h_1(t) = h_{1,I}(t) + jh_{1,Q}(t)$, and $h_2(t) = h_{2,I}(t) + jh_{2,Q}(t)$ are generally complex-valued. The operation is called widely-linear because it involves filtering both the non-conjugate and conjugate versions of the signal $x(t)$. Some authors use the term linear–conjugate-linear filtering [16], [41].

The corresponding frequency-domain relation for a deterministic $x(t)$ with FT $X(f)$, and denoting the transfer functions of the filters as $H_1(f)$ and $H_2(f)$, is

$$Y(f) = H_1(f)X(f) + H_2(f)X^*(-f)\,. \tag{2.18}$$

The crosstalk between $X(f)$ and $X^*(-f)$ induced by WL filtering is herein called *mirror-frequency interference* (MFI).

Widely linear filtering is a natural extension to strictly linear filtering in the context of *nonproper* or *noncircular* complex random signals [120], which will be reviewed in Chapter 3. Widely linear signal models are encountered in several communications signal processing problems, such as in channel equalization, interference mitigation, and array processing under noncircular modulations, and signals under TX or RX I/Q imbalance [P2], [43], [120], [148].

For practical implementations, it may be useful to write (2.17) in terms of the real-valued signals and filters, yielding

$$y(t) = h_I(t) \star x_I(t) + h_Q(t) \star x_Q(t) \tag{2.19}$$

where

$$\begin{aligned} h_I(t) &= h_{1,I}(t) + h_{2,I}(t) + j(h_{1,Q}(t) + h_{2,Q}(t)) \\ h_Q(t) &= h_{2,Q}(t) - h_{1,Q}(t) + j(h_{1,I}(t) - h_{2,I}(t)) \end{aligned} \tag{2.20}$$

Thus, instead of two complex filters operating on two complex signals as in (2.17), the equivalent form in (2.19) has two complex filters operating on two *real-valued* signals. The complexity of WL filtering using the form in (2.19) is, in terms of number of multiplications and additions, therefore exactly the same as for filtering a complex signal with a strictly linear, complex, filter.

2.3 I/Q Imbalance Modeling, Implications, and Mitigation

This subsection introduces the baseband signal models of direct-conversion systems affected by TX and RX I/Q imbalances. First, the models for individual transmitters and receivers are given (shown in Figure 2-3), followed by two link-level models with 1 transmitter and 2 transmitters that contain, in addition to the I/Q imbalances, also the frequency-selective fading channels and additive noise. These link models are shown in Figure 2-9. In this subsection, the focus is on the mirror-frequency problem and its implications, while the interactions of TX I/Q imbalance and PA nonlinearity will be introduced in subsection 2.5. Interactions between I/Q imbalances and other RF impairments shall be discussed in subsection 2.6, as well as in subsection 3.5 from the second-order statistics point of view.

2.3.1 I/Q Imbalance in Individual Transmitters and Receivers

Equations (2.12) and (2.14) establish the relations between the complex envelope, or the I and Q signals, and the real-valued bandpass signal in DCRs and DCTs, respectively. The corresponding receiver and transmitter structures were introduced in Figure 1-1. Suppose now, that the upconverting (downconverting) cosine and sine oscillator signals have a *phase mismatch* of ϕ_{TX} (ϕ_{RX}; both in radians), i.e. the oscillator signals are not in perfect phase quadrature, and that the amplitudes of the oscillator signals have a relative mismatch g_{TX} (g_{RX}), called *gain mismatch*. Furthermore, assume that the total impulse responses of the I and Q signal paths have an *impulse response mismatch* $h_{TX}(t)$ ($h_{RX}(t)$), due to for example differences in LPF, amplifier, and DAC/ADC passband gain characteristics over frequency, and/or LPF cutoff frequencies. Then, denoting the *ideal complex envelope* under perfect I/Q matching by $z_{TX}(t)$ ($z_{RX}(t)$), the mismatch model described above results in the following transformations of the complex envelopes [8], [143], [160]:

$$\begin{aligned} x_{TX}(t) &= g_{1,TX}(t) \star (c_{TX}(t) \star z_{TX}(t)) + g_{2,TX}(t) \star (c_{TX}(t) \star z_{TX}(t))^* \\ &= c_{TX}(t) \star [g_{1,TX}(t) \star z_{TX}(t) + g_{2,TX}(t) \star z_{TX}^*(t)] \end{aligned} \tag{2.21}$$

$$\begin{aligned} x_{RX}(t) &= c_{RX}(t) \star [g_{1,RX}(t) \star z_{RX}(t) + g_{2,RX}(t) \star z_{RX}^*(t)] \\ &= g_{1,RX}(t) \star (c_{RX}(t) \star z_{RX}(t)) + g_{2,RX}(t) \star (c_{RX}(t) \star z_{RX}(t))^* \end{aligned} \tag{2.22}$$

where $c_{TX}(t)$ and $c_{RX}(t)$ denote the (real-valued) *common impulse responses* of the transmitter and receiver I and Q signal paths. The *I/Q imbalance filters* $g_{1,TX}(t)$, $g_{2,TX}(t)$, $g_{1,RX}(t)$, and $g_{2,RX}(t)$ depend on the actual imbalance parameters $\{g_{TX}, \phi_{TX}, h_{TX}(t)\}$ and $\{g_{RX}, \phi_{RX}, h_{RX}(t)\}$ as

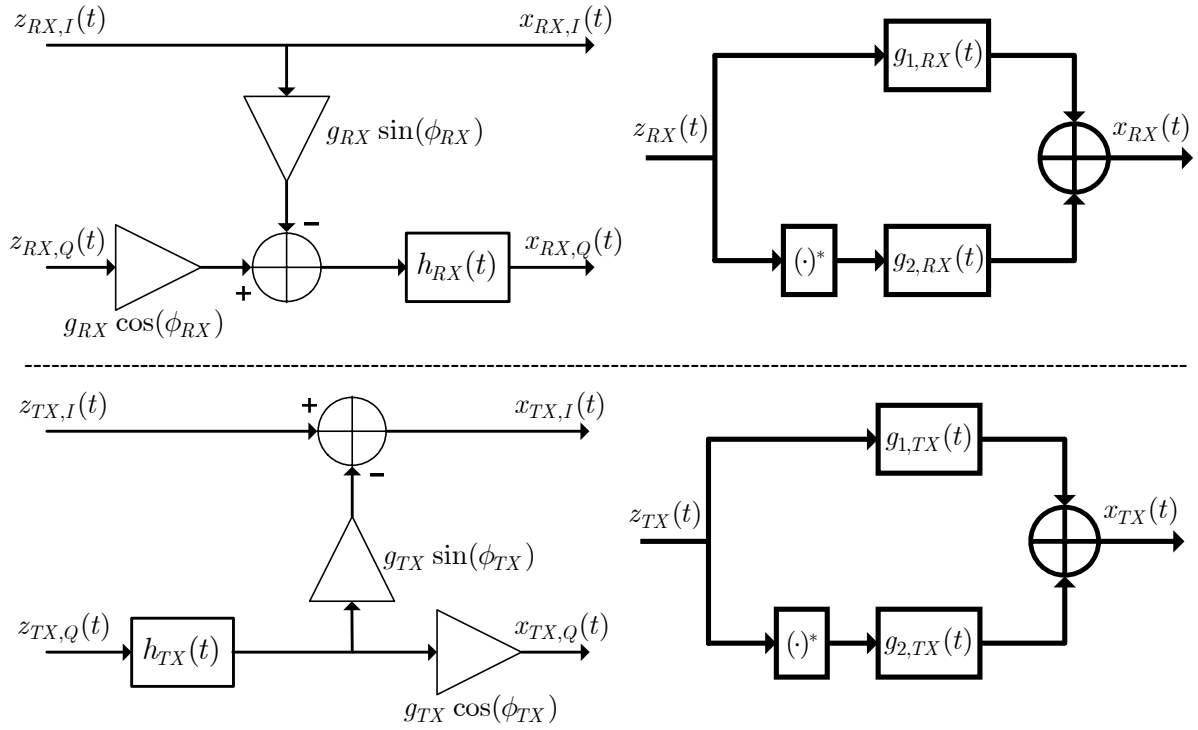

Figure 2-3: *Baseband I/Q imbalance models for direct-conversion transmitters (top) and receivers (bottom), using real-valued signal notations (left) and complex-valued signals (right).*

$$\begin{aligned} g_{1,TX}(t) &= (\delta(t) + h_{TX}(t) g_{TX} e^{j\phi_{TX}})/2, \qquad & g_{2,TX}(t) &= (\delta(t) - h_{TX}(t) g_{TX} e^{j\phi_{TX}})/2 \\ g_{1,RX}(t) &= (\delta(t) + h_{RX}(t) g_{RX} e^{-j\phi_{RX}})/2, \qquad & g_{2,RX}(t) &= (\delta(t) - h_{RX}(t) g_{RX} e^{j\phi_{RX}})/2 \end{aligned} \tag{2.23}$$

where $\delta(t)$ is the Dirac delta function. The common impulse response $c_{TX}(t)$ ($c_{RX}(t)$) does not affect the relative strengths of the two signal components $z_{TX}(t)$ and $z_{TX}^*(t)$ ($z_{RX}(t)$ and $z_{RX}^*(t)$), and is therefore typically dropped, yielding simpler models of the form

$$x_{TX}(t) = g_{1,TX}(t) \star z_{TX}(t) + g_{2,TX}(t) \star z_{TX}^*(t) \tag{2.24}$$

$$x_{RX}(t) = g_{1,RX}(t) \star z_{RX}(t) + g_{2,RX}(t) \star z_{RX}^*(t). \tag{2.25}$$

These are the most common frequency-selective I/Q imbalance models used in the literature [103], [143], [164], [P2]. Figure 2-3 shows these baseband I/Q imbalance models with complex signal notations as well as with real-valued I and Q signals.

In some studies only the mixing stage mismatches $\{g_{TX}, \phi_{TX}\}$ or $\{g_{RX}, \phi_{RX}\}$ are considered, yielding the frequency-independent (instantaneous) I/Q imbalance models of the form [11], [113], [144],

$$x_{TX}(t) = K_{1,TX} z_{TX}(t) + K_{2,TX} z_{TX}^*(t) \tag{2.26}$$

$$x_{RX}(t) = K_{1,RX} z_{RX}(t) + K_{2,RX} z_{RX}^*(t) \tag{2.27}$$

with

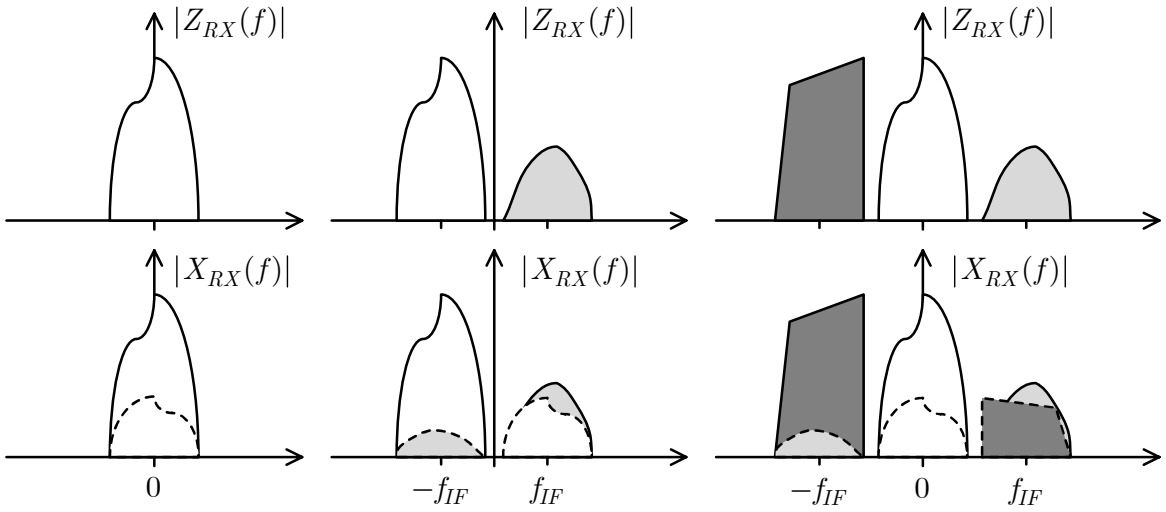

Figure 2-4: *Ideal complex envelopes (top) and the corresponding mismatched complex envelopes (bottom) for different DCR variants.*

$$\begin{aligned} K_{1,TX} &= (1 + g_{TX}e^{j\phi_{TX}})/2, \quad & K_{2,TX} &= (1 - g_{TX}e^{j\phi_{TX}})/2 \\ K_{1,RX} &= (1 + g_{RX}e^{-j\phi_{RX}})/2, \quad & K_{2,RX} &= (1 - g_{RX}e^{j\phi_{RX}})/2. \end{aligned} \tag{2.28}$$

From (2.24) and (2.25), it is evident that I/Q mismatch results in a *widely-linear transformation of the ideal complex envelope*, since the conjugate of the complex envelope is showing up. The FTs of (2.24) and (2.25) are obtained by applying (2.18), as

$$X_{TX}(f) = G_{1,TX}(f)Z_{TX}(f) + G_{2,TX}(f)Z^*_{TX}(-f) \tag{2.29}$$

$$X_{RX}(f) = G_{1,RX}(f)Z_{RX}(f) + G_{2,RX}(f)Z^*_{RX}(-f)\,, \tag{2.30}$$

where the transfer functions are

$$\begin{aligned} G_{1,TX}(f) &= (1 + H_{TX}(f)g_{TX}e^{j\phi_{TX}})/2, \quad & G_{2,TX}(f) &= (1 - H_{TX}(f)g_{TX}e^{j\phi_{TX}})/2 \\ G_{1,RX}(f) &= (1 + H_{RX}(f)g_{RX}e^{-j\phi_{RX}})/2, \quad & G_{2,RX}(f) &= (1 - H_{RX}(f)g_{RX}e^{j\phi_{RX}})/2. \end{aligned} \tag{2.31}$$

Equations (2.29) and (2.30) clearly reveal the *mirror-frequency interference* (MFI) that results from the conjugate signal terms $g_{2,TX}(t) \star z^*_{TX}(t)$ and $g_{2,RX}(t) \star z^*_{RX}(t)$. Depending on the DCR/DCT type, MFI results in either self-interference or adjacent/ alternate channel interference. This is illustrated on a conceptual level in Figure 2-4, which shows the spectra of different variants of DCRs (after I/Q downconversion and lowpass filtering), without (top) and with I/Q imbalance (bottom). The left-most spectra are for single-channel DCR, where the received signal under I/Q imbalance suffers from self-interference. The middle spectra are for a low-IF receiver, where the signals suffer adjacent channel interference. Here, the level of MFI experienced by the two users will depend heavily on the actual power difference between the signals. The spectra of a multi-channel DCR is shown on the right, where the middle signal suffers from self-interference and the two low-IF signals experience MFI from alternate

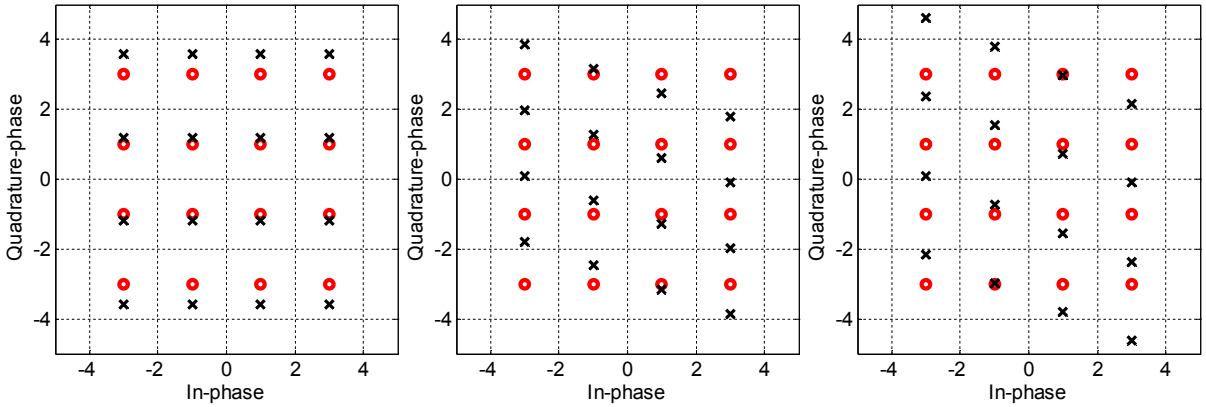

Figure 2-5: *Scatter plots of a noiseless 16-QAM signal under 20 % gain imbalance (left), 20 degrees phase imbalance (middle), and both gain and phase imbalance (right). The red circles denote the ideal symbols and the black crosses the imbalanced symbols.*

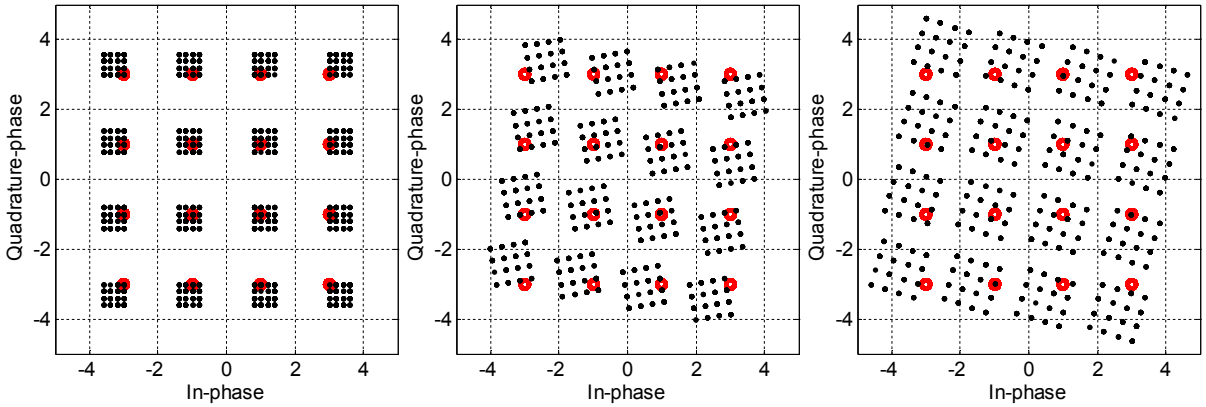

Figure 2-6: *Scatter plots of a noiseless 16-QAM OFDM signal under 20 % gain imbalance (left), 20 degrees phase imbalance (middle), and both gain and phase imbalance (right). The red circles denote the ideal symbols and the black points the imbalanced symbols, being interfered by the mirror subcarriers.*

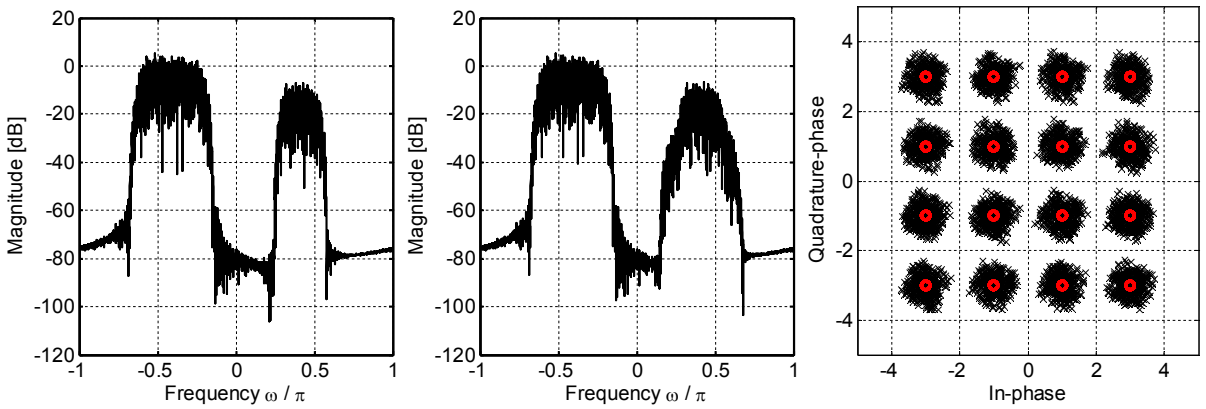

Figure 2-7: *Spectrum of the ideal complex envelope (left), spectrum of the mismatched complex envelope (middle), and the scatter plot of the weaker signal (right) in a 2-carrier low-IF receiver. 16-QAM signals, I/Q imbalances of 4%/4 degrees (IRR=28 dB), PSD level difference of 10 dB between the signals, no noise.*

channels. The actual impact of MFI on signal quality and system performance will thus heavily depend on the DCR/DCT type, as well as a number of other variables, which will be discussed in the two subsections to follow.

The effect of frequency-independent I/Q imbalance on noiseless 16-QAM symbol constellations is illustrated in Figure 2-5 for a single-carrier DCR, in Figure 2-6 for an OFDM DCR, and in Figure 2-7 for a two-carrier low-IF receiver with a PSD level difference of 10 dB between the signals. For the single-carrier DCR, the constellation is *expanded* and *skewed*. In OFDM DCR, there is *mirror-subcarrier interference* as well as *gain* and *common phase error terms*. In the low-IF receiver case, the MFI is pure additive noise, whose level depends on the power difference of the mirror signal bands and the IRR.

A few remarks are in order regarding the *differences* between the TX and RX I/Q imbalance models in (2.24) and (2.25). Even though they appear to be exactly the same, their implications differ, stemming from the interpretations of the ideal complex envelope $z_{TX}(t)$ or $z_{RX}(t)$. On the transmitter side, in the absence of LO leakage, the ideal complex envelope of the I/Q modulator output ($z_{TX}(t)$) is equal to the original transmit baseband signal, up to scaling and phase shift. On the other hand, in the receiver the ideal complex envelope $z_{RX}(t)$ is only ideal in the sense that it contains no I/Q imbalances. Compared to the original transmit signal, it is in general affected by the radio channel and additive noise, as well as any other possible system impairments such as time and frequency synchronization uncertainties. Importantly, it may also be constructed of any number of signals, from any number of transmitters, which may in turn include an arbitrary number of antennas. The structures of the ideal complex envelopes are therefore very different, and these will in turn make a difference on the relative effects of TX and RX I/Q imbalances on system performance. These will be elaborated on in the following subsections.

Using the relations (2.29) and (2.30), we can quantify the quality of an individual radio front-end in terms of its mirror-frequency rejection, by defining the *image rejection ratio* (IRR), given respectively for the TX and RX as

$$IRR_{TX}(f) = \frac{\left|G_{1,TX}(f)\right|^2}{\left|G_{2,TX}(f)\right|^2} \quad \text{and} \quad IRR_{RX}(f) = \frac{\left|G_{1,RX}(f)\right|^2}{\left|G_{2,RX}(f)\right|^2}. \tag{2.32}$$

In essence, the IRR measures how much the interference term falling on frequency *f* from the mirror-frequency *–f* will be attenuated. The IRR is the performance criterion used in analog RF design to assess the mirror-frequency attenuation of an *individual radio front-end* [27], [111]. Sometimes the inverse of the IRR, called image leakage ratio (ILR) is used [160], as was also done in [P8]. Typically, without any digital enhancement, IRR values between 25-40 dB are reported [27], [90], [111]. Figure 2-8 shows the measured IRR of a state-of-the-art direct-conversion receiver chip designed for the 3GPP LTE uplink, showing IRR's in the range of 33-40 dB as a function of frequency. The horizontal axis represents frequency offset

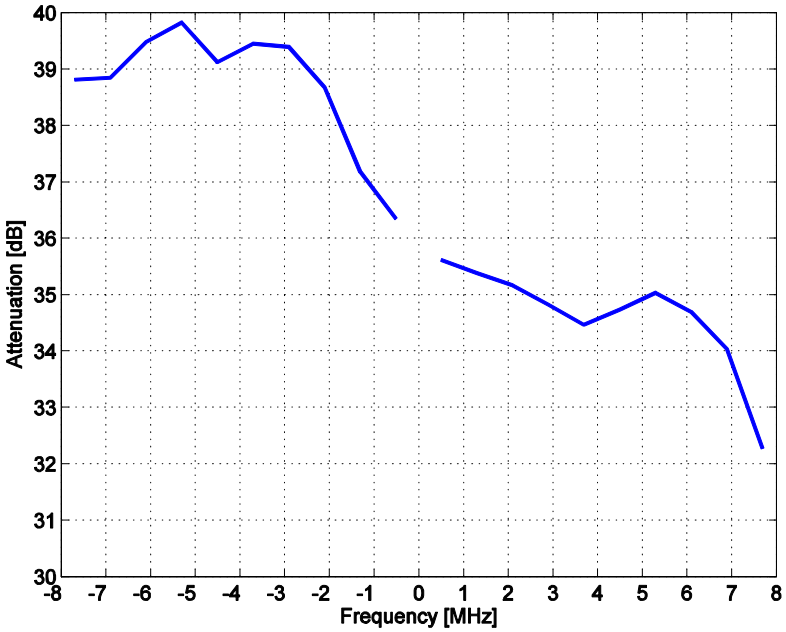

Figure 2-8. *Image attenuation of a state-of-the-art direct-conversion receiver.*

from the carrier frequency, which is 2 GHz in this case. In many cases IRRs in the typical range 25-40 dB yield unsatisfactory signal quality, while in some cases, such as with single-channel DCT/DCR systems under a frequency non-selective channel, they may be enough. The next subsections deal with these questions.

The techniques in this thesis are mostly concerned with *digitally enhancing the IRR* in individual radio transmitters and receivers, and therefore the IRR is the performance metric of choice. However, IRR alone tells little about how I/Q imbalances affect the symbol-error rate (SER) of a communication link or system, which is always the ultimate physical layer performance metric. In addition to the actual IRRs of the radios, the SER performance of a given system under I/Q imbalances depends on a multitude of factors, such as channel type and DCT/DCR type. For the sake of completeness, therefore, two simple link models will be introduced next. These will shed light on the different relative effects that TX and RX I/Q imbalances have on received signal quality, and are a big motivator for the algorithm developments in [P1]-[P7]. Only an intuitive, qualitative, account will be given, based on SIR expressions with deterministic signals and channels. For more thorough analyses, the reader is referred to the original works in [117], [160], [163], [172], from where this subsection partly draws.

The following discussion assumes that the LOs used for upconversion and downconversion use the same frequency. We also assume that TX I/Q imbalance is *not* corrected at the source, but the TX-induced image is actually emitted from the TX. However, it should be noted that RF system specifications of current standards, or regulatory bodies, usually do not allow emission of out-of-band interference on the level that TX I/Q imbalance may produce.

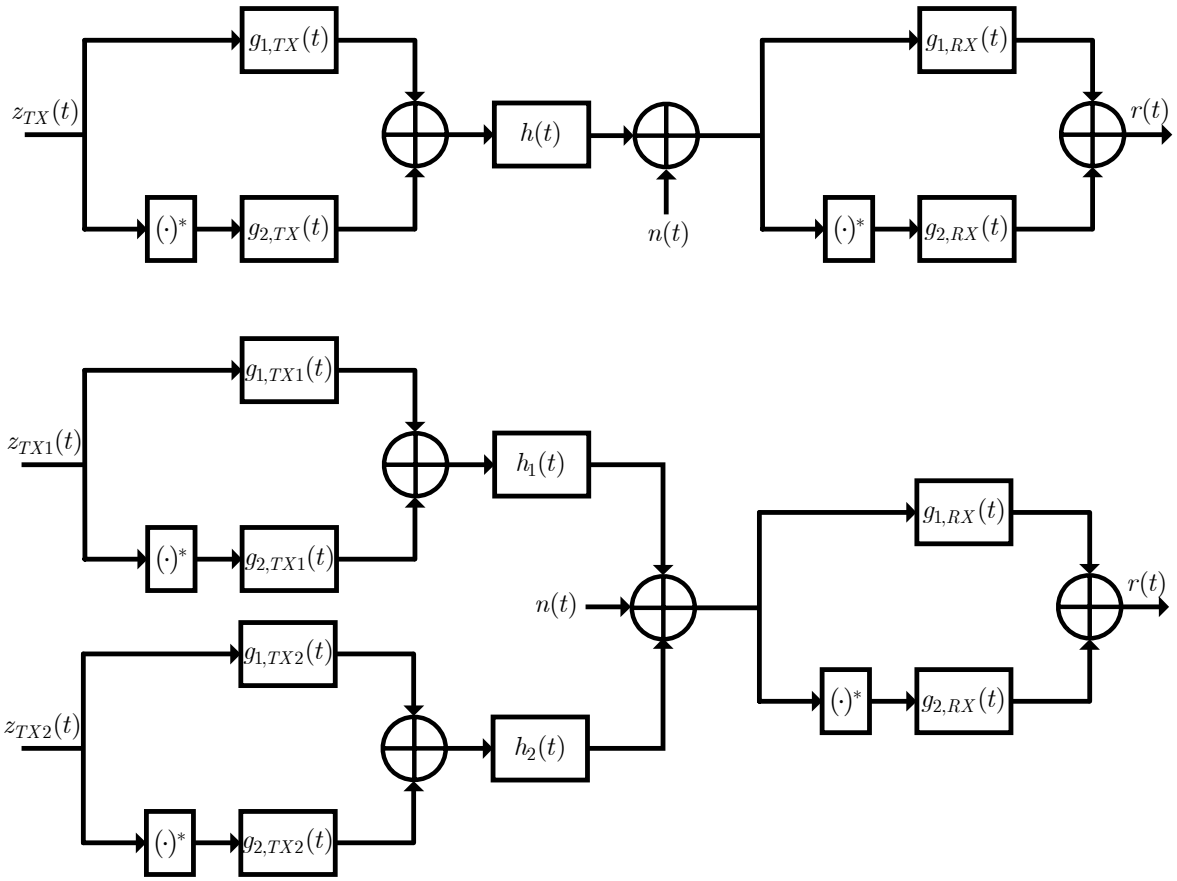

Figure 2-9: *Baseband link models with 1 transmitter (top) and 2 transmitters, containing TX and RX I/Q imbalances, frequency-selective channels, and additive noise.*

2.3.2 Zero-IF Single-User Link Model With I/Q Imbalances

Consider now a TX-RX link, where a single transmitter and receiver are connected through a radio channel with baseband equivalent response $h(t) \leftrightarrow H(f)$, as shown in Figure 2-9. Both the TX and RX contain I/Q imbalances, as described by (2.24) and (2.25). The received signal is then [115], [130], [149]

$$\begin{aligned} r(t) = {} & [g_{1,RX}(t) \star h(t) \star g_{1,TX}(t) + g_{2,RX}(t) \star h^*(t) \star g_{2,TX}^*(t)] \star z_{TX}(t) \\ & + [g_{1,RX}(t) \star h(t) \star g_{2,TX}(t) + g_{2,RX}(t) \star h^*(t) \star g_{1,TX}^*(t)] \star z_{TX}^*(t) \\ & + g_{1,RX}(t) \star n(t) + g_{2,RX}(t) \star n^*(t) \,, \end{aligned} \tag{2.33}$$

or equivalently in frequency domain, assuming deterministic transmit signal $z_{TX}(t) \leftrightarrow Z_{TX}(f)$:

$$\begin{aligned} R(f) = {} & [G_{1,RX}(f)H(f)G_{1,TX}(f) + G_{2,RX}(f)H^*(-f)G_{2,TX}^*(-f)]Z_{TX}(f) \\ & + [G_{1,RX}(f)H(f)G_{2,TX}(f) + G_{2,RX}(f)H^*(-f)G_{1,TX}^*(-f)]Z_{TX}^*(-f) \\ & + G_{1,RX}(f)N(f) + G_{2,RX}(f)N^*(-f) \,. \end{aligned} \tag{2.34}$$

The overall link model is thus also a WL transformation of the transmit signal $z_{TX}(t)$, but now the impulse responses filtering $z_{TX}(t)$ and $z_{TX}^*(t)$ include not only the I/Q imbalance filters of the TX and RX, but also the channel response $h(t) \leftrightarrow H(f)$. Therefore, the transformation will in general be heavily frequency-selective. Furthermore, the total image at frequency f is now a sum of the TX-induced image, which has travelled through the effective channel $G_{1,RX}(f)H(f)G_{2,TX}(f)$, and the RX-induced image with effective channel response $G_{2,RX}(f)H^*(-f)G_{1,TX}^*(-f)$. These are in general *non-separable*, and only their joint effect is observed and can be estimated[1].

From (2.34), we can obtain the SIR of the whole link for a deterministic transmit signal $z_{TX}(t)$ with power spectrum $P_{TX}(f)$, and deterministic channel $H(f)$, as

$$SIR_{TX-RX}(f) = \frac{\left|G_{1,RX}(f)H(f)G_{1,TX}(f) + G_{2,RX}(f)H^*(-f)G_{2,TX}^*(-f)\right|^2}{\left|G_{1,RX}(f)H(f)G_{2,TX}(f) + G_{2,RX}(f)H^*(-f)G_{1,TX}^*(-f)\right|^2} \cdot \frac{P_{TX}(f)}{P_{TX}(-f)} \tag{2.35}$$

From this, by setting $\{G_{1,RX}(f) = 1, G_{2,RX}(f) = 0\}$ or $\{G_{1,TX}(f) = 1, G_{2,TX}(f) = 0\}$, we obtain the SIR expressions for systems with TX or RX I/Q imbalances only, as

$$SIR_{TX}(f) = \frac{\left|G_{1,TX}(f)\right|^2}{\left|G_{2,TX}(f)\right|^2} \cdot \frac{P_{TX}(f)}{P_{TX}(-f)} = IRR_{TX}(f) \cdot \frac{P_{TX}(f)}{P_{TX}(-f)} \quad \text{and} \tag{2.36}$$

$$SIR_{RX}(f) = \frac{|H(f)|^2}{|H(-f)|^2} \cdot \frac{\left|G_{1,RX}(f)\right|^2}{\left|G_{2,RX}(f)\right|^2} \cdot \frac{P_{TX}(f)}{P_{TX}(-f)} = IRR_{RX}(f) \cdot \frac{|H(f)|^2}{|H(-f)|^2} \cdot \frac{P_{TX}(f)}{P_{TX}(-f)}. \tag{2.37}$$

These expressions hint at rather different effects of TX and RX I/Q imbalances on system performance. First, under TX imbalance only, the received SIR does *not* depend on the channel, but is completely defined by the TX IRR, and the power difference between the mirror frequencies of the transmit signal. If the transmit power at mirror frequencies is equal, which is usually the case in a DCT unless water-filling is utilized, the SIR is fully determined by $IRR_{TX}(f)$. If $IRR_{TX}(f)$ is in the 25-40 dB range, the overall SINR of the received signal will in most cases be dominated by the additive noise, thus suggesting a rather mild effect of TX imbalances in the single-user case considered here. The SIR under RX I/Q imbalance, on the other hand, is affected by the ratio of channel power responses at mirror frequencies, in addition to RX IRR and transmit power difference. Considering a multi-path, frequency selective radio channel, $SIR_{RX}(f)$ will thus be *heavily frequency-selective*, suggesting more severe effects.

Analytical results of these effects have been obtained in [160] for single-user SISO-OFDM systems under RX I/Q imbalances, and in [117] for single-user MIMO-OFDM systems with spatial multiplexing, and under TX and RX I/Q imbalances. Schenk [117]

[1] A carrier frequency offset or a time-varying channel (Doppler) can decouple the TX and RX I/Q imbalances (see Chapter 3 as well as [P2], [P8], [36], [56], [129] for details), but this is irrelevant to the current discussion.

found, that practical TX I/Q imbalance levels in zero-forcing single-user (SISO or MIMO) OFDM systems have very little effect on symbol-error-rate (SER) in neither AWGN nor Rayleigh fading channels, as the above analysis also suggested. RX I/Q imbalances only have a small effect in an AWGN or flat-fading channel [160], but in a frequency-selective fading channel (e.g., Rayleigh), the effects will be significant [160], and will still be amplified in MIMO-OFDM with spatial multiplexing [117]. The results in [117] are complemented by the comprehensive SIR analysis in [172] for both space-time coded and spatial multiplexing MIMO systems. Altogether, these studies have demonstrated that the effects of I/Q imbalances on received SIR and link SER will generally be more severe in multi-antenna systems compared to single-antenna systems. Intuitively, this can be explained by the fact that each received signal in a MIMO system is affected by mirror-frequency interference from *all* the transmit streams.

2.3.3 Low-IF Two-User Link Model With I/Q Imbalances

Now we consider the two-user system shown in Figure 2-9, with 2 transmitters and a single receiver. The two transmitters have I/Q imbalance filters $\{ g_{1,TX1}(t),\ g_{2,TX1}(t) \}$ and $\{ g_{1,TX2}(t),\ g_{2,TX2}(t) \}$ with FTs $g_{k,TXl}(t) \leftrightarrow G_{k,TXl}(f)$, $k,l \in \{1,2\}$, and deterministic channel responses $h_1(t) \leftrightarrow H_1(f)$ and $h_2(t) \leftrightarrow H_2(f)$. The received signal is

$$\begin{aligned} r(t) = & [g_{1,RX}(t) \star h_1(t) \star g_{1,TX1}(t) + g_{2,RX}(t) \star h_1^*(t) \star g_{2,TX1}^*(t)] \star z_{TX1}(t) \\ & + [g_{1,RX}(t) \star h_1(t) \star g_{2,TX1}(t) + g_{2,RX}(t) \star h_1^*(t) \star g_{1,TX1}^*(t)] \star z_{TX1}^*(t) \\ & + [g_{1,RX}(t) \star h_2(t) \star g_{1,TX2}(t) + g_{2,RX}(t) \star h_2^*(t) \star g_{2,TX2}^*(t)] \star z_{TX2}(t) \\ & + [g_{1,RX}(t) \star h_2(t) \star g_{2,TX2}(t) + g_{2,RX}(t) \star h_2^*(t) \star g_{1,TX2}^*(t)] \star z_{TX2}^*(t) \\ & + g_{1,RX}(t) \star n(t) + g_{2,RX}(t) \star n^*(t) \,, \end{aligned} \tag{2.38}$$

whose FT is

$$\begin{aligned} R(f) = & [G_{1,RX}(f)H_1(f)G_{1,TX1}(f) + G_{2,RX}(f)H_1^*(-f)G_{2,TX1}^*(-f)]Z_{TX1}(f) \\ & + [G_{1,RX}(f)H_1(f)G_{2,TX1}(f) + G_{2,RX}(f)H_1^*(-f)G_{1,TX1}^*(-f)]Z_{TX1}^*(-f) \\ & + [G_{1,RX}(f)H_2(f)G_{1,TX2}(f) + G_{2,RX}(f)H_2^*(-f)G_{2,TX2}^*(-f)]Z_{TX2}(f) \\ & + [G_{1,RX}(f)H_2(f)G_{2,TX2}(f) + G_{2,RX}(f)H_2^*(-f)G_{1,TX2}^*(-f)]Z_{TX2}^*(-f) \\ & + G_{1,RX}(f)N(f) + G_{2,RX}(f)N^*(-f) \,. \end{aligned} \tag{2.39}$$

If the two signals occupy each others' mirror frequencies, such as in the middle spectra of Figure 2-4, we can obtain two frequency-domain observations $R_1(f)$ and $R_2(f)$ through ideal (bandpass) filtering, yielding

$$\begin{aligned} R_1(f) &= [G_{1,RX}(f)H_1(f)G_{1,TX1}(f) + G_{2,RX}(f)H_1^*(-f)G_{2,TX1}^*(-f)]Z_{TX1}(f) \\ &\quad + [G_{1,RX}(f)H_2(f)G_{2,TX2}(f) + G_{2,RX}(f)H_2^*(-f)G_{1,TX2}^*(-f)]Z_{TX2}^*(-f) + N_1(f) \\ R_2(f) &= [G_{1,RX}(f)H_2(f)G_{1,TX2}(f) + G_{2,RX}(f)H_2^*(-f)G_{2,TX2}^*(-f)]Z_{TX2}(f) \\ &\quad + [G_{1,RX}(f)H_1(f)G_{2,TX1}(f) + G_{2,RX}(f)H_1^*(-f)G_{1,TX1}^*(-f)]Z_{TX1}^*(-f) + N_2(f). \end{aligned} \tag{2.40}$$

The total image for user 1 (user 2) at frequency f is now a sum of the TX-induced image, which has travelled through the effective channel $G_{1,RX}(f)H_2(f)G_{2,TX2}(f)$ ($G_{1,RX}(f)H_1(f)G_{2,TX1}(f)$) and the RX-induced image with effective channel response $G_{2,RX}(f)H_2^*(-f)G_{1,TX2}^*(-f)$ ($G_{2,RX}(f)H_1^*(-f)G_{1,TX1}^*(-f)$). In a frequency-selective channel, these responses are in general very different (depending somewhat on the coherence bandwidth of the channel and the absolute distance of f and $-f$).

The SIRs for the two users of (2.40) are

$$SIR_{TX-RX,1}(f) = \frac{\left|G_{1,RX}(f)H_1(f)G_{1,TX1}(f) + G_{2,RX}(f)H_1^*(-f)G_{2,TX1}^*(-f)\right|^2}{\left|G_{1,RX}(f)H_2(f)G_{2,TX2}(f) + G_{2,RX}(f)H_2^*(-f)G_{1,TX2}^*(-f)\right|^2} \cdot \frac{P_{TX1}(f)}{P_{TX2}(-f)} \tag{2.41}$$

$$SIR_{TX-RX,2}(f) = \frac{\left|G_{1,RX}(f)H_2(f)G_{1,TX2}(f) + G_{2,RX}(f)H_2^*(-f)G_{2,TX2}^*(-f)\right|^2}{\left|G_{1,RX}(f)H_1(f)G_{2,TX1}(f) + G_{2,RX}(f)H_1^*(-f)G_{1,TX1}^*(-f)\right|^2} \cdot \frac{P_{TX2}(f)}{P_{TX1}(-f)} \tag{2.42}$$

With TX or RX I/Q imbalances only, the SIR expressions for user 1 reduce to

$$SIR_{TX,1}(f) = \frac{\left|H_1(f)\right|^2}{\left|H_2(f)\right|^2} \cdot \frac{\left|G_{1,TX1}(f)\right|^2}{\left|G_{2,TX2}(f)\right|^2} \cdot \frac{P_{TX1}(f)}{P_{TX2}(-f)} \text{ and} \tag{2.43}$$

$$SIR_{RX,1}(f) = \frac{\left|H_1(f)\right|^2}{\left|H_2^*(-f)\right|^2} \cdot \frac{\left|G_{1,RX}(f)\right|^2}{\left|G_{2,RX}(f)\right|^2} \cdot \frac{P_{TX1}(f)}{P_{TX2}(-f)} \tag{2.44}$$

Similar expressions can be easily obtained for user 2 from (2.42). Both (2.43) and (2.44) depend on the ratio of the mirror-frequency transmit powers of users 1 and 2 ($P_{TX1}(f)$ and $P_{TX2}(-f)$), which are generally *not* equal, unlike in the single-user scenario. The SIR expression under TX I/Q imbalance is also markedly different from the single-user zero-IF case (2.36) in the sense that (2.43) now depends on the ratio of the channel responses $H_1(f)$ and $H_2(f)$. Thus, in the two-user low-IF scenario, and in multi-user FDMA systems in general, the effects of TX vs. RX I/Q imbalances are expected to be rather similar, i.e., *equally severe*. Generalization from the two-user system to multi-user FDMA systems with more than two users is easily established (see [163]), and will not be elaborated further here.

The exact effects of I/Q imbalances on detection performance in multi-user systems is still an open question. IRR analysis for a two-user low-IF system, similar to the above case, was done in [149]. An SIR analysis was done for OFDMA and SC-FDMA systems under frequency-independent TX and RX I/Q imbalances by Yoshida et al. in [163]. In line with the

above analysis, [163] revealed that transmitter I/Q imbalances will be a potentially bigger problem in FDMA, compared to the single-user direct-conversion case. Intuitively, and as the above analysis for the two-user system revealed, this can be explained by the TX-induced images experiencing different (and possibly better) channel responses than the direct signal terms, due to the images emerging from different TX's.

It is also worth noting, that the two link-level models described above are still simplified models. Certain other physical impairments, namely carrier frequency offsets (CFO), phase noise, and Doppler effects of the mobile radio channel, will create inter-carrier interference (ICI), and will thus break the exact mirror-frequency structure in (2.34) and (2.39). More complex modeling and mitigation approaches may be needed in these cases, depending on the severity of these additional impairments in the system under study. The reader is referred to [38], [124], [129], [136], [138] for modeling approaches for CFO and to [94] for Doppler in conjunction with I/Q imbalance in OFDM systems, and to [54]-[56], [131] for details on CFO and to [108], [168] for phase noise in conjunction with I/Q imbalance in MIMO-OFDM systems.

2.3.4 Further Research Topics on Performance Analysis

The analytical performance studies in [117], [160], [163], [172] have only looked at *linear receivers*, i.e., receivers with zero-forcing or MMSE equalization. There remain many open issues, such as how I/Q imbalances affect system performance in general in *nonlinear receivers*, and in particular, what are their ultimate implications in nonlinear multi-user and multi-antenna receivers. In FDMA and CDMA, I/Q imbalances create multi-user interference (MUI), while in multi-antenna systems, inter-stream interference is created. Indeed, these would be best handled with nonlinear receivers such as joint maximum likelihood (ML) detection, or other more practical multi-user detection (MUD) techniques such as serial or parallel interference cancellation (SIC and PIC, respectively) [153]. What would make the MUD studies interesting, is the fact that TX I/Q imbalances create *frequency diversity* due to the TX-induced MFI. The diversity could be fully exploited by joint ML detection, or partially exploited by other nonlinear receivers such as SIC, as was demonstrated experimentally for single-user OFDM in [64], and later confirmed in [69]. However, when weighed against the implementation complexity of nonlinear receivers, the small SNR improvements may prove too expensive. Anyhow, the effects of I/Q imbalances in multi-user and multi-antenna systems with nonlinear receivers, are an interesting topic for further research.

2.3.5 I/Q Imbalance Compensation Structures

There are various approaches for mitigating the effects of I/Q imbalances. This thesis focuses on correcting the I/Q imbalance *at the source*, i.e, TX I/Q imbalances on the transmitter side and RX I/Q imbalances on the receiver side. TX I/Q imbalance can be

corrected also in the receiver, but in this case the system specifications must allow for the TX-induced image to be emitted in the first place. In single-user direct-conversion systems the TX-induced image is not a big concern [117], [160] but, e.g., in FDMA systems it may create considerable interference on the band of another user, as discussed in subsection 2.3.3. The allowable levels of such interferences are strictly governed by standardization or regulatory bodies, and may be easily violated with practical IRR levels. Second, TX I/Q imbalance interacts with PA nonlinearity and PA predistortion, generating additional IMD terms at the PA output, and creating an upper bound on the spectral regrowth mitigation capabilities of conventional predistorters [22], [34] (this issue will be addressed in Subsection 2.5). Third, RX-based TX I/Q imbalance compensation with linear techniques makes the additive noise *noncircular*, as well as *enhances the noise* in a similar fashion as linear equalization does. These effects will affect detection performance somewhat, although they are expected to be rather mild with practical levels of I/Q imbalances. These are the three main reasons for concentrating on mitigation of TX I/Q imbalances at the source.

I/Q imbalance is a widely-linear transformation, given as $x_i(t) = g_{1,i}(t) \star z_i(t) + g_{2,i}(t) \star z_i^*(t)$, with $i = \{TX, RX\}$, and therefore a natural form for a compensator or equalizer is another widely-linear transformation. Assuming FIR filters, the compensators for TX and RX I/Q imbalances are given as

$$z_{TX}^{pre}(t) = w_{1,TX}(t) \star z_{TX}(t) + w_{2,TX}(t) \star z_{TX}^*(t) \tag{2.45}$$

$$z_{RX}^{post}(t) = w_{1,RX}(t) \star x_{RX}(t) + w_{2,RX}(t) \star x_{RX}^*(t). \tag{2.46}$$

Notice that the TX I/Q imbalance compensator operates on the transmit signal $z_{TX}(t)$, and it is the compensator output signal $z_{TX}^{pre}(t)$ which then experiences the I/Q imbalance, while in the receiver, the compensator operates on the imbalanced signal $x_{RX}(t)$. The ideal, zero-forcing solutions for the equalizers are, in frequency domain,

$$\begin{cases} W_{1,i}^{id}(f) = \dfrac{G_{1,i}^*(-f)}{G_{1,i}(f)G_{1,i}^*(-f) - G_{2,i}(f)G_{2,i}^*(-f)} \\ W_{2,i}^{id}(f) = \dfrac{-G_{2,i}(f)}{G_{1,i}(f)G_{1,i}^*(-f) - G_{2,i}(f)G_{2,i}^*(-f)} \end{cases} \tag{2.47}$$

with $i = \{TX, RX\}$. Applying these in (2.45) and (2.46) will yield $x_{TX}(t) = z_{TX}(t)$ in the TX I/Q modulator output, and $z_{RX}^{post}(t) = z_{RX}(t)$ in the receiver compensator's output, thus evidencing perfect equalization of the I/Q imbalances. The impulse responses $w_{1,i}^{id}(t)$, $w_{2,i}^{id}(t)$ corresponding to the ideal equalizers are well-behaving (stable) and finite in length, even though in theory they are infinitely long. This is because with any practical I/Q imbalance values, the denominator $G_{1,i}(f)G_{1,i}^*(-f) - G_{2,i}(f)G_{2,i}^*(-f)$ in (2.47) generally does not contain any zeros, and is close to unity for the whole range of frequencies.

Another option for the compensator is the *asymmetrical WL filter*

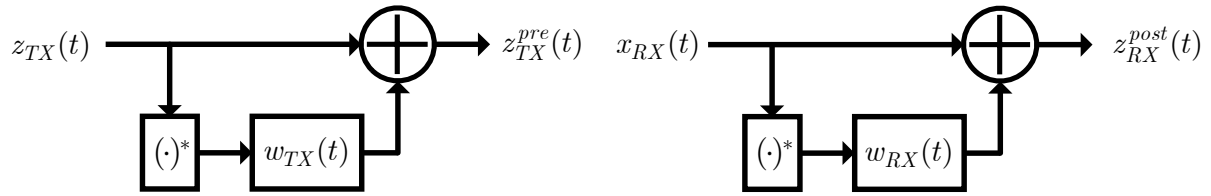

Figure 2-10: *Asymmetric WL compensators for TX I/Q imbalance (left) and RX I/Q imbalance.*

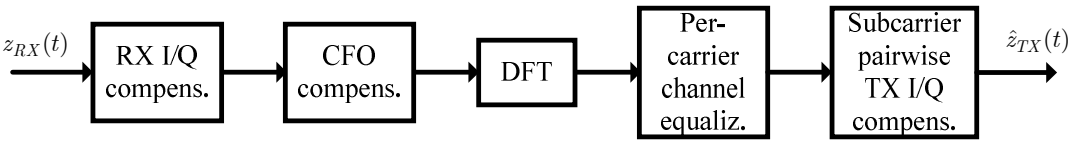

Figure 2-11: *Conceptual single-user OFDM receiver structure under TX and RX I/Q imbalance, CFO, and frequency-selective channel.*

$$z_{TX}^{pre}(t) = z_{TX}(t) + w_{TX}(t) \star z_{TX}^{*}(t) \tag{2.48}$$

$$z_{RX}^{post}(t) = x_{RX}(t) + w_{RX}(t) \star x_{RX}^{*}(t) \tag{2.49}$$

where filtering is only done on the conjugate signal. The compensation structures for these are given in Figure 2-10. The compensation developments for I/Q imbalance in [P1], [P2], [P5]-[P8] utilize the asymmetrical compensator, while the joint PA and I/Q modulator predistortion studies in [P3], [P4] assume the symmetric form.

The ideal frequency-domain solutions for (2.48) and (2.49), in the sense that they mitigate the conjugate term completely, are [P1], [P2]

$$W_{TX}^{id}(f) = -\frac{G_{2,TX}(f)}{G_{1,TX}(f)} \tag{2.50}$$

$$W_{RX}^{id}(f) = -\frac{G_{2,RX}(f)}{G_{1,RX}^{*}(-f)} \tag{2.51}$$

Applying the above compensators in (2.48)-(2.49) yields $x_{TX}(t) \cong g_{1,TX}(t) \star z_{TX}(t)$ in the TX I/Q modulator output, and $z_{RX}^{post}(t) \cong g_{1,RX}(t) \star z_{RX}(t)$ in the receiver compensator's output, thus showing perfect mitigation of MFI, even though some mild linear distortion remains in the compensated signals [P1], [P2]. These residual linear distortions are merged into the channel impulse response, and will be handled by the channel equalizer/detector later on in the receiver chain.

Frequency-domain compensator structures can be obtained from (2.48)-(2.49) through FT, yielding

$$Z_{TX}^{pre}(f) = Z_{TX}(f) + W_{TX}(f)Z_{TX}^{*}(-f) \tag{2.52}$$

$$Z_{RX}^{post}(f) = X_{RX}(f) + W_{RX}(f)X_{RX}^{*}(-f) \tag{2.53}$$

which can be easily applied in an OFDM system on a mirror-subcarrier pair basis [7], [171].

An example of a RX-based compensation structure for a link containing both TX and RX I/Q imbalances is given in Figure 2-11. This example scenario assumes a single-user single-antenna OFDM system, and includes the effects of the channel and CFO. Here, RX I/Q imbalance and CFO are corrected in time domain, while channel equalization and TX I/Q imbalance are compensated after the DFT in the frequency domain, either jointly or separately. The impairments are dealt with in the reverse order of appearance, and in a decoupled manner, facilitating efficient estimation of the compensators, as well as yielding a simple overall compensation structure. This type of structure has been used in several SISO-OFDM and MIMO-OFDM (with respective modifications) compensation studies, for example in [54], [56], [69], [83], [129], [131].

2.4 Power Amplifier Nonlinearity

The power amplifier (PA) is the device which is responsible for amplifying the transmitted signal such, that it arrives at the receiver with adequate power for successful detection. Ideally, amplification is a purely linear operation, so that the input-output (voltage) relation can be described as

$$v_{out}(t) = G_L \cdot v_{in}(t) \tag{2.54}$$

where G_L is the linear (voltage) gain of the ideal amplifier, and $v_{in}(t)$ and $v_{out}(t)$ denote the amplifier input and output signals, respectively.

Amplifiers are, however, inherently nonlinear devices, and can be described by the general input-output relation

$$v_{out}(t) = G(v_{in}(t)), \tag{2.55}$$

where $G(\cdot)$ denotes the nonlinearity, whose exact structure is dependent on the actual circuit topology and implementation technology of the amplifier. Some popular PA models will be reviewed in subsection 2.4.3.

Nonlinearity creates *harmonic* and *intermodulation distortion* (HD and IMD, respectively), which can potentially corrupt not only the desired signal, but also the adjacent and alternate channel signals, as well as signals occupying the harmonic zones of the desired signal band [67]. Fortunately, in current radio communication systems with relatively narrowband signal bands, all the harmonic zones are typically sufficiently distant from the desired signal band so that they are effectively filtered out by a bandpass filter or the antenna circuitry before transmission [67]. Empirical PA modeling and predistortion approaches thus usually only consider the vicinity of the desired signal band, also known as the *fundamental*

zone. In the fundamental zone, only *odd-order IMD products* of $v_{in}(t)$ are known to be present (subsection 2.4.3 presents the actual signal models; see (2.56)). For a more detailed discussion of these issues, the reader is referred to [26], [67], [104], [135].

2.4.1 Envelope Dynamics, PAPR, Back-Off, and Power Efficiency

If the signal going through a nonlinearity has a *constant envelope* (CE), only HD is created, meaning that the fundamental zone is basically unaffected by the nonlinearity [26], [67]. For this reason, CE modulations (e.g., MSK, GMSK, FM, PM) or nearly CE modulations (such as offset-QPSK) have been strongly favored in the past. However, in order to meet the spectral efficiency requirements of current and future communication systems, the use of non-constant envelope (NCE) modulations, is seen inevitable. The vast majority of digital modulation formats, such as *M*-QAM and *M*-PSK, OFDM, and CDMA, fall into this category of signals. Moreover, multicarrier transmission through, e.g., carrier aggregation has been considered for increasing data rates (cf. 3GPP LTE-A considerations [3]), unavoidably implicating larger envelope dynamics in the transmitted signal.

A useful and popular measure of the envelope characteristics of NCE signals is the peak-to-average power ratio (PAPR), defined for the PA input signal $v_{in}(t)$ as

$$\mathrm{PAPR}(v_{in}(t)) = \frac{\max_{t\in T}(|v_{in}(t)|^2)}{E[|v_{in}(t)|^2]} \tag{2.56}$$

where T is some finite observation interval (for example the length of a single OFDM symbol). For a random signal $v_{in}(t)$ the PAPR is clearly a random variable. Its statistics are usually measured with the complementary cumulative distribution function (CCDF), defined as $p(\gamma) = \Pr\{\mathrm{PAPR} > \gamma_0\}$. The CCDF thus tells that a PAPR level γ_0 is exceeded in signal blocks of duration T with probability $p(\gamma_0)$. The level γ_0 is sometimes called the clipping level, and it is an important design parameter for the dimensioning of the transmitter. CE signals have a PAPR of 0 dB, while for example the PAPR of a continuous-time OFDM symbol with 1024 subcarriers exceeds 11.1 dB with a probability of 1/100 [12].

An important requirement for any PA is its *power efficiency*, which is defined as the fraction of DC supply power delivered to the RF output:

$$\eta = \frac{P_{RF}}{P_{DC}}, \tag{2.57}$$

where P_{RF} is the power of the PA output signal, and P_{DC} is the supply power [26], [67]. Power efficiency affects both the battery life and the heat generated by the amplifier, and it is thus especially important for small battery-powered devices such as mobile phones, as well as satellite and high altitude platform (HAP) transceivers.

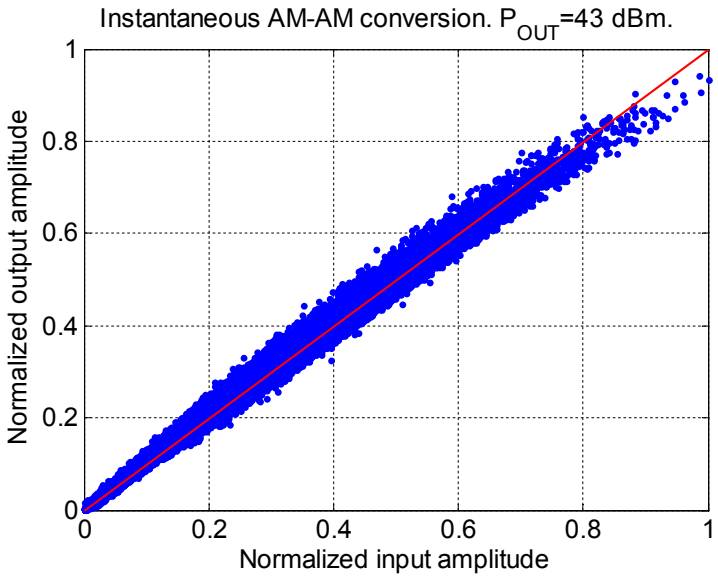

Figure 2-12: *Instantaneous AM-AM curve for an AR KMW2026M25 power amplifier at output power of 43 dBm.*

Ideal Class A and B amplifiers[2] have maximum power efficiencies of 50 and 78.5 %, respectively, which may be achieved with CE signals [26], [67]. With NCE signals, the power efficiency of the PA depends on the applied back-off, which in turn is largely determined by the PAPR of the signal. If the PA has a maximum (instantaneous) output power P_{sat}, the output power must be backed off from this level by at least the PAPR in order to prevent clipping. With a PAPR of 10 dB, for example, average power efficiencies of 5% and 28% are obtained for Class A and B amplifiers, respectively [104]. The efficiency of the amplifiers thus suffers immensely as a result of using NCE signals with high PAPR. PAPR mitigation techniques have therefore been a topic of intense research during the last 15 years, having the potential for great efficiency improvements (see [63] for a review of PAPR reduction techniques).

Besides saturation or clipping, amplifiers generally exhibit *compressive* nonlinear behavior (gain roll-off), as well as linear and nonlinear *time dispersion* (memory) at amplitude levels well below the clipping level [26], [67], [121] [154]. Figure 2-12 shows the instantaneous AM-AM response of an AR KMW2026M25 100-W solid-state power amplifier at output power of 46 dBm, and the ideal linear response as a reference. The signal was an OFDM signal with 160 active subcarriers, 16-QAM subcarrier modulation, a bandwidth of 7.5 MHz, and the carrier frequency was 490 MHz. The PA exhibits clear compressive behavior at higher envelope values, as well as memory effects, manifested as spreading of the instantaneous AM-AM curve[3].

[2] The efficiency of a Class AB amplifier lies between those of Class A and B amplifiers.

[3] The spreading can in principle be caused by mechanisms other than PA memory effects, such as filtering in other components in the measurement chain, and measurement noise. Here, these variables were controlled for and do not contribute to the spreading.

As with clipping, the conservative way to deal with the compressive nonlinear behavior is to drive the amplifier in its "linear region", i.e., to back off the amplifier's input power from the input saturation point. The linear region should here be understood to mean a power level where the transmitted signal fulfills certain quality constraints in terms of self-interference (EVM; see (2.65)), adjacent/alternate channel interference (ACPR; see (2.64)), or some other linearity measure. The needed power back-off is at least as large as the PAPR of the signal to be transmitted.

In order to obtain good power efficiency with general non-constant envelope signals, without corrupting the transmitted signal or creating interference on neighboring channels, three complementary strategies can be used. First, the efficiency of the transmitter can be improved through using linear transmitter architectures (see next subsection). Second, the PAPR of the signal can be reduced through sophisticated digital signal processing, thus facilitating more efficient amplification. Third, some kind of *linearization technology* can be adopted, to overcome the nonlinear (compressive) behavior and the memory effects of the amplifier. PA linearization techniques will be briefly reviewed next, with a focus on digital predistortion.

2.4.2 PA Linearization Techniques

Linearity is becoming increasingly important in PA design due to the adoption of higher-order modulation formats with non-constant envelopes. First, higher-order modulations are inherently more vulnerable to any system nonlinearities. Second, compared to constant envelope signals, non-constant envelope signals are more likely to create undesired nonlinear distortions on adjacent channels. Therefore, development of more linear transmitter architectures, PAPR mitigation, and *linearization* of existing PA technologies, are considered important ingredients in present and future radio transmitters that utilize non-constant envelope signals. Linear transmitter architectures include, for example, linear amplification using nonlinear components (LINC), envelope elimination and restoration (EER), envelope tracking (ET), dynamic load modulation techniques, and Doherty amplifiers. Even though termed "linear transmitter architectures", the main goal of these techniques is to improve the *power efficiency* of the transmitter, without sacrificing too much linearity. The reader is referred to [67], [104], [105] for more details on linear transmitter architectures, as they are out of the scope of this thesis. For details on PAPR mitigation, the reader is referred to [63] and the references therein.

Linearization techniques are explicitly aiming at improving the linearity of the PA, and they include:

(1) Feedforward linearization; for the traditional analog implementation, see [67], and for digitally-oriented implementations, see [47], [24], [17],

(2) Feedback linearization; these techniques can be divided into four categories: RF feedback, envelope feedback, polar feedback, and Cartesian feedback [26], [67]

(3) Analog RF and IF predistortion [66]

(4) Baseband digital predistortion

The details and relative merits of each technique are discussed for example in [26], [67], [71], [104]. In terms of signal bandwidth, feedback linearization is the most narrowband technique, and is not suitable for modern wideband applications. Feedforward, analog predistortion, and digital predistortion are all considered "wideband" techniques, in the sense that they can all be used to linearize signals with several MHz bandwidth. For bandwidths above 100 MHz, analog predistortion is currently the only feasible technology [66], [104], while feedforward is applicable up to around 100 MHz [104]. However, for bandwidths below 100 MHz, digital predistortion is considered the most promising linearization technology in terms of efficiency and linearity improvements, and flexibility, [44], [66], [70]. Fueled by Moore's law and the advancement of DAC and ADC technologies, DPD will be able to handle wider and wider bandwidths in the future. This thesis deals with DSP-based techniques only, and will therefore only consider linearization through DPD.

In terms of performance, it suffices to say here that a comprehensive and fair comparison between the techniques is extremely difficult to do, and is rarely attempted. We are aware of only one study [71], where the authors linearized a 300-W PEP Doherty power amplifier with feedforward and digital predistortion. There, it was found that for a fixed ACPR of -45 dBc, digital predistortion gave approximately 8 percentage points better power efficiency compared to feedforward, for PAPRs ranging from 5.5 to 9.8 dB. On the other hand, with smaller PAPR values, digital predistortion required larger back-off than feedforward to obtain the same level of ACPR. This can be explained by the fact that as the PA is driven deeper into saturation, higher and higher polynomial terms would be needed in the predistorter. This can become restrictive in terms of the needed bandwidth as well as sensitivity to noise and modeling errors in PD parameter estimation [13], [48].

The basic idea behind DPD (and predistortion in general) is to apply a nonlinear transformation, which is an inverse of the PA nonlinear function, on the baseband signal before passing it through the PA. Figure 2-13 illustrates this idea, by showing the input-output envelope relation of a predistorter (left), a memoryless PA (middle), and the cascade of the predistorter and the PA (right). The ideal linearized PA is thus an *ideal soft limiter*, i.e., is linear up to the saturation level. The saturation level is in practice determined by the DC supply power of the PA [67].

Digital predistorters are usually based on so-called *behavioral* PA models [44], [121]. Behavioral models are black-box models that aim at characterizing the input-output relation of the amplifier as accurately as possible with a finite set of parameters, without considering details about the physical circuit-level characteristics of the device, although some physical insights may be incorporated into the models (see, e.g., [166]). Behavioral models usually come in the form of *polynomial* or *envelope-phase* (AM/AM and AM/PM) PA models, either with or without memory, or on look-up-table (LUT) techniques, or combinations of these [44].

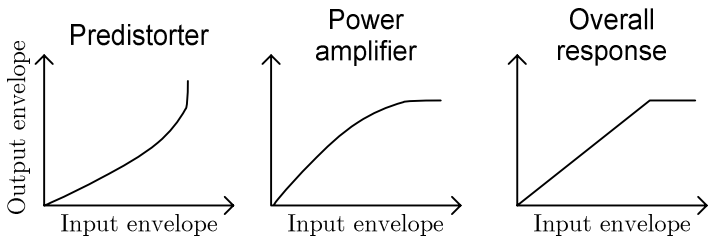

Figure 2-13: *Predistortion principle of operation.*

LUT techniques are out of the scope of this thesis. The next subsection will review behavioral PA modeling approaches.

2.4.3 Overview of Behavioral PA Models

This subsection gives a brief introduction to PA modeling approaches. The treatment is limited to polynomial-based *behavioral baseband models* of bandpass nonlinearities instead of physical circuit-level models, or other parametric models, because these facilitate straightforward estimation of the PA model parameters, or of the predistorter parameters.

The simplest baseband models of power amplifiers are based on polynomial (Taylor series) approximations of bandpass nonlinearities, yielding models of the form [67], [135]

$$\begin{aligned} z_{PA}(t) &= \sum_{\substack{p=1, \\ p \text{ odd}}}^{P} b_p \left|z(t)\right|^{p-1} z(t) \\ &= b_1 z(t) + b_3 \left|z(t)\right|^2 z(t) + ... + b_P \left|z(t)\right|^{P-1} z(t) \end{aligned} \tag{2.58}$$

where b_p are the PA model parameters. When the model parameters are real-valued, the PA model is said to be *strictly memoryless*. Strictly memoryless nonlinearities only affect the envelope of the signal, not the phase, and are typical models for narrowband signals. When b_p are complex-valued, the PA model is called *quasi-memoryless*.

For a general memoryless PA, denoting the complex envelope of the PA input signal in polar form as $z(t) = a(t)\exp(\theta(t))$, the output signal can be expressed as [135]

$$z_{PA}(t) = A[a(t)]e^{j(\theta(t)+\Phi[a(t)])}, \tag{2.59}$$

where $A[a(t)]$ represents the amplitude modulation-to-amplitude modulation (AM/AM) response, and $\Phi[a(t)]$ is the amplitude modulation-to-phase modulation (AM/PM) response of the amplifier. AM/AM and AM/PM responses are commonly used to characterize the envelope and phase shaping properties of memoryless PAs. A strictly memoryless nonlinearity is completely characterized by its AM/AM response, while quasi-memoryless PAs also affect the phase of the signal, as characterized by the AM/PM response. For the polynomial PA model in (2.58), the AM/AM and AM/PM responses can be obtained from the relation [135]

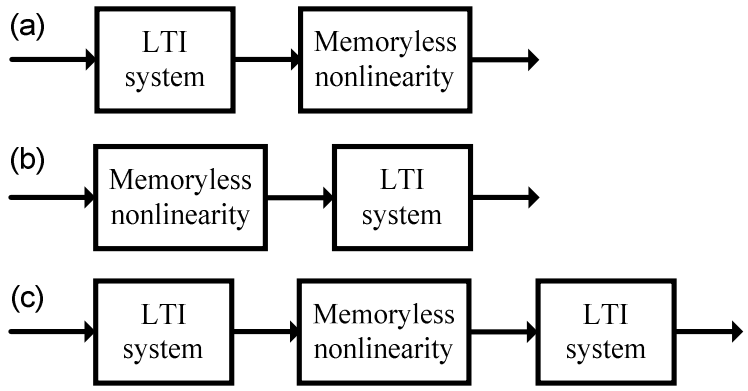

Figure 2-14: *(a) Wiener system, (b) Hammerstein system, and (c) Wiener-Hammerstein system.*

$$A[a(t)]e^{j\Phi[a(t)]} = \sum_{\substack{p=1,\\ p\ \text{odd}}}^{P} b_p a^p(t)\,. \tag{2.60}$$

Memoryless PA models are, however, not accurate enough in current and future wideband systems, because PAs invariably exhibit significant memory effects, manifested as spreading of the AM/AM and AM/PM response curves, and asymmetric IMD in two-tone or multi-tone tests [154], [20]. The memory effects can be broadly divided into electrical and electro-thermal memory effects (see [154], [20], [97], [155] for details). Depending on the time constant of the effect, a division between short-term and long-term memory effects is often made. Short-term memory effects are characterized by the inverse of the time constant being of the same order of magnitude as the bandwidth of the information signal. DPD linearization is usually restricted to dealing with short-term memory effects, because the filters needed to tackle long-term memory would grow impractically long and complex.

PA models that take into account the memory effects can be obtained by cascading memoryless PA models with filters in its output and/or input, by having parallel connections of such systems, by using memory polynomials, or by utilizing Volterra filters [121], [44], [98], [30], [13], [32]. The cascade of an LTI filter with a memoryless nonlinearity is called a Wiener system. Changing the order of the memoryless nonlinearity and the LTI filter gives a so-called Hammerstein system. The combination of Wiener and Hammerstein systems is called a Wiener-Hammerstein system. These are illustrated in Figure 2-14. A parallel connection of Hammerstein systems is naturally called a parallel Hammerstein (PH) system, which is shown in Figure 2-15. The PH system has been shown to be a versatile tool for both direct and inverse (predistortion) modeling of PA's [30], [59], [60], [98]. The PH system is used also in [P3] and [P4] for predistortion purposes.

In a PH system, the branch nonlinearities are commonly polynomials of different orders. In the PA modeling or predistortion context, at digital baseband, the branch nonlinearities are polynomials of the form

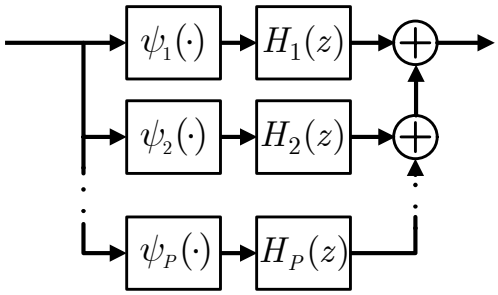

Figure 2-15: *Parallel Hammerstein nonlinearity.*

$$\psi_p(x_n) = \sum_{k \in I_{P;p}} u_{k,p} \, |x_n|^{k-1} x_n \ , \ p \in I_P \tag{2.61}$$

with $x_n = x_{n,I} + jx_{n,Q}$ denoting the baseband equivalent input signal to the nonlinearity, P the polynomial order, I_P the set of used polynomial orders, and $u_{k,p}$ the polynomial weights [98], [30], [106], [59], [P3]. If all polynomial orders up to P are used in (2.61), $I_P = \{1,2,3,...,P\}$, and if only odd orders are included, $I_P = \{1,3,5,...,P\}$. The subset of I_P in which orders only up to p are retained, is denoted by $I_{P;p}$. The filters $H_p(z)$, in turn, are usually finite impulse response (FIR) filters for implementation and parameter estimation simplicity.

The Volterra series expansion is the ultimate way to model a nonlinear system with memory. It can be considered a "Taylor series with memory". The baseband Volterra series model of a bandpass nonlinearity is given as [135]

$$v(x_n) = \sum_{p=0}^{\frac{P-1}{2}} v_{2p+1}(x_n) \triangleq \sum_{p=0}^{\frac{P-1}{2}} \sum_{d_1=0}^{M} \cdots \sum_{d_{2p+1}=0}^{M} h_{2p+1}(\mathbf{d}_{2p+1}) \prod_{i=1}^{p+1} x_{n-d_i} \prod_{i=p+2}^{2p+1} x_{n-d_i}^* \ , P \text{ odd} \tag{2.62}$$

where $\mathbf{d}_l = [d_1, d_2, ..., d_l]$, $h_l(\mathbf{d}_l)$ is the *l*-th order Volterra kernel, M is the memory depth (assumed equal for all dimensions), and P is the nonlinearity order, assumed odd. The model can be broken down to a sum of Volterra nonlinearities that contain only terms of order $2p+1$, $v_{2p+1}(x_n)$. Basically all other polynomial based PA models, for example those in Figure 2-14 and Figure 2-15, can be shown to correspond to certain approximations or simplifications of the Volterra series model [30], [98], [92], [121].

Some clarifications about the connection between behavioral PA models and PA predistorters are in order. Most often when deciding on the type of predistorter to be used for a real system, the first step is to find a good parametric model for the device under test (DUT). Then, the task of choosing the predistorter type becomes a problem of determining the inverse system for that particular PA model. If the Wiener model, for example, is found to be a good model for the DUT, the ideal PD structure is a Hammerstein system, and vice versa. More generally, the inverse of a Volterra nonlinearity is another Volterra nonlinearity. The parameters of the chosen PD structure can then be found through

two different strategies, *direct learning* or *indirect learning*. Direct learning finds a pre-inverse for the PA utilizing the learned PA model explicitly [165], but the cost function is always non-quadratic regardless of the PD structure, and can thus lock to *local minima* of the cost function. Indirect learning, on the other hand, utilizes actual measured data of the PA input and the PA output in estimating the parameters of the chosen PD structure. If a suitable PD structure such as parallel Hammerstein or Volterra is used with indirect learning, the cost function is always quadratic in the estimated parameters, thus avoiding the local minima problem and facilitating efficient estimation with mean-square or least squares error minimization techniques [30], [32], [92], [P3], [P4].

2.4.4 Impact of PA Nonlinearity on System Performance

To shortly analyze the effects of an instantaneous (memoryless) nonlinearity, we consider the case of a 3rd order polynomial PA model from (2.58), yielding the input-output relation

$$z_{PA}(t) = b_1 z(t) + b_3 |z(t)|^2 z(t) \tag{2.63}$$

where $z(t)$ is the PA input signal, and b_1, b_3, with $b_1 > b_3$, are the first and third order PA model parameters. The FT of (2.63) yields

$$Z_{PA}(f) = b_1 Z(f) + b_3 Z(f) \star Z(f) \star Z^*(-f)$$

which follows directly from the properties of the FT. The resulting third-order distortion term is thus a convolution of the spectra of the input signal with itself and its frequency-mirrored complex conjugate, leading to the well-known spectral widening, or *spectral regrowth*. Third order nonlinearity thus has a total bandwidth that is three times that of the original signal, in terms of the absolute bandwidth. More generally, *N*th order nonlinearity results in *N*-fold bandwidth compared to the original signal.

The amount or severity of the spectral regrowth is often measured by the adjacent-channel power ratio, defined as

$$\mathrm{ACPR}_{\mathrm{dB}} = 10 \log_{10} \frac{\int_{W_A} S_{PA}(f) df}{\int_{W_D} S_{PA}(f) df}, \tag{2.64}$$

where $S_{PA}(f)$ denotes the power spectral density (PSD) of the PA output signal $z_{PA}(t)$, and W_A and W_D the frequency band of the (worse) adjacent channel and the desired channel, respectively. Communications standard bodies always specify the maximum levels of allowable ACPR on the adjacent channels, as well as the channels further away, herein called *alternate channels*. These specifications come in the form of a *spectral mask* or *interference mask*, which the power spectral density of the transmitted signal must satisfy.

To quantify the amount of self-interference generated by a nonlinearity (or any nonideality) in a transmitter, the error-vector magnitude (EVM), or signal vector error, is often used. It is defined as the RMS error of the transmitted signal constellation points,

$$EVM = \sqrt{\frac{\frac{1}{N}\sum_{n=1}^{N}\left|S_{ideal,n} - S_{meas,n}\right|^2}{\frac{1}{N}\sum_{n=1}^{N}\left|S_{ideal,n}\right|^2}}, \tag{2.65}$$

where $S_{ideal,n}$ and $S_{meas,n}$ are actual and measured transmitted symbols, respectively, and N is the number of symbols (large) used for estimation. The EVM is usually given in percentage, or sometimes in dB as $20\log_{10}(EVM)$.

2.5 Joint Effects of PA Nonlinearity, Tx I/Q Imbalance, and LO Leakage

The main implementation impairments in a direct-conversion transmitter are PA nonlinear distortion, I/Q imbalance, and local oscillator (LO) leakage. Modeling and compensation of PA nonlinearity and I/Q imbalance have been treated separately and extensively in the literature, and also in the preceding subsections. What is often overlooked in the literature, however, is that in direct-conversion transmitters these impairments interact in a manner that may severely cripple the overall transmitted signal quality. In addition to the obvious effects of I/Q imbalance and LO leakage (mirror-frequency interference and spurious signal energy at the LO frequency, respectively), there are other significant performance-degrading phenomena arising from their interaction with the PA that need addressing. First, I/Q imbalance and LO leakage cause extra intermodulation distortion (IMD) products to appear at the PA output [34], [22], [151]. Effectively this means that even with access to ideal PA predistorter coefficients (e.g., in *p*th order inverse sense), spectral regrowth will not be fully mitigated. Second, the extra IMD products at the PA output will interfere with the estimation of an adaptive PA PD [34], [22], [151]. In other words, if the PA PD is trained with no regard for I/Q imbalance and LO leakage, the resulting PD will be biased, and thus the overall transmitted signal quality will be further compromised. Third, PA nonlinearity interferes with the estimation of the I/Q modulator (IQM) predistorter, yielding biased estimates. This makes it challenging to estimate and compensate for IQM impairments prior to PA PD estimation. Therefore, joint processing of the three main impairments seems the only option in light of the current literature[4].

Now, we couple the frequency-independent TX I/Q mismatch model from (2.26), the polynomial PA model of (2.58), and LO leakage, to see their joint effects. This is done for motivational purposes, to illustrate the effects that the IQM impairments have on the inter-

[4] However, expression (17) in [P8] suggests, that the CACF of the PA output signal is only slightly affected by PA nonlinearity, thus implying that a circularity-based estimation algorithm may possibly be used to estimate the TX I/Q imbalance even under PA nonlinearity. This forms an interesting topic for further research.

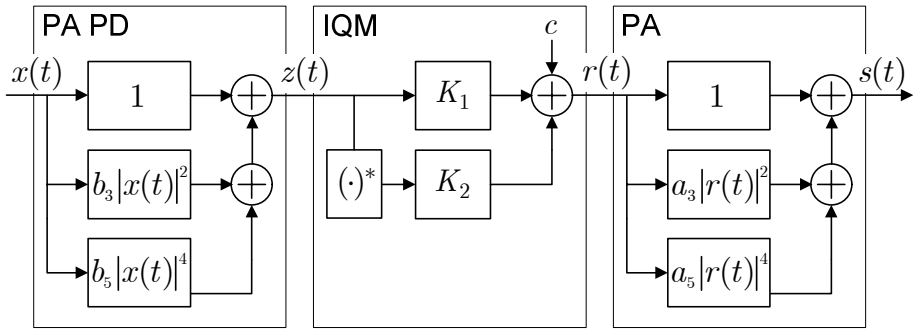

Figure 2-16: *Memoryless baseband signal model for a transmitter, with fifth-order polynomial PA predistorter (PA PD), I/Q modulator (IQM) with mismatch and LO leakage, and fifth-order polynomial PA model.*

modulation products created by the PA, and on the estimation of the PA predistorter parameters. In the publications [P3] and [P4], frequency-dependent behavior for both I/Q mismatch and PA nonlinearity have been assumed.

With reference to Figure 2-16, we denote the baseband I/Q signal, exiting the PA predistorter, as $z(t) \triangleq z_I(t) + jz_Q(t)$. If the IQM is ideal, i.e., it has no impairments, $z(t)$ is also the complex envelope of the IQM output signal. Under I/Q mismatch and LO leakage, the complex envelope of the IQM output is written as

$$r(t) = K_1 z(t) + K_2 z^*(t) + c\,, \tag{2.66}$$

where

$$K_1 = \frac{1 + g\exp(j\phi)}{|1 + g\exp(j\phi)|},\; K_2 = \frac{1 - g\exp(j\phi)}{|1 + g\exp(j\phi)|}$$

are the baseband I/Q mismatch coefficients, and $c = |c|\exp(j\angle c)$ is the LO leakage signal. Notice that K_1 and K_2 are scaled versions of the I/Q parameters introduced in (2.28). This scaling simply eliminates the level mismatch caused by the used I/Q imbalance model in (2.66), which is known to have its own independent effects on the IMD levels of the PA output [34]. In the following analysis we are interested in the effects of the MFI term $K_2 z^*(t)$, not of the level mismatch. The effects of level mismatch on the IMD products were analyzed in [34].

With the IQM output signal (2.66) as input to a 5th order polynomial PA model, the complex envelope of the PA output signal is expressed as

$$s(t) = H(r(t)) = r(t) + a_3 |r(t)|^2 r(t) + a_5 |r(t)|^4 r(t)\,, \tag{2.67}$$

where the linear gain term has been set to unity. With a perfect IQM ($K_1 = 1$, $K_2 = c = 0$), the PA output takes the form

$$s(t) = H(z(t)) = z(t) + a_3 |z(t)|^2 z(t) + a_5 |z(t)|^4 z(t). \tag{2.68}$$

We can see the effect of LO leakage on the PA output signal by plugging (2.66) into (2.67) and setting $K_1 = 1$ and $K_2 = 0$, yielding

$$\begin{aligned} s(t) = z(t) + 2a_3 c|z(t)|^2 + a_3 c^* z(t)^2 + a_3 |z(t)|^2 z(t) + a_5 c^{*2} z(t)^3 \\ + 3a_5 c|z(t)|^4 + 2a_5 c^* |z(t)|^2 z(t)^2 + a_5 |z(t)|^4 z(t) + c \end{aligned} \tag{2.69}$$

where higher than fifth order terms have been neglected. Compared to the case of no IQM impairments in (2.68), two second-order products $|z(t)|^2$ and $z(t)^2$, one third-order product $z(t)^3$ and two fourth-order products $|z(t)|^4$ and $|z(t)|^2 z(t)^2$, appear. These create additional in-band and adjacent/alternate channel interference.

Under I/Q mismatch, we insert (2.66) into (2.67) and set $c = 0$, resulting in

$$\begin{aligned} s(t) = A_{iq1} z(t) + A_{iq2} z(t)^* + A_{iq3} |z(t)|^2 z(t) + A_{iq4} |z(t)|^2 z(t)^* \\ + A_{iq5} z(t)^3 + A_{iq6} z(t)^{*3} + A_{iq7} |z(t)|^4 z(t) + A_{iq8} |z(t)|^4 z(t)^* \\ + A_{iq9} |z(t)|^2 z(t)^3 + A_{iq10} |z(t)|^2 z(t)^{*3} + A_{iq11} z(t)^5 + A_{iq12} z(t)^{*5} \end{aligned} \tag{2.70}$$

where the terms of order higher than 5 have been neglected. Extra intermodulation products again appear compared to (2.68), now due to I/Q mismatch. These are the first-order image interference term $x(t)^*$, three third-order products $|x(t)|^2 x(t)^*$, $x(t)^3$ and $x(t)^{*3}$, and five fifth-order products $|x(t)|^4 x(t)^*$, $|x(t)|^2 x(t)^3$, $|x(t)|^2 x(t)^{*3}$, $x(t)^5$, and $x(t)^{*5}$. The exact expressions for the complex coefficients $A_{iqj}, j = 1...12$ in (2.70) are listed in Table 17-2 of [150], as well as in [30] (although with a different parameterization), and are not reproduced here.

The effects of the extra IMD terms on adaptive PA PD parameter estimation were assessed in [22] and [150], as well as experimentally in [P3], [P4]. There, it was found that the resulting parameter estimates will be biased, further compromising the spectral regrowth mitigation capabilities of PA predistortion, and in some cases possibly resulting in amplification, instead of attenuation, of total IMD at the PA output.

2.6 Other Essential Impairments in Direct-Conversion Links

Other essential impairments, related to circuit implementations or the radio channel, include carrier frequency offset, receiver DC offsets, and additive noise. Here, special interest is on the *interactions* that these impairments have with I/Q imbalances or their compensation. The following results are compiled from [P8], [P2], [120]. These will be elaborated on in Section 3.5, from the viewpoint of second-order statistics.

2.6.1 Carrier Frequency Offset

The received signal with carrier frequency offset and RX I/Q imbalance is [138], [145]

$$x_{RX}(t) = g_{1,RX}(t) \star (e^{j\Delta\omega t} z_{RX}(t)) + g_{2,RX}(t) \star (e^{-j\Delta\omega t} z^*_{RX}(t)) \tag{2.71}$$

whose FT is

$$\begin{aligned} X_{RX}(f) &= G_{1,RX}(f) Z_{RX}(f - \Delta f) + G_{2,RX}(f) Z^*_{RX}(-f + \Delta f) \\ &= G_{1,RX}(f) \tilde{Z}_{RX}(f) + G_{2,RX}(f) \tilde{Z}^*_{RX}(-f) \end{aligned} . \tag{2.72}$$

where $\tilde{Z}_{RX}(f) = Z_{RX}(f - \Delta f)$. The mirror-frequency interference interpretation of I/Q imbalance thus holds also under CFO. Now, if CFO is corrected, the signal model becomes

$$\tilde{X}_{RX}(f) = G_{1,RX}(f + \Delta f) Z_{RX}(f) + G_{2,RX}(f + \Delta f) Z^*_{RX}(-f + 2\Delta f) , \tag{2.73}$$

where the mirror-frequency structure is now "broken". RX I/Q imbalance compensation should therefore be performed *before* any digital CFO compensation. TX I/Q imbalance compensation, on the other hand, if to be done at the receiver side, should (at least in single-user systems) be done *after* fine frequency correction. Often in the literature it is done jointly with channel equalization, in which case the equalizer/detector assumes a widely-linear form, or equivalently in the frequency-domain, a mirror subcarrier pair wise form as in (2.52) (see also [54], [56], [69], [77], [129], [134], [163]).

Modern wireless communication systems invariably have frequency offset present, and it is therefore imperative to take it into account when deriving I/Q imbalance compensation algorithms. In RX I/Q imbalance compensation, blind (non-data-aided) estimation algorithms relying on second-order statistics of the received signal are typically immune to CFO, whereas data-aided estimators always need to estimate (but not compensate) CFO before estimating RX I/Q imbalance parameters.

2.6.2 DC Offsets

Receiver DC offsets are due to *signal leakages* from one mixer port to another, and subsequent *self-mixing* [3], [35], [110], [127]. When the LO signal leaks to the RF signal input and mixes with itself, the result is a constant voltage at zero-frequency (DC). When the received signal leaks to the mixer's LO port, the resulting self-mixing product is the signal squared, which results in a time-varying signal-dependent low-frequency signal with a strong DC component. Hence it is often called "dynamic DC offset", although it is in fact second-order intermodulation (IM2) of the mixer's input frequency band, therefore having frequency content also around DC [35]. If there is a strong signal ("blocker") present within the mixer's input band, the dynamic DC offset has the potential to destroy detection of the desired signal. In addition, the IM2 has a symmetric spectrum. Therefore, it creates correlation between the

mirror frequencies of the received signal and can potentially have implications on RX I/Q imbalance estimation [P8]. This will be elaborated on in Section 3.5.

2.6.3 Additive Noise

Assuming that the baseband additive noise $n(t)$ is white complex-circular Gaussian (AWGN) with zero mean and variance σ_n^2, the received signal under frequency-independent RX I/Q imbalance becomes

$$\begin{aligned} x_{RX}(t) &= K_{1,RX}(r(t) + n(t)) + K_{2,RX}(r^*(t) + n^*(t)) \\ &= K_{1,RX}r(t) + K_{2,RX}r^*(t) + K_{1,RX}n(t) + K_{2,RX}n^*(t) \end{aligned}$$

where $r(t)$ is the noiseless received signal. Circularity is here defined as $\mathrm{E}[n^2(t)] = 0$, which for a Gaussian distributed $n(t)$ implies rotational invariance of the pdf (see Sections 3.4 and 3.5 and [120] for more details). Now under I/Q imbalance, the noise term $n_{RX}(t) = K_{1,RX}n(t) + K_{2,RX}n^*(t)$ is clearly *not* circular anymore, because $\mathrm{E}[n_{RX}^2(t)] = 2K_{1,RX}K_{2,RX}\sigma_n^2 \neq 0$. On the other hand, RX I/Q imbalance compensation restores the circularity of the noise. Anyhow, the noncircular noise has implications on optimum maximum likelihood (ML) estimation of I/Q imbalance parameters, because the typical assumption of circular noise no longer holds.

Chapter 3

Second-Order Statistics of I/Q Signals

This section introduces the second-order statistics of complex random signals or processes, giving the basic time-domain and frequency-domain expressions. We begin with the general case of nonstationary signals, and then introduce the statistics for second-order stationary and cyclostationary signals. The concepts of circularity and properness are explained, as they apply to this thesis. Time-average properness, which is an important concept for understanding mirror-frequency interference with cyclostationary signals, is introduced. An intuitive spectral interpretation of time-average properness is given, essentially saying that it is equivalent to the signal being free of mirror-frequency interference. The effects of various RF impairments on the second-order statistics of communication signals are also addressed. These results form the theoretical basis upon which Chapter 4 and the contributions therein, as well as parts of Chapter 5, build upon.

3.1 Definitions

The mean of a general *nonstationary* complex-valued random signal $x(t) = x_I(t) + jx_Q(t)$ is given as

$$\mu_x(t) \triangleq \mathrm{E}[x(t)] = \mathrm{E}[x_I(t)] + j\mathrm{E}[x_Q(t)]. \tag{3.1}$$

In the continuation, to simplify notation, we assume that all signals are *zero-mean* unless otherwise stated.

The *cross-correlation function* of two complex-valued random signals $x(t) = x_I(t) + jx_Q(t)$ and $y(t) = y_I(t) + jy_Q(t)$ is denoted by

$$\gamma_{xy}(t,\tau) = \mathrm{E}[x(t+\tau)y^*(t)] \tag{3.2}$$

and their *complementary cross-correlation function* is given by

$$c_{xy}(t,\tau) = \mathrm{E}[x(t+\tau)y(t)], \tag{3.3}$$

in terms of the *global time variable* t and the *local time variable* τ. In general, for a complete joint second-order description of $x(t)$ and $y(t)$, both moments are needed [120].

Using the definitions in (3.1) and (3.2), we define the *autocorrelation function* (ACF) and the *complementary autocorrelation function* (CACF) of a complex random signal $x(t)$ as

$$\gamma_{xx}(t,\tau) = \mathrm{E}[x(t+\tau)x^*(t)] \tag{3.4}$$

$$c_{xx}(t,\tau) = \mathrm{E}[x(t+\tau)x(t)]\,. \tag{3.5}$$

Both of these moments are generally needed for a complete second-order description of $x(t)$ [95], [101]. The CACF can also be viewed as the cross-correlation function of $x(t)$ and its complex-conjugate $x^*(t)$, since clearly $c_{xx}(t,\tau) = \mathrm{E}[x(t+\tau)(x^*(t))^*] = \gamma_{xx^*}(t,\tau)$.

We then define the *spectral correlation* $\mathbb{P}_{xx}(v,f)$ and the *complementary spectral correlation* $\mathbb{C}_{xx}(v,f)$ as the two-dimensional Fourier transforms of $\gamma_{xx}(t,\tau)$ and $c_{xx}(t,\tau)$, respectively:

$$\mathbb{P}_{xx}(v,f) = \int_{\mathbb{R}^2} \gamma_{xx}(t,\tau)e^{-j2\pi(vt+f\tau)}\mathrm{d}\tau\mathrm{d}t \tag{3.6}$$

$$\mathbb{C}_{xx}(v,f) = \int_{\mathbb{R}^2} c_{xx}(t,\tau)e^{-j2\pi(vt+f\tau)}\mathrm{d}\tau\mathrm{d}t\,. \tag{3.7}$$

The above is the so-called Cramér-Loève spectral representation of $x(t)$, and it requires that $x(t)$ is *harmonizable*[5].

3.2 Second-Order Stationary and Wide-Sense Stationary Signals

We say that $x(t)$ is *wide-sense stationary* (WSS) if its mean and ACF are independent of *t*, and *second-order stationary* (SOS) if, in addition, its CACF is independent of *t* [101]. These are indicated by dropping the *t*-argument in (3.1), (3.4), and (3.5), and writing them as μ_x, $\gamma_{xx}(\tau)$, and $c_{xx}(\tau)$. With similar conditions on the ordinary and complementary cross-correlation functions of two random signals $x(t)$ and $y(t)$, they are called *jointly WSS* or *jointly SOS*, respectively. Stationarity is a typical assumption often made in communications literature to make the analysis more tractable.

For a SOS signal $x(t)$ the spectral correlations are zero outside the line $v = 0$ (a.k.a. the *stationary manifold*). Evaluating (3.6) and (3.7) on $v = 0$ we obtain the *power spectral density* (PSD) and the *complementary power spectral density* (CPSD) of $x(t)$, as

$$P_{xx}(f) \triangleq \mathbb{P}_{xx}(0,f) = \int_{-\infty}^{\infty} \gamma_{xx}(\tau)e^{-j2\pi f\tau}d\tau \tag{3.8}$$

[5] Harmonizability of a nonstationary random signal $x(t)$ means that it can be represented as $x(t) = \int \mathrm{d}\xi(f)e^{j2\pi ft}$, where $\xi(f)$ is a spectral process with correlated increments $\mathrm{d}\xi(f)$ [80], [120].

$$C_{xx}(f) \triangleq \mathbb{C}_{xx}(0,f) = \int_{-\infty}^{\infty} c_{xx}(\tau) e^{-j2\pi f\tau} d\tau \,. \tag{3.9}$$

In the SOS case, the spectral correlations are thus reduced to one-dimensional Fourier transforms of $\gamma_{xx}(\tau)$ and $c_{xx}(\tau)$, as is well known [101], [120].

$P_{xx}(f)$ and $C_{xx}(f)$ are valid PSD and CPSD if the following three conditions are fulfilled for all f [101]:

$$\begin{aligned} &1.\ P_{xx}(f) \geq 0 \\ &2.\ C_{xx}(f) = C_{xx}(-f) \\ &3.\ |C_{xx}(f)|^2 \leq P_{xx}(f)P_{xx}(-f) \end{aligned} \tag{3.10}$$

3.2.1 Ergodicity

The concept of *ergodicity* needs to be invoked when building practical estimators for stationary random signals. Broadly speaking, ergodicity means that certain time-average moments of a random process are equal to the corresponding ensemble averages. One can define different orders of ergodicity, for example ergodicity in mean, in mean square, in correlation function, and in pdf [126]. In a particular estimation problem, ergodicity should in principle be established for all the moments or statistics that are to be estimated.

A SOS random process $x(t)$ is *ergodic in the mean* if and only if the time average of a sample function of $x(t)$ is equal to the ensemble average of $x(t)$, i.e.,

$$\overline{\mu}_x \triangleq \lim_{T_0\to\infty} \frac{1}{T_0} \int_{-T_0/2}^{T_0/2} x(t)dt = \mu_x \,. \tag{3.11}$$

A sufficient condition for (3.11) and therefore for ergodicity in the mean is that

$$\int_{-\infty}^{\infty} |\gamma_{xx}(\tau)| d\tau < \infty \,, \tag{3.12}$$

meaning that the ACF be *absolutely integrable* [126].

A SOS random process $x(t)$ is *ergodic in correlation function* for shift τ if and only if

$$\overline{\gamma}_{xx}(\tau) \triangleq \lim_{T_0\to\infty} \frac{1}{T_0} \int_{-T_0/2}^{T_0/2} x(t+\tau)x^*(t)dt = \gamma_{xx}(\tau) \tag{3.13}$$

$$\overline{c}_{xx}(\tau) \triangleq \lim_{T_0\to\infty} \frac{1}{T_0} \int_{-T_0/2}^{T_0/2} x(t+\tau)x(t)dt = c_{xx}(\tau) \,. \tag{3.14}$$

If we define the random processes $\Phi_\lambda(t) = x(t+\lambda)x^*(t)$ and $\Theta_\lambda(t) = x(t+\lambda)x(t)$ for each λ, and assume that $x(t)$ has stationary second and fourth-order moments, the sufficient conditions for ergodicity in correlation function are obtained as

$$\int_{-\infty}^{\infty} \left|\gamma_{\Phi_\lambda\Phi_\lambda}(\tau)\right| d\tau < \infty \tag{3.15}$$

$$\int_{-\infty}^{\infty} \left| \gamma_{\Theta_\lambda \Theta_\lambda}(\tau) \right| d\tau < \infty, \tag{3.16}$$

where $\gamma_{\Phi_\lambda \Phi_\lambda}(\tau) = \mathrm{E}[\Phi_\lambda(t+\tau)\Phi_\lambda^*(t)] = \mathrm{E}[x(t+\tau+\lambda)x^*(t+\tau)x^*(t+\lambda)x(t)]$ and $\gamma_{\Theta_\lambda \Theta_\lambda}(\tau) = \mathrm{E}[\Theta_\lambda(t+\tau)\Theta_\lambda^*(t)] = \mathrm{E}[x(t+\tau+\lambda)x(t+\tau)x^*(t+\lambda)x^*(t)]$ [126]. In other words, ergodicity in correlation function requires that the fourth-order moments $\gamma_{\Phi_\lambda \Phi_\lambda}(\tau)$ and $\gamma_{\Theta_\lambda \Theta_\lambda}(\tau)$ are absolutely integrable. In the vast majority of practical estimation problems, and in particular those dealing with communications signals, the second and fourth-order moments are finite in magnitude and tend to zero as $\tau \to \infty$, meaning that (3.12), (3.15), and (3.16) will almost certainly hold. Ergodicity (or a related concept for cyclostationary signals called *cycloergodicity*; see for example [40]) will thus be assumed in the remainder of this thesis without explicit proofs. Further discussion of ergodicity is out of our scope, so the interested reader is referred to [126] for more details.

3.2.2 Sample Estimates of Second-Order Moments

Invoking ergodicity, natural estimators for the autocorrelation functions of SOS signals are the *sample estimates*

$$\hat{\gamma}_{xx}(\tau) = \frac{1}{T_C} \int_0^{T_C} x(t+\tau)x^*(t)dt \tag{3.17}$$

$$\hat{c}_{xx}(\tau) = \frac{1}{T_C} \int_0^{T_C} x(t+\tau)x(t)dt \tag{3.18}$$

with observation time T_C. The corresponding sample estimators for *discrete-time signals* are

$$\hat{\gamma}_{xx}(\tau) = \frac{1}{N_C} \sum_{n=0}^{N_C-1} x(n+\tau)x^*(n) \tag{3.19}$$

$$\hat{c}_{xx}(\tau) = \frac{1}{N_C} \sum_{n=0}^{N_C-1} x(n+\tau)x(n), \tag{3.20}$$

where N_C is the observation block size in samples.

3.3 Cyclostationary Signals

The complex envelope of a real-valued RF noise process in the radio front-end is SOS [120]. However, practical communication signals are usually *not* SOS or WSS, because their second-order moments (and in some cases also the first-order moment) are *periodic* or *cyclic* in *t* due to for example data modulation, carrier modulation, or coding. Such random signals are called *second-order cyclostationary* (cyclostationary (CS) in short) or periodically stationary [39], and their second-order moments have the properties

$$\gamma_{xx}(t,\tau) = \gamma_{xx}(t+T,\tau) \tag{3.21}$$

$$c_{xx}(t,\tau) = c_{xx}(t+T,\tau) \tag{3.22}$$

with the fundamental period T. As $\gamma_{xx}(t,\tau)$ and $c_{xx}(t,\tau)$ are periodic, they can be expressed as *Fourier series* [39]

$$\gamma_{xx}(t,\tau) = \sum_{n=-\infty}^{\infty} \gamma_{xx}^{n}(\tau) \cdot e^{j2\pi nt/T} \tag{3.23}$$

$$c_{xx}(t,\tau) = \sum_{n=-\infty}^{\infty} c_{xx}^{n}(\tau) \cdot e^{j2\pi nt/T} \tag{3.24}$$

where the frequencies $n/T \triangleq v$, $n \in \mathbb{Z}$, are called *cyclic frequencies*, and the *Fourier series coefficients* corresponding to the cyclic frequencies are given as

$$\gamma_{xx}^{n}(\tau) = \frac{1}{T}\int_{0}^{T} \gamma_{xx}(t,\tau)e^{-j2\pi nt/T}dt \tag{3.25}$$

$$c_{xx}^{n}(\tau) = \frac{1}{T}\int_{0}^{T} c_{xx}(t,\tau)e^{-j2\pi nt/T}dt\,. \tag{3.26}$$

Functions (3.25) and (3.26) are known as the *cyclic autocorrelation function* (c-ACF) and *cyclic complementary autocorrelation function* (c-CACF), respectively [39], [120].

Taking the Fourier transforms of the c-ACF and c-CACF in τ yields the *cyclic power spectral density* (c-PSD) and the *cyclic complementary PSD* (c-CPSD) as

$$P_{xx}^{n}(f) = \int_{-\infty}^{\infty} \gamma_{xx}^{n}(\tau)e^{-j2\pi f\tau}d\tau \tag{3.27}$$

$$C_{xx}^{n}(f) = \int_{-\infty}^{\infty} c_{xx}^{n}(\tau)e^{-j2\pi f\tau}d\tau\,. \tag{3.28}$$

The c-ACF and c-CACF (and therefore the c-PSD and c-CPSD) are generally non-zero only at some of the cyclic frequencies, but not necessarily on the same cyclic frequencies [120]. These cyclic statistics find application in many signal processing tasks in communications, e.g., symbol and carrier synchronization, signal detection, spectrum sensing, and modulation classification [42].

An important pair of statistics for the purposes of this thesis is obtained by calculating $\gamma_{xx}^{n}(\tau)$ and $c_{xx}^{n}(\tau)$ on the stationary manifold $v = n/T = 0$, yielding [102], [120]

$$\gamma_{xx}^{0}(\tau) = \frac{1}{T}\int_{0}^{T} \gamma_{xx}(t,\tau)dt \triangleq \overline{\gamma}_{xx}(\tau) \tag{3.29}$$

$$c_{xx}^{0}(\tau) = \frac{1}{T}\int_{0}^{T} c_{xx}(t,\tau)dt \triangleq \overline{c}_{xx}(\tau)\,. \tag{3.30}$$

$\overline{\gamma}_{xx}(\tau)$ and $\overline{c}_{xx}(\tau)$ are called the *time-average ACF* and *time-average CACF*, respectively. The periodicities in $\gamma_{xx}(t,\tau)$ and $c_{xx}(t,\tau)$ are simply removed by averaging over the period, thus yielding functions in one dimension. For a non-zero CS random signal $x(t)$, $\gamma_{xx}^{0}(\tau) \neq 0$, meaning that CS processes always have a "stationary component" at $v = 0$. An often-used trick to make a cyclostationary signal SOS is to model the time reference or phase of the process as a random variable, distributed uniformly over T [73], [39]. The ACF and CACF of the phase-randomized SOS process equal the time-average ACF and CACF of the original CS process, respectively [39].

Equations (3.25), (3.26), (3.29), and (3.30) give the expressions for a single period T. If there are two (or more) distinct periods in $\gamma_{xx}(t,\tau)$ and/or $c_{xx}(t,\tau)$, say T_1 and T_2, the integration is done over the *least common multiple* (LCM) of these periods [120], [41]. If T_1 and T_2 are incommensurate, their LCM equals ∞. These kinds of processes are generally known as *almost cyclostationary processes* [42]. The second-order cyclic statistics of CS processes are generalized to the almost CS case by taking the limit values of (3.25) and (3.26) as T tends to infinity [120].

The *time-average PSD* and *time-average CPSD* are then obtained as the Fourier transforms of $\overline{\gamma}_{xx}(\tau)$ and $\overline{c}_{xx}(\tau)$, respectively, or equivalently by evaluating the c-PSD and c-CPSD on the stationary manifold $v = n/T = 0$:

$$P_{xx}^{0}(f) = \int_{-\infty}^{\infty} \gamma_{xx}^{0}(\tau) e^{-j2\pi f\tau} d\tau \triangleq \overline{P}_{xx}(f) \tag{3.31}$$

$$C_{xx}^{0}(f) = \int_{-\infty}^{\infty} c_{xx}^{0}(\tau) e^{-j2\pi f\tau} d\tau \triangleq \overline{C}_{xx}(f). \tag{3.32}$$

These are equivalent to the PSD and CPSD of SOS signals, in the sense that a *spectrum analyzer* analyzing a CS signal will draw (a sample estimate of) the time-average PSD, whereas for a SOS signal it will draw (a sample estimate of) the PSD [89].

The sample estimates for the time-average ACF and CACF are the same as for SOS signals, defined in (3.17)-(3.20). However, for a CS signal, the integration or summation in (3.17)-(3.20) should in principle be done over an integer multiple of the cyclostationary period T, or in case of an almost CS signal, with $T \to \infty$.

As a final note for this subsection, the time-average statistics are in fact more relevant than the cyclic statistics for the analysis of the circularity-based algorithms in Section IV. This is because those algorithms explicitly utilize sample estimates of the *time-average autocorrelation functions*, or in other words, are only concerned with the *stationary components* of the processed signals. Therefore, whenever dealing with CS signals in the remainder of this thesis and in [P1]-[P8], unless otherwise stated, ACF, CACF, PSD, and CPSD will be understood to mean their *time-average counterparts*, and properness to mean *time-average properness* (see next subsection).

3.4 Circularity and Properness

Now, we define *circularity* and *properness* of complex random variables, vectors, and signals. These concepts have been introduced and analyzed in the seminal works by Brown [16], Picinbono [99], [101], van den Bos [152], Gardner [41], Neeser [95], Schreier [119] and their colleagues, and have been utilized by the author of this thesis for I/Q imbalance analysis and compensation in [P1-P8].

3.4.1 Random Variables

For a complex-valued random variable x, *circularity* is defined as x and $e^{j\alpha}\mathrm{x}$, for any $\alpha \in [0,2\pi)$, having the *same probability distribution* [99]. The term "circularity" is due to the fact that the probability density function (pdf) of a circular random variable x, assuming that the pdf exists, has circular contour lines [120]. Here, we refer to these kinds of random variables as *strictly circular*.

Strict circularity is difficult to measure in practice. A weaker form of circularity called *moment circularity* or *Nth order circularity* is defined as x and $e^{j\alpha}\mathrm{x}$, for any $\alpha \in [0,2\pi)$, having *equal moments up to order N*. *N*th order moments are defined as

$$m_x(k,l) = \mathrm{E}[x^k x^{*l}], \tag{3.33}$$

with $k+l=N$ and $k,l \in \mathbb{N}_0$. This implies, that for an *N*th order circular random variable, its only non-zero moments up to order *N* are the ones with an *equal number of nonconjugated and conjugated terms*, since only in these cases the phase terms cancel out [99]. The conditions for *second-order circularity* are thus

$$\begin{aligned} m_x(1,0) &= \mathrm{E}[x] = 0 \\ m_x(2,0) &= \mathrm{E}[x^2] = 0 \end{aligned} \tag{3.34}$$

All variables, vectors, and signals will be assumed *zero-mean* in the continuation, unless otherwise stated, so the zero-mean condition will not be explicitly mentioned when discussing circularity or properness. The condition in (3.34) is also known as *properness*, and the terms second-order circularity and properness are often used interchangeably. Strict circularity implies moment circularity, but not vice versa in general. For a complex Gaussian random variable, with mean zero, properness implies strict circularity. This is a special property of the family of *complex elliptical distributions* [96] (to which the complex Gaussian distribution also belongs), and cannot be generalized to other distributions.

It is worth mentioning that only proper Gaussian variables have the pdf of the form

$$p_x(x) = \frac{1}{\pi\sqrt{\gamma_{xx}}} \exp\left(-\frac{|x|^2}{\gamma_{xx}}\right) \tag{3.35}$$

which is a direct extension of the real case and the one used almost exclusively in the literature. However, in general there is no reason to assume that properness holds. A complete description of a complex-valued Gaussian variable/process also takes into account the CACF. For a scalar variable x, the *generalized complex Gaussian* pdf is given as [120]

$$p_x(x) = \frac{1}{\pi\sqrt{\gamma_{xx}(1-|\rho|^2)}} \exp\left(-\frac{|x|^2 - \mathrm{Re}\{\rho x^{*2}\}}{\gamma_{xx}(1-|\rho|^2)}\right) \tag{3.36}$$

where ρ is the *circularity coefficient* defined as

$$\rho = \frac{c_{xx}}{\gamma_{xx}}, \tag{3.37}$$

and $\gamma_{xx} \triangleq m_x(1,1) = \mathrm{E}[|x|^2]$ and $c_{xx} \triangleq m_x(2,0) = \mathrm{E}[x^2]$. Clearly when x is proper, $\rho = 0$ and (3.36) simplifies to the circular pdf in (3.35).

3.4.2 Random Vectors

We first introduce the definitions of *mean*, *covariance matrix* and *complementary covariance matrix* of a complex-valued random vector $\mathbf{x} \triangleq [x_1, x_2, ..., x_n]^{\mathrm{T}}$:

$$\begin{aligned} \boldsymbol{\mu}_{\mathbf{x}} &= \mathrm{E}[\mathbf{x}] \\ \boldsymbol{\Gamma}_{\mathbf{xx}} &\triangleq \mathrm{E}[\mathbf{x}\mathbf{x}^{\mathrm{H}}] \\ \mathbf{C}_{\mathbf{xx}} &\triangleq \mathrm{E}[\mathbf{x}\mathbf{x}^{\mathrm{T}}]. \end{aligned} \tag{3.38}$$

We then define the augmented vector $\tilde{\mathbf{x}} = [\mathbf{x}^{\mathrm{T}}, \mathbf{x}^{\mathrm{H}}]^{\mathrm{T}}$, whose mean vector and covariance matrix are given as

$$\tilde{\boldsymbol{\mu}}_x \triangleq \mathrm{E}[\tilde{\mathbf{x}}] = \begin{bmatrix} \boldsymbol{\mu}_x \\ \boldsymbol{\mu}_x^* \end{bmatrix}$$

$$\tilde{\boldsymbol{\Gamma}}_{\mathbf{xx}} \triangleq \mathrm{E}[\tilde{\mathbf{x}}\tilde{\mathbf{x}}^{\mathrm{H}}] = \begin{bmatrix} \boldsymbol{\Gamma}_{\mathbf{xx}} & \mathbf{C}_{\mathbf{xx}} \\ \mathbf{C}_{\mathbf{xx}}^* & \boldsymbol{\Gamma}_{\mathbf{xx}}^* \end{bmatrix}$$

These are called the *augmented mean* and *augmented covariance matrix* of $\mathbf{x}$.

The concept of circularity is extended to random vectors as follows. A complex random vector $\mathbf{x}$ is called circular (or strictly circular) if $\mathbf{x}$ and $e^{j\alpha}\mathbf{x}$, for any $\alpha \in [0, 2\pi)$, have the *same probability distribution*. A complex random vector $\mathbf{x}$ is defined *proper* or *second-order circular* if $\mathbf{x}$ and $e^{j\alpha}\mathbf{x}$ have equal second-order moments, or equivalently, if

$$\mathbf{C}_{\mathbf{xx}} = \mathbf{0}. \tag{3.39}$$

The pdf of a general complex Gaussian random vector is given by [152]

$$p(\mathbf{x}) = \frac{1}{\pi^n \det^{1/2} \tilde{\mathbf{\Gamma}}_{\mathbf{xx}}} \exp\left\{-\tfrac{1}{2}(\tilde{\mathbf{x}} - \tilde{\boldsymbol{\mu}}_x)^{\mathrm{H}} \tilde{\mathbf{\Gamma}}_{\mathbf{xx}}^{-1} (\tilde{\mathbf{x}} - \tilde{\boldsymbol{\mu}}_x)\right\}. \tag{3.40}$$

The univariate pdf in (3.36) is a special case of this for $n = 1$. Only when $\mathbf{x}$ is proper does (3.40) take the form

$$p(\mathbf{x}) = \frac{1}{\pi^n \det \mathbf{\Gamma}_{\mathbf{xx}}} \exp\left\{-(\mathbf{x} - \boldsymbol{\mu}_x)^{\mathrm{H}} \mathbf{\Gamma}_{\mathbf{xx}}^{-1} (\mathbf{x} - \boldsymbol{\mu}_x)\right\}, \tag{3.41}$$

which is the familiar formula for the pdf of a complex-circular Gaussian random vector. The circular pdf is completely described by $\boldsymbol{\mu}_x$ and $\mathbf{\Gamma}_{\mathbf{xx}}$, so clearly properness implies circularity also in the multivariate Gaussian case. Again, this is a special characteristic of the family of complex elliptical distributions [96], and cannot be generalized to other distributions.

3.4.3 Random Signals

Properness can be established for random SOS signals as follows [99]. A random SOS signal $x(t) = u(t) + j \cdot v(t)$ is defined *proper* or *second-order circular*, if

$$c_{xx}(\tau) = 0, \forall \tau, \tag{3.42}$$

or equivalently, if

$$C_{xx}(f) = 0, \forall f. \tag{3.43}$$

Properness can also be interpreted as $x(t)$ being *uncorrelated with its own complex-conjugate*, since $c_{xx}(\tau) = E[x(t+\tau)x(t)] = E[x(t+\tau)(x^*(t))^*] = \gamma_{xx^*}(\tau)$.

When viewed in terms of the real and imaginary parts of $x(t)$, we obtain the following equivalent conditions for properness:

$$\gamma_{uu}(\tau) = \gamma_{vv}(\tau) \quad \text{and} \quad \gamma_{uv}(\tau) = -\gamma_{vv}(-\tau), \forall \tau \tag{3.44}$$

or

$$P_{uu}(f) = P_{vv}(f) \quad \text{and} \quad \mathrm{Re}\{P_{uv}(f)\} = 0, \forall f. \tag{3.45}$$

In terms if the real-valued signals $u(t)$ and $v(t)$, properness of $x(t)$ thus means that $u(t)$ and $v(t)$ have equal autocorrelation functions and an odd-symmetric crosscorrelation function. Odd-symmetry implies that $\gamma_{uv}(0) = 0$.

Properness is preserved under linear filtering and modulation, but generally not under widely linear filtering (of which I/Q imbalance is a special case). The sum of two (or more) proper random signals is proper, while the sum of a proper and nonproper signal, or the sum of several nonproper signals, is generally nonproper [120].

Two jointly SOS random signals $x(t) = x_I(t) + jx_Q(t)$ and $y(t) = y_I(t) + jy_Q(t)$ are called *mutually proper* if their complementary cross-correlation function vanishes, i.e.,

$$c_{xy}(t,\tau) = \mathrm{E}[x(t+\tau)y(t)] = 0\,. \tag{3.46}$$

Define the vector-valued random signal $\mathbf{x}(t) \triangleq [x_1(t), x_2(t), ..., x_n(t)]^{\mathrm{T}}$. Its covariance and complementary covariance matrices are given as

$$\boldsymbol{\Gamma}_{\mathbf{xx}}(\tau) \triangleq \mathrm{E}[\mathbf{x}(t+\tau)\mathbf{x}^{\mathrm{H}}(t)]$$

$$\mathbf{C}_{\mathbf{xx}}(\tau) \triangleq \mathrm{E}[\mathbf{x}(t+\tau)\mathbf{x}^{\mathrm{T}}(t)]\,.$$

It is defined proper, if

$$\mathbf{C}_{\mathbf{xx}}(\tau) = \mathbf{0}\,, \tag{3.47}$$

meaning that the elements of **x** be individually proper and mutually proper [P2].

3.4.4 Properness Measures for Random Signals

The typical properness measure for SOS random signals is the CACF, or the normalized CACF $\rho_{xx}(\tau) = c_{xx}(\tau)/\sigma_x^2$. For CS signals, properness is defined by a *vanishing c-CACF*. We argue in the following that in many cases, such as analysis and mitigation of mirror-frequency interference, a useful measure of properness for CS signals is the *time-average CACF*.

Definition 3-1.
A CS random signal $x(t)$ is called *time-average proper*, if its time-average CACF vanishes, i.e.,

$$\overline{c}_{xx}(\tau) = 0, \forall\tau\,, \tag{3.48}$$

or equivalently, if its time-average CPSD equals zero:

$$\overline{C}_{xx}(f) = 0, \forall f\,. \tag{3.49}$$

For SOS/WSS signals properness and time-average properness are clearly identical concepts, but for cyclostationary signals the time-average measure gives a simpler expression, because it is a function of only the delay τ. Using the time-average CACF as a measure of properness allows broadening the class of proper random signals in a useful manner for our purposes, and will also allow for an intuitive spectral interpretation of properness.

Example 3-1.

An example of a signal that is nonproper by the classical definition (3.42), but proper by the time-average properness measure (3.48), is the analytic bandpass signal $y(t) = e^{j2\pi f_0 t}x(t)$ with a SOS *nonproper* complex envelope $x(t)$, i.e., $c_{xx}(\tau) \neq 0$. The nonproperness of $x(t)$ could be for example due to data modulation or modulator I/Q imbalance, or both. The classical properness measure yields $c_{yy}(t,\tau) = \mathrm{E}[y(t)y(t+\tau)] = e^{j2\omega_0 t}e^{j\omega_0\tau}c_{xx}(\tau)$, which is clearly non-zero. It is also periodic in *t*, with period $2\pi / 2\omega_0 = T_0 / 2$. Calculating the time-average CACF of $y(t)$, by averaging $c_{yy}(t,\tau)$ over $[0, T_0/2]$, gives

$$\begin{aligned}\overline{c}_{yy}(\tau) &= \frac{1}{T_0/2}\int_0^{T_0/2} c_{yy}(t,\tau)\mathrm{d}t \\ &= \frac{1}{T_0/2}\int_0^{T_0/2} e^{j(2\omega_0 t+\omega_0\tau)}c_{xx}(\tau)\mathrm{d}t \\ &= \frac{1}{T_0/2}e^{j\omega_0\tau}c_{xx}(\tau)\int_0^{T_0/2} e^{j2\omega_0 t}\mathrm{d}t = 0,\end{aligned} \tag{3.50}$$

thus demonstrating time-average properness. If the complex envelope $x(t)$ is nonproper and *cyclostationary* with period T_1, the integration in the first row of (3.50) is done over the LCM of $T_0/2$ and T_1. Then, a sufficient condition for time-average properness is that $2/T_0 \neq n/T_1$, which is to avoid the situation where the carrier modulation moves some of the spectral "replicas" of $x(t)$ on the stationary manifold. The number of relevant cyclic frequencies is dependent on the pulse shape of the signal (see [120] for more details).

Thus, by using the time-average CACF as the measure of properness, properness can be established not only to analytic SOS signals, but also to analytic CS signals with generally *nonproper* complex envelopes (under the above condition on the cyclic frequencies).

It is clear, however, that the time-average CACF does not utilize all the available second-order information, because the c-CACF may be nonzero also outside $v = n/T = 0$. This extra information could possibly be utilized in analysis and/or practical compensation developments for the impairments considered in this thesis, but this hasn't been explored yet[6]. It should be noted, however, that to be able to use the cyclic statistics efficiently in practice, one must know the period(s). This may be difficult or even impossible in some cases, for example under CFO or sampling clock frequency offset. For the estimation of the stationary components of the cyclic statistics ($n = 0$), the period(s) need not be known exactly, because the integration can always be done with $T \to \infty$. This is a very useful property from practical implementation point of view. Exploiting the cyclic statistics anyway provides an interesting direction for further studies.

[6] An attempt was made in [173] to exploit the cyclic statistics in compensating I/Q imbalance of receivers, and a slight improvement over the technique from [P5] was found, but the Author of this thesis was unable to replicate the results. The method in [173] used a flawed noise model, which may have affected the original results.

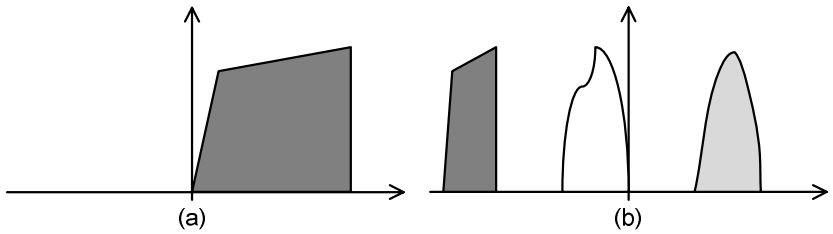

Figure 3-1: *PSD of (a) an analytic signal and (b) a generalized analytic signal.*

3.4.5 Spectral Interpretations of Properness and Nonproperness

It is well known, that an analytic SOS signal is proper [101], or more generally, that a SOS signal whose spectral support is disjoint from the spectral support of its complex conjugate is proper [119], [P2]. The latter type of signal is called generalized analytic [119]. These signal types are illustrated in Figure 3-1.

This is of course not the whole story, because a signal whose spectral support overlaps with the spectral support of its complex conjugate can also be proper. For SOS signals, a more general result states that a signal is proper if and only if $\mathrm{E}[\mathrm{d}\xi(f)\mathrm{d}\xi(-f)] = 0$ [120], where $\mathrm{d}\xi(f)$ are the increments of the spectral process of $x(t)$, related as

$$x(t) = \int_{-\infty}^{\infty} \mathrm{d}\xi(f) e^{j2\pi ft} \,. \tag{3.51}$$

Simple examples of such signals are the complex envelope of a bandpass WSS real-valued signal (e.g., thermal noise), or a QPSK modulated baseband signal [101], [120]. Notice that $\mathrm{E}[\mathrm{d}\xi(f)\mathrm{d}\xi(-f)] = 0$ implies that the signal is *free of mirror-frequency interference*. This result applies also to time-average statistics of CS signals [120]. For CS signals this connection between properness and mirror-frequency interference has not been explicitly stated before, but it follows directly from Result 10.1 in [120]. The interested reader is referred to [120] and the references therein for details.

3.4.6 Most Communications Signals are Proper

Single-Carrier M-PSK and M-QAM

M-PSK (with $M > 2$) and square *M*-QAM alphabets with equally probable symbols are proper. Real-valued modulations such as *M*-PAM and BPSK are nonproper, as are also offset QAM modulations. Linear filtering preserves properness or nonproperness, so the pulse-shaped versions of these data modulation formats remain proper or nonproper.

OFDM and SC-FDMA

An OFDM signal that is composed of proper symbol alphabets, and whose subcarrier symbols are mutually proper, is of course proper. Using the notion of time-average properness, we can also say that an OFDM signal constructed of *improper* alphabets is proper

as long as mirror subcarrier symbols are mutually proper (true if they are independent), and the DC subcarrier is proper (or zero). A SOS SC-FDMA waveform is proper if the individual signals are mutually and individually proper [6]. Through the definition of time-average properness, properness can be established also for SC-FDMA waveforms that are composed of individually and mutually proper CS signals.

General Multi-Carrier Signals

A general multi-carrier signal that is constructed of individually and mutually proper SOS signals is proper [P2]. With the results of this Section, properness can be said to hold for a multi-carrier signal that is made up of individually and mutually proper CS signals.

CDMA

Direct-spread CDMA signals are proper if the symbols are proper, or if the signature sequence is proper in the time-average sense.

3.5 Effects of Physical Non-idealities on Properness

Now, the effects on properness of certain non-idealities related to analog circuit impairments and the radio channel are reviewed. They have been assessed in our works [P2], [P8], [6], [148], as well as the work of others, e.g., [101], [119]. They are an important part of the thesis contribution, and a motivator for the receiver I/Q imbalance compensation studies to be reviewed in Chapter 4.

3.5.1 Power Amplifier Nonlinearity

There are no general results available in the literature on the effects of nonlinearities on properness. However, third order polynomial nonlinearity, which is the dominant nonlinear term created for example by RF power amplifiers, was shown in [P8] to preserve the properness or nonproperness of a signal.

3.5.2 The Radio Channel

The radio channel is modeled as a linear time-variant FIR filter with impulse response $h(t,\lambda_k)$, where λ_k, with $k = 1,2,...,N_\lambda$, denotes the propagation delay of the *k*th distinct multipath component arriving at the receiver. N_λ is finite, and λ_{N_λ} corresponds to the *delay spread* of the channel. The channel output signal is thus

$$r(t) = \sum_{k=1}^{N_\lambda} h(t,\lambda_k) s(t-\lambda_k)\,. \tag{3.52}$$

The CACF of the channel output signal becomes [P2], [P8]

$$\begin{aligned} c_{rr}(\tau) &= \mathrm{E}[\sum_{k=1}^{N_\lambda}\sum_{l=1}^{N_\lambda} h(t,\lambda_k)h(t-\tau,\lambda_l) \\ &\qquad \times s(t-\lambda_k)s(t-\tau-\lambda_l)] \\ &= \sum_{k=1}^{N_\lambda}\sum_{l=1}^{N_\lambda} \mathrm{E}[h(t,\lambda_k)h(t-\tau,\lambda_l)] \\ &\qquad \times c_{ss}(\tau+\lambda_l-\lambda_k) \end{aligned} \quad . \tag{3.53}$$

With independently fading, WSS, and circular taps (e.g., Rayleigh fading), the received signal is made circular by the time-varying channel, regardless of the circularity of $s(t)$ [P2], [P8]. If the channel is deterministic (fixed taps), the properness of $r(t)$ is determined by the properness of $s(t)$.

3.5.3 Additive Noise

The complex envelope of a stationary real-valued bandpass signal is proper [101]. Thus, the additive noise generated in the antenna and RF parts of a radio receiver (usually assumed to be AWGN) is proper. The sum of two proper random signals is proper, while the sum of a nonproper and proper signal is nonproper. Hence, proper additive noise emanating from the RF parts of the receiver does not affect properness or nonproperness of the received signal.

If the mixers or the baseband parts of an I/Q receiver (up to and including the ADCs) contribute significantly to the noise figure (which is an unusual situation), the additive noise can become nonproper due to relative power differences of the I and Q signal path noise processes. However, the LNA is known to be the most important component contributing to the noise figure, and the baseband parts are regarded as having very little effect on it [19], [111]. Thus, while the baseband parts have the potential to generate nonproper noise, we have chosen to ignore it due to its small contribution to the overall noise figure, as is invariably done in the literature.

3.5.4 Carrier Frequency Offset

Properness is preserved under complex mixing [120], and therefore under carrier frequency offset. For a nonproper SOS signal $x(t)$, however, the CACF of the frequency-shifted version $y(t) = e^{j\omega_0 t}x(t)$ is $c_{yy}(t,\tau) = \mathrm{E}[y(t)y(t+\tau)] = e^{j2\omega_0 t}e^{j\omega_0\tau}c_{xx}(\tau)$, which is non-zero. But as was seen in Example 3-1 and (3.50), the time-average CACF of $y(t)$ *vanishes*. Complex mixing thus, while preserving the properness of a proper signal, also *makes a nonproper signal proper*. If we evaluate the c-CACF of $y(t)$ at the first cyclic frequency $n = 1$, or $v = 1/(T_0/2) = 2\omega_0$, we obtain

$$c_{yy}^1(\tau) = e^{j\omega_0\tau}c_{xx}(\tau)\cdot\frac{1}{T_0/2}\int_0^{T_0/2} e^{j2\omega_0 t}e^{-j2\omega_0 t}dt = e^{j\omega_0\tau}c_{xx}(\tau), \tag{3.54}$$

meaning that the frequency offset ω_0 has moved the CACF of $x(t)$ to $n = 1$ and thus *off the stationary manifold*, in effect making the signal (time-average) proper.

The circularizing effect of CFO was established in [P8], however not through the time-average CACF explicitly, but by looking at the expected value of the sample estimate of the CACF in (3.20), assuming that $x(t)$ was SOS. The result in (3.50) and Example 3-1 is more general, since it applies to a CS $x(t)$ also.

3.5.5 Phase Noise

In [P8], it was shown that Wiener phase noise tends to make nonproper signals proper, in the time average sense. On the other hand, using a general PLL-type phase noise model, such an effect is not seen [P8].

3.5.6 Receiver Nonlinearities and DC Offsets

Properness is defined by a vanishing CACF and a zero mean. Thus, a DC level, arising for example from LO signal self mixing, will make a signal nonproper. Static DC offset is easy to estimate and remove from the received signal, and cancellation is usually done already before the AD interface to avoid ADC saturation, usually by high-pass/notch filtering ("AC coupling"). Any residual static DC offset is removed in the digital domain by subtracting the mean of the signal from the signal itself.

Even-order nonlinearities, for example the second-order intermodulation created by signal self-mixing in a DCR ("dynamic DC offset"; see, e.g., [35]), can make a signal nonproper [P8]. The magnitude of the effect depends on the RF-to-LO isolation of the mixers, i.e., how much the RF signal leaking to the LO input of the mixer is attenuated. This was studied in [P8], and the effect on circularity-based I/Q imbalance compensation was shown to be negligible under realistic RF-to-LO isolation values in the order of 35-50 dB, and in the absence of blocker signals.

3.5.7 I/Q Imbalance

The I/Q imbalance phenomenon was introduced in subsection 2.3, and it was shown to effectively be a widely-linear filter. WL filtering is generally known to make a proper signal nonproper [120]. To see this in more detail, first assume that the perfectly balanced signal $z(t)$ is proper with $c_{zz}(\tau) = 0\ \forall\tau$, and denote its ACF by $\gamma_{zz}(\tau)$. Then, after some rather straight-forward manipulations, the second-order statistics of the imbalanced signal $x(t) = g_1(t) \star z(t) + g_2(t) \star z^*(t)$ can be written as

$$\begin{aligned}\gamma_{xx}(\tau) &\triangleq \mathrm{E}[\,x(t+\tau)x^*(t)\,] \\ &= g_1(\tau) \star g_1^*(-\tau) \star \gamma_{zz}(\tau) + g_2(\tau) \star g_2^*(-\tau) \star \gamma_{zz}(-\tau)\end{aligned} \tag{3.55}$$

and

$$\begin{aligned} c_{xx}(\tau) &\triangleq \mathrm{E}[\,x(t+\tau)x(t)\,] \\ &= g_1(\tau) \star g_2(-\tau) \star \gamma_{zz}(\tau) + g_1(-\tau) \star g_2(\tau) \star \gamma_{zz}(-\tau) \end{aligned} \tag{3.56}$$

thus revealing the nonproperness of the imbalanced signal. This same effect is seen with both TX and RX I/Q imbalances, but the forms of the filters $g_1(t)$ and $g_2(t)$ are slightly different (see (2.23) for details).

Now that properness is properly defined, and established for the vast majority of practical communication signals, we proceed to use it in receiver front-end signal processing, as the leading principle in I/Q imbalance compensation. It can also be used for the same purpose in direct-conversion transmitters, as outlined in [P1], and recapped in Chapter 5.

Chapter 4

Digital I/Q Imbalance Compensation in Direct-Conversion Receivers

In this Chapter, the contributions to receiver I/Q imbalance compensation in [P2], [P5]-[P7] are reviewed. These can be divided into techniques considering frequency-independent I/Q imbalances in [P5] and [P7], and methods capable of compensating frequency-selective I/Q mismatches in [P2] and [P6]. In all these studies, the asymmetrical widely-linear compensator structure, introduced in (2.49) and drawn in Figure 4-1, is utilized. The algorithms are based on so-called recircularization of the received, imbalanced signal, i.e., on explicitly forcing the compensator output proper. The methods are all blind, in the sense that they do not need any specific training data for parameter estimation.

4.1 Background and Prior Art

4.1.1 Data-Aided Estimation Techniques

Many of the practical compensation developments in the literature involve training signal based estimation of the imbalance parameters $g_{1,RX}(t)$, $g_{2,RX}(t)$, or of the optimum compensators in (2.47), (2.50), and (2.51) directly. Particular interest has been on OFDM systems under TX and/or RX I/Q imbalance, where estimation is done at the receiver side utilizing system-specific preamble symbols or pilot subcarriers. In such a scenario, the coupled parameters multiplying $Z_{TX}(f)$ and $Z_{TX}^{*}(-f)$ in the link model (2.34) can be identified using, e.g., least-squares type model fitting, minimum mean-square error (MMSE), or maximum likelihood (ML) based estimation. Such work has been reported, e.g., in [7], [81], [114], [122], [132], [137] for estimation of RX I/Q imbalances and the channel, and for example in [134], [78], [82] considering both TX and RX I/Q imbalances along with the channel. Extensions to these approaches, taking into account also CFO, are detailed in [14], [38], [124], [129], [136], [138], [161]. Extensions to spatial multiplexing multi-antenna MIMO-OFDM systems are then considered in [54], [56], [108], [116], [117], [131], [133], [168] with different mixtures of RX and TX I/Q imbalances, CFO, and phase noise, as well as

in [169], [170], [172] considering the space-time coded (STC) multi-antenna OFDM case. More general, modulation-independent, preamble based formulations in *time-domain* have been proposed in [69], [125], [162] for the single-antenna case, and in [55] for a general MIMO case with RX I/Q imbalance.

4.1.2 Blind Statistical Estimation Techniques

An alternative approach to RX I/Q imbalance estimation and compensation is to utilize the *statistical properties* of the used communications waveforms, so that no explicit knowledge of the transmit waveforms is needed. Two different approaches have been established - one based on the statistics of the real-valued I and Q signals and another one based on the statistics of the corresponding complex signals. In general, blind statistical methods are particularly well suited for receiver I/Q imbalance mitigation where, by default, the ideal received waveform $z_{RX}(n)$ is unknown due to channel noise, multipath, and lack of synchronization information, etc. [P2], [P8], [45], [144], [160]. Data-aided estimation may also be feasible, but because RX I/Q imbalance is the last in the chain of analog system impairments, any data-aided estimator basically needs to take into account all the other system impairments. This leads to needlessly complicated estimators for a simple impairment, especially so in multi-user scenarios. A further advantage of using blind methods for RX I/Q imbalance compensation is that all subsequent signal processing blocks, such as carrier frequency offset (CFO) compensation and channel estimation and equalization, remain unchanged compared to a system without I/Q imbalance.

The techniques utilizing real-valued I/Q signal models and the corresponding I/Q signal statistics build on the fact that I/Q imbalances create correlation (or statistical dependence more generally) between the observed I and Q signals. Second-order statistics based techniques to remove this correlation are proposed, e.g., in [50], [146], shown to be robust also against for example CFO. Higher-order statistical techniques, based on blind signal separation (BSS) of the I and Q signals, are in turn proposed in [147], also taking into account CFO and channel equalization.

Using complex-valued signals, various statistical techniques have been proposed for both low-IF and direct-conversion type radio architectures. In the low-IF case, one well-established approach is to downconvert the signals from both positive and negative IF's to baseband in the receiver digital front-end. Using these IF observations, either adaptive interference cancellation (AIC) or BSS based signal estimation techniques have been proposed, e.g., in [58], [144], [142], [143], [164] for both frequency-independent and frequency-dependent imbalance scenarios. Alternative moment estimation based approaches are described for the low-IF case in [45] and [157], in the OFDM direct-conversion receiver context in [61], and for a general I/Q receiver in [46][7]. In [103] and [148], BSS type adaptive techniques, based on

[7] The algorithm in [46] is identical to the one proposed in [P5].

decorrelating the received signal with its complex conjugate, are proposed for a general I/Q receiver. The algorithm in [103] utilizes the properness feature implicitly, and is also capable of compensating frequency-selective I/Q imbalances, whereas [148] is the first work in the literature that utilizes properness explicitly, although in a frequency-independent imbalance setting. The work in [148] was the initial inspiration for the work that culminated in the publications [P2], [P5], [P6], [P7], and [P8].

The contributions in [P2], [P5], [P6], [P7], and [P8] also utilize the statistical properties of complex-valued signals, but they differ from most of the above mentioned techniques in the sense that they are applicable with any modulation format and in any I/Q receiver setting, whether a single-user direct-conversion or low-IF receiver, or a multi-channel/multi-user direct-conversion receiver. From the state-of-the art literature, only [46], [50], [103], [146], [147], [148] consider this general I/Q receiver setting, with all except [103] focusing on the frequency-independent I/Q imbalance case.

4.2 Blind Circularity-Based Algorithms

The recircularization algorithms are based on the observations, that the received signal without RX I/Q imbalance is proper (as argued in Subsection 3.4.6 and Section 3.5 based on [P8], [P2]), while I/Q imbalance makes it nonproper (as shown in (3.56)). A natural strategy for I/Q imbalance compensation is then to make the received signal proper again. If the premise of an originally proper signal holds, this will implicitly remove the mirror-frequency interference [P2]. In light of subsection 3.4.5, stating that a signal is proper if and only if it is free of mirror-frequency interference, this is an obvious result.

The compensator structure that was used in [P2], [P5], [P6], [P7], and [P8] is the *asymmetric widely-linear filter*, shown in Figure 4-1. This structure has a single FIR filter (of length N_W) in the conjugate signal branch, denoted here by $\mathbf{w}_{RX} \triangleq [w_{RX,1}, w_{RX,2}, ..., w_{RX,N_W}]^{\mathrm{T}}$. The compensator output signal is $y(n) = x_{RX}(n) + \mathbf{w}_{RX}^T \mathbf{x}_{RX}^*(n)$, where $x_{RX}(n)$ denotes the input signal, and $\mathbf{x}_{RX}^*(n) = [x_{RX}(n)\ x_{RX}(n-1) \cdots x_{RX}(n-N_W+1)]^T$. The objective of the algorithms is to make the output signal proper for the span of the filter, i.e., to have

$$E[\mathbf{y}(n)y(n)] = \mathbf{0}\,, \tag{4.1}$$

where $\mathbf{y}(n) = [y(n)\ y(n-1) \cdots y(n-N_W+1)]^T$ and $\mathbf{0}$ is a vector of all zeros. In [P2], it was shown that there are two solutions to (4.1); the one in (2.51) which suppresses the conjugate signal term, and the mirror solution $W_{RX}^m(f) = 1/W_{RX}^{id*}(f)$, which mitigates the desired non-conjugate signal. Convergence to the mirror solution can be avoided by design in

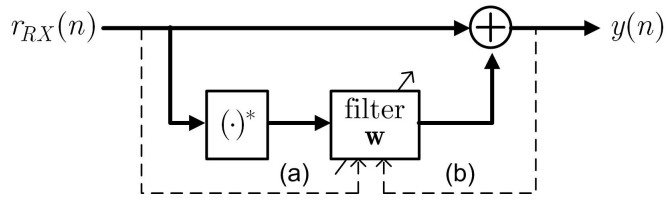

Figure 4-1. Asymmetric widely-linear I/Q imbalance compensator structure in (a) block processing and (b) iterative modes of operation.

the block processing algorithm, and by proper initialization in the iterative algorithm, as described in [P2].

4.2.1 Frequency-selective estimators

The algorithms proposed in [P2], [P6] are now shortly reviewed, and the reader is referred to the original articles for full details. The technique in [P2] is based on estimating the ACF and CACF of the received waveform $x_{RX}(n)$ explicitly using sample estimates, and then solving for the compensator filter using these statistics only. First, expand (4.1) and write it as a function of the input signal statistics, as [P2]

$$\mathbf{c}_{RX} + \mathbf{\Gamma}_{RX}\mathbf{w}_{RX} + \bar{\mathbf{\Gamma}}_{RX}\mathbf{w}_{RX} + \mathbf{W}\mathbf{C}^*_{RX}\mathbf{w}_{RX} = \mathbf{0}\,, \tag{4.2}$$

where the matrices $\mathbf{\Gamma}_{RX}$ and $\bar{\mathbf{\Gamma}}_{RX}$ are constructed from the ACF of $x_{RX}(n)$, i.e., $\gamma_{RX}(l) = \mathrm{E}[x^*_{RX}(n)x_{RX}(n+l)]$, while the entries of $\mathbf{C}^*_{RX}$ and $\mathbf{c}_{RX}$ are from the CACF of $x_{RX}(n)$, defined as $c_{RX}(l) = \mathrm{E}[x_{RX}(n)x_{RX}(n+l)]$. For the exact definitions of these matrices and vectors, the interested reader is referred to [P2]. Noting that the last term on the LHS of (4.2) is vanishingly small compared to the other terms (see also [P2], [8]), we can ignore it and obtain a *closed-form approximate solution* for the compensator filter as [P2]

$$\mathbf{w}_{RX} = -(\mathbf{\Gamma}_{RX} + \bar{\mathbf{\Gamma}}_{RX})^{-1}\mathbf{c}_{RX}\,. \tag{4.3}$$

Given $\gamma_{RX}(l)$ and $c_{RX}(l)$, this approximate solution is very close to the optimum solution in (2.51), and in the single-tap (memoryless) compensator case has been shown to triple the dB-value of the front-end IRR [P5]. The approximate solution can be further refined with a simple iteration if needed, as described in [P2]. One option for estimating $\gamma_{RX}(l)$ and $c_{RX}(l)$ is through the natural sample estimates, given as

$$\hat{\gamma}_{RX}(l) = \frac{1}{N}\sum_{n=0}^{N-1} x^*_{RX}(n)x_{RX}(n+l) \tag{4.4}$$

$$\hat{c}_{RX}(l) = \frac{1}{N}\sum_{n=0}^{N-1} x_{RX}(n)x_{RX}(n+l) \tag{4.5}$$

where N denotes the estimator block size. The finite accuracy of the sample statistics will affect the achievable performance to some extent, depending essentially on the block-size.

An iterative algorithm for nulling (4.1) was proposed in [P6]. The algorithm is iterated for $n = 0,1,2,...$ as

$$\begin{aligned} y(n) &= x_{RX}(n) + \mathbf{w}_{RX,n}^{\mathrm{T}}\mathbf{x}_{RX}^{*}(n) \\ \mathbf{w}_{RX,n+1} &= \mathbf{w}_{RX,n} - \lambda\mathbf{y}(n)y(n) \end{aligned} \tag{4.6}$$

where λ denotes the adaptation step-size. The only stability point of this algorithm is the point where $E[\mathbf{y}(n)y(n)] = \mathbf{0}$, i.e., when the compensator output signal is *proper*. By initializing the filter as $\mathbf{w}_0 = \mathbf{0}$ practically guarantees that the iteration converges towards the optimum solution given in (2.51) instead of the mirror solution [P2], [P6]. To give some further formal justification to the algorithm, it can be viewed as a "stochastic" Newton zero search in the function $\mathbf{f}(\mathbf{w}) = \mathrm{E}[\mathbf{y}(n)y(n)]$. The exact convergence speed and the obtained steady-state estimation performance depend on the applied step-size value as well as the actual PSD of the processed signal [P2], [P6].

A modification to the basic iterative solution was introduced in [P2] in order to reduce the residual steady-state variance of the filter coefficients. It involves simple low-pass filtering of the coefficients with a first-order recursion, as

$$\begin{aligned} \mathbf{w}_{n+1} &= \mathbf{w}_n - \lambda\mathbf{y}(n)y(n) \\ \tilde{\mathbf{w}}_{n+1} &= \alpha\tilde{\mathbf{w}}_n + (1-\alpha)\mathbf{w}_{n+1} \end{aligned} \tag{4.7}$$

where $\alpha \in [0,1)$ is the smoothing parameter. The smoothing parameter adjusts the memory of the algorithm, which is approximately given by $1/(1-\alpha)$. This means that the convergence of (4.7) is delayed by $1/(1-\alpha)$ with respect to the basic iterative solution in (4.6), even though their rates of convergence are otherwise the same.

4.2.2 Frequency-independent compensators

Frequency-independent or memoryless compensators can be obtained as special cases of the previous multi-tap solutions. However, for the single-tap version of the block estimator in (2.51), an *exact closed-form solution* can be obtained, as [P5]

$$w = -\frac{c_{r_{RX}}}{\gamma_{r_{RX}} + \sqrt{\gamma_{r_{RX}}^2 - \left|c_{r_{RX}}\right|^2}}, \tag{4.8}$$

where $\gamma_{RX} \triangleq \gamma_{RX}(0)$ and $c_{RX} \triangleq c_{RX}(0)$. An approximation to the above, which avoids the square root operation, can be obtained by ignoring $|c_{RX}|^2$ in the denominator [P5], leading to

$$w = -\frac{c_{r_{RX}}}{2\gamma_{r_{RX}}}. \tag{4.9}$$

This solution is the single-tap version of (4.3), and was shown in [P5] to give a maximum 3-fold increase (in dBs) to the front-end IRR, as mentioned already earlier.

The single-tap version of the adaptive compensator (4.6) assumes a particularly simple form:

$$\begin{aligned} y(n) &= r_{RX}(n) + w_n r_{RX}^*(n) \\ w_{n+1} &= w_n - \lambda y^2(n) \end{aligned} \tag{4.10}$$

In [P7] an alternative formulation for output circularization was given, based on gradient descent minimization of the cost function

$$J(w) = \left| E[y^2(n)] \right|^2 = \left| E[(x_{RX}(n) + w x_{RX}^*(n))^2] \right|^2. \tag{4.11}$$

The solution proposed in [P7] is

$$\begin{aligned} \hat{\gamma}_{RX,n} &= \alpha \hat{\gamma}_{RX,n-1} + (1-\alpha)|r_{RX}(n)|^2 \\ \hat{c}_{RX,n} &= \alpha \hat{c}_{RX,n-1} + (1-\alpha) r_{RX}^2(n) \\ \hat{\nabla}_w J_n(w) &= 4 w_n \hat{\gamma}_{RX,n}^2 + 2 w_n^* \hat{c}_{RX,n}^2 + 2 \hat{\gamma}_{RX,n} \hat{c}_{RX,n} \\ w_{n+1} &= w_n - \mu \hat{\nabla}_w J_n(w) \end{aligned} \tag{4.12}$$

where $n = 0,1,2,...$ is the iteration index, the first two rows are recursive estimates of the statistics γ_{RX} and c_{RX}, $\alpha \in [0,1)$ is the recursion coefficient, and $\hat{\nabla}_w J_n(w)$ is the estimate of the gradient of (4.11). This algorithm was shown in [P7] to converge faster than the basic iterative algorithm in (4.10) and the IF decorrelation method from [58], or from another viewpoint, to give a lower steady-state variance when convergence speeds are equal.

4.3 Simulation and Measurement Examples

Now, simulation and RF laboratory measurement examples are given for the blind circularity-based algorithms presented above. Most of these results are reproduced from [P2], [P5]-[P8].

4.3.1 Simulation example 1 – IRR in a 2-carrier low-IF receiver

The first simulation scenario assumed here is a 2-carrier low-IF receiver operating at 2 GHz RF range. Both carriers have 16-QAM data modulation, ordinary raised-cosine pulse-shaping, and 25% roll-off. A symbol rate of 3.84 MHz complying with the 3GPP specifications is assumed, yielding individual waveform bandwidths of about 5 MHz. In the receiver analog front-end, the two incoming carriers are I/Q downconverted symmetrically around DC, being then located at ±3 MHz IF's, and sampled at a sampling rate of 15.36 MHz (4 times oversampling). The simulation model contains also independently fading multipath channels for the two carrier signals, with their power delay profiles following the Extended Vehicular A model described in [128]. A mobility of 120 km/h is assumed as a challenging

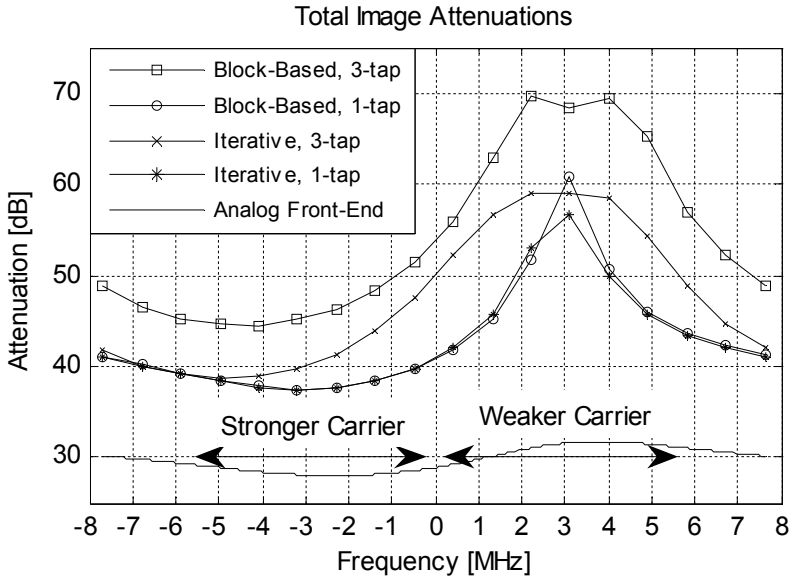

Figure 4-2. Compensated IRRs for the circularity-based iterative and block algorithms, with 1-tap and 3-tap compensation filters, in a two-carrier low-IF receiver. Both signals are 16-QAM, and they have an RF power difference of 30 dB. Extended Vehicular A (120 km/h) channel and received SNR = 10 dB. Frequency-dependent analog front-end I/Q imbalances, resulting in IRR varying between 27-33dB.

example case. The channel model also includes additive white Gaussian noise (AWGN), with the weaker carrier having an effective in-band signal-to-noise ratio (SNR) of 10 dB. The receiver analog front-end model has frequency-dependent I/Q imbalances, with the resulting IRR varying smoothly between 27…33 dB. For comparison purposes, both 1-tap and 3-tap versions of the algorithms are implemented.

Figure 4-2. shows the obtained image attenuation curves of the iterative compensator in (4.6) and the block-compensator in (4.3), plotted as a function of frequency, and assuming 30 dB RF power difference between the two carriers. Also shown is the corresponding IRR curve of the analog front-end alone. The shown IRR curves represent an average value obtained in 100 independent simulation runs (ensemble averaging). All algorithms utilize 50,000 samples for estimation, and the step-sizes of the iterative algorithms are chosen such that the coefficients have converged in this time. The first important observation is that the obtained image attenuation is clearly better with 3-tap compensators, compared to the 1-tap algorithms. This is indeed due to the frequency-selective nature of the imbalances, which the 1-tap compensators do not account for. A very desirable feature of the compensators is that they are tuning most of the attenuation to those frequencies which experience the *most* mirror-frequency interference, which in this case is the band of the weaker carrier. Another key observation is that while both the iterative and block approaches are providing very high IRR at the weaker carrier band, the performance of the block algorithm is still considerably better. Thus in this sense, the block algorithm is using the available data more efficiently. Even though this is somewhat dependent on the step-size of the adaptive algorithm, these kinds of

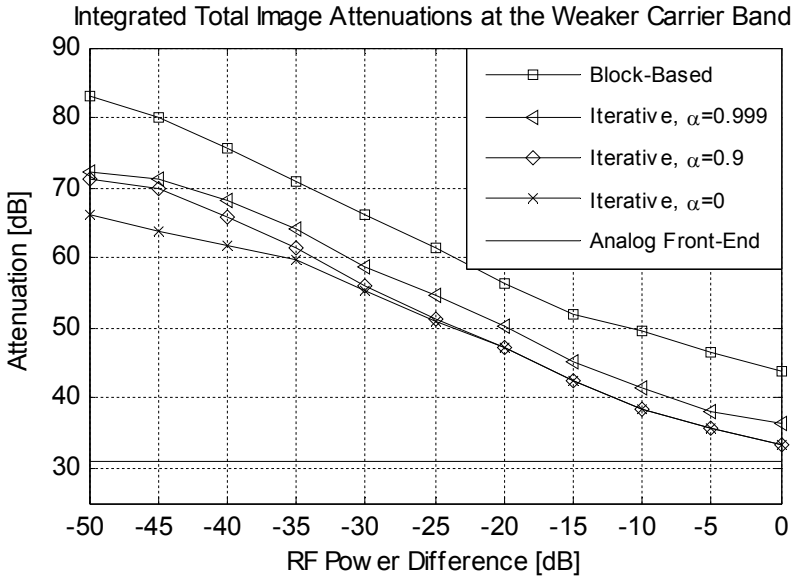

Figure 4-3. Integrated total in-band image attenuations at the weaker carrier band as a function of received RF power difference between two carriers with 16-QAM data modulation, Extended Vehicular A (120 km/h) channel model and received SNR = 10 dB. The iterative and block-processing based methods (3-tap compensators) are simulated with α denoting the coefficient smoothing parameter in the iterative solutions. Frequency-dependent analog front-end I/Q imbalances, resulting in 31 dB integrated image attenuation at the weaker carrier band.

conclusions are typical in the estimation literature, when the parameters (here imbalances) are *not* changing in time.

Next, we simulate the 3-tap iterative and block-based algorithms, and vary the RF power difference of the two carriers between 0 dB and 50 dB. Coefficient smoothing for the iterative algorithm is also included to illustrate its effects. Otherwise, the simulation scenario is identical to the previous one. Again, all the step-sizes of the adaptive algorithms are selected such that similar convergence properties are obtained, and the overall number of received samples used for the adaptation and/or estimation is 50,000. The obtained results in terms of the *total integrated IRR* within the weaker carrier band are shown in Figure 4-3. The most important observation is that the overall IRR is increasing with increasing power difference between the signals. Thus essentially, the algorithms are able to keep a relatively *constant signal-to-interference ratio* (SIR) at the compensator output. Again, the block algorithm gives a consistently higher level of performance compared to the iterative algorithm. The effect of coefficient smoothing is also clearly observed in Figure 4-3. With $\alpha = 0.999$, the integrated IRR is improved by 3-5 dB's compared to $\alpha = 0$ (the basic iterative algorithm), depending on the RF power difference.

4.3.2 Simulation example 2 – IRR in 3GPP LTE uplink with several RF impairments

Now, from [P8], the circularity-based RX I/Q imbalance mitigation algorithms in (4.3) and (4.6) are tested under other impairments, namely TX I/Q imbalance, time-varying channel, CFO, and DC offsets, to verify the analysis made in [P8]. We consider the 3GPP Long-Term

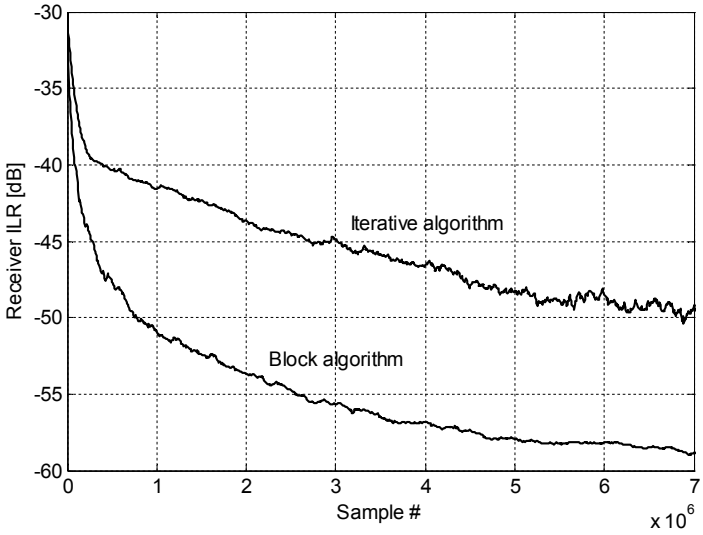

Figure 4-4. Receiver image leakage ratio vs. sample index in 3GPP LTE basestation receiver. Shown are the ILRs for the block algorithm in (4.3) and the iterative algorithm in (4.6) with step-size $3 \cdot 10^{-6} / \sigma_{RX}^2$, *where* $\sigma_{RX}^2 = \mathrm{E}[|x_{RX}(n)|^2]$.

Evolution (LTE) uplink, which employs single-carrier frequency-division multiple access (SC-FDMA) [1], as a practical example case. We assume the 10 MHz mode, which has 1024 total subcarriers, out of which a maximum of 600 are used for transmission. The number of users varies from subframe (1 ms) to subframe, with user bandwidths, subcarrier allocations, CFOs, TX I/Q imbalances, and channel impulse responses drawn randomly for each user in each subframe. Spectral occupancy is 75 % on average. CFO range is +/- 0.15 ppm, which for 2 GHz carrier frequency corresponds to +/- 300 Hz. TX IRRs vary between 26…∞ dB, with an average of about 33 dB. The channels are assumed block-fading, and they follow the Extended Vehicular A power delay profile from [128]. RF-to-LO isolation is 45 dB, LO-to-RF isolation is 47 dB, and average in-band SNR equals 15 dB. RX I/Q imbalance is frequency-selective, and varying between 27-34 dB within the signal band. RX imbalance compensator filter has 3 taps.

Figure 4-4. shows the ILRs[8] of the 3-tap block and iterative algorithms from (4.3) and (4.6) as a function of sample index, ensemble averaged over 100 independent realizations. The algorithms are clearly able to compensate for the majority of the RX imbalance, in spite of the other impairments. The block-based algorithm is using the available data more efficiently, giving 55-60 dB IRR, with a continuing downward trend as N grows. For the iterative algorithm, to obtain smaller steady-state variance (and hence smaller ILR), the step-size should be made smaller.

It is also worth noting that the 3GPP LTE uplink is, from the viewpoint of the properness of the received signal, perhaps one of the most challenging scenarios. This is because the mobile transmitters will invariably transmit nonproper waveforms due to TX I/Q imbalance,

[8] Image leakage ratio was used as a figure of merit in [P8] due to presentational clarity.

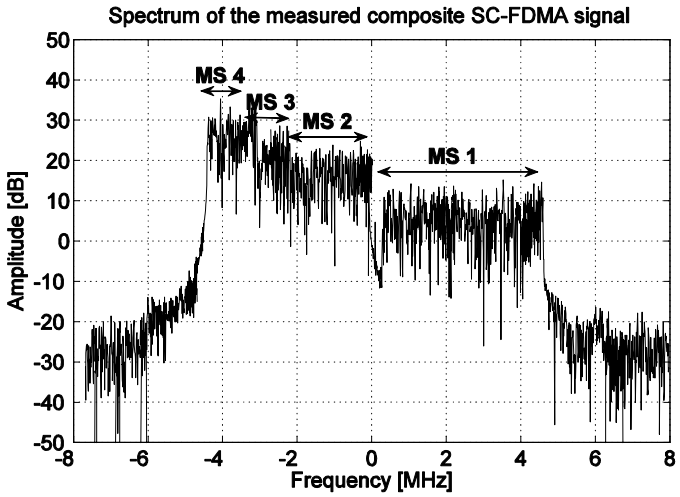

Figure 4-5. Example measured spectrum with 3G-LTE SC-FDMA waveforms after analog front-end I/Q downconversion and filtering. 10 MHz overall spectrum deployment. The individual mobile station (MS) bands are also shown in the figure. The relative spectral density levels are {0, 10, 15, 20} dB, for MS1-4, respectively.

while their CFO's will be tightly synchronized to the basestation LO (specified mobile LO uncertainty is ±0.1 ppm, corresponding to ±200 Hz at 2 GHz LO frequency), thus providing a very slow circularizing effect. On the other hand, the channels are time varying, making the received signal circular under the assumption of circular, independently fading taps. Altogether, even though properness is established for the received signal, a somewhat slower convergence rate is seen in this case, compared to a system without TX I/Q imbalances. The DC offsets can also in principle affect the obtainable ILR slightly, even though their effect was shown in [P8] to be small with practical RF-to-LO isolation values. In summary, this experiment largely verifies the analysis made in Section 3.5 and [P8], and builds confidence on the practical feasibility of the circularity-based algorithms in challenging scenarios such as the LTE uplink.

4.3.3 Measurement example

A RF measurement example from [P2] is given, to illustrate the effectiveness of the techniques in a real I/Q demodulator chip. These 600 subcarriers are allocated to four different mobile stations (MS) as {300, 150, 75, 75}, yielding mobile bandwidths around {4.5, 2.25, 1.125, 1.125} MHz, for the MS1-MS4, respectively. At the receiver input, the relative spectral density levels of the four signals are {0, 10, 15, 20} dB, respectively, representing a challenging yet practical example case of overall RF dynamics in the order of 20 dB. The measured spectrum is shown in Figure 4-5..

In this case, the most wideband mobile (MS1) is interfered by the other three mobiles at its mirror-frequency band, and vice versa. In the following, we detect only this most wideband mobile signal since it is the weakest one and thus most sensitive to mirror-frequency interference.

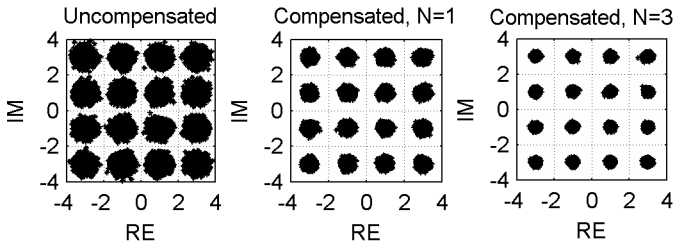

Figure 4-6. Example demodulated symbol rate 16-QAM constellations for mobile station 1 without and with compensation (with the block-algorithm). The measurement system circuit noise is roughly 30dB below the target signal level.

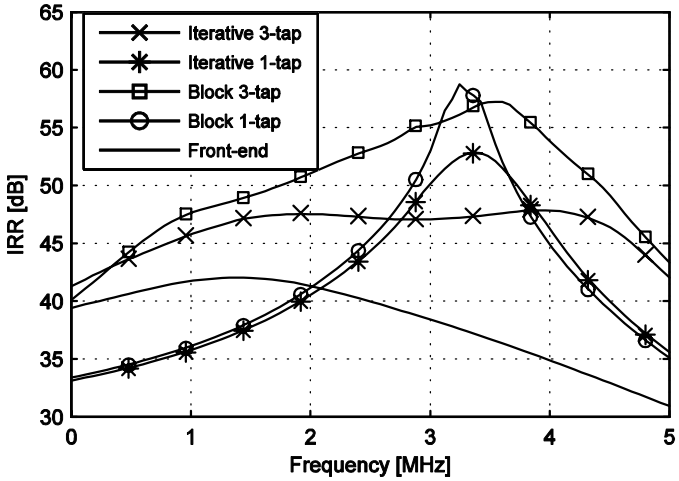

Figure 4-7. Obtained IRR's with measured 3G-LTE SC-FDMA signals at the wideband mobile (MS1) band.

An example of demodulated symbol rate constellations, with 16-QAM data modulation at the active subcarriers, is shown in Figure 4-6, without and with compensation. Here, 1-tap and 3-tap versions of the block-compensator are used as an example. Clearly, there is considerable amount of mirror-frequency interference in the constellation without compensation, while the remaining dispersion in the compensated constellations is mainly due to residual synchronization errors, inevitable circuit and measurement noise, and possible residual ISI due to the on-chip analog baseband filters. Based on the measured spectrum in Figure 4-5., the circuit and measurement noise floor is approximately 30 dB below the wideband mobile (MS1) signal level.

Following the front-end imbalance parameter estimation approach in [P2], Figure 4-7. shows the calculated uncompensated and compensated IRR values in the band of the weakest mobile (MS1) in the previous measured SC-FDMA example case. The compensated IRR is ensemble averaged over 20 independent measurements. For the block algorithm, the compensator coefficients are estimated from a block of 50000 samples, while for the iterative algorithm, a suitable step-size is selected such that the algorithm reaches steady-state after about 40-50000 iterations. The 3-tap compensators give more consistent performance over the interesting band, while the 1-tap compensators tune most of their attenuation to approximately

the center of the band with the strong interference (as discussed earlier). The block-solutions are again seen to outperform the corresponding iterative solutions. Within the wideband mobile band, the 3-tap block algorithm gives 2…20 dB increase in the IRR.

4.4 Practical Aspects and Conclusions

The properness-based algorithms provide a practical and effective "plug-and-play" solution to the problem of I/Q imbalance in all receivers utilizing direct I/Q downconversion. They are robust in the face of multipath, additive noise, CFO, phase noise, PA nonlinearity, and practical levels of DC offsets [P2], [P8]. Furthermore, under time-varying channel or CFO, both of which are invariably present in most practical situations, the proposed techniques can also tolerate nonproper transmitted waveforms, arising from either nonproper data modulations or TX I/Q imbalances, as shown analytically in Section 3.5 and [P8], and experimentally above.

The proposed techniques are particularly attractive in cases where several signals are received simultaneously, such as in FDMA systems, or in multi-standard software defined radios, where the variety of received waveforms is large and may evolve over time. In an FDMA receiver (such as in LTE uplink), any data-aided estimator would become unnecessarily complex, having to take into account the channel responses, CFOs, and pilot data of *all* the individual users. In SDRs, on the other hand, a data-aided I/Q imbalance estimator would have to be tailored for each waveform independently, leading to unnecessary complexity. Due to the very slow time variations of the I/Q imbalances, the slower convergence rates of the proposed blind algorithms are not a concern. Altogether, the above considerations make the proposed algorithms of significant practical interest.

Chapter 5

Digital Calibration Techniques for Direct-Conversion Transmitters

This Chapter reviews the contributions to digital calibration of direct-conversion transmitters in [P1], [P3], and [P4]. In [P1], solutions for estimating and compensating frequency-dependent TX I/Q imbalances are proposed, while [P3] and [P4] present techniques for the joint estimation and compensation of frequency-dependent PA nonlinearity and I/Q imbalance, as well as LO leakage. The compensation processing, herein referred to as *predistortion*, takes place at digital baseband, in the digital front-end of the transmitter. The predistorters are linear with respect to their parameters, therefore facilitating efficient estimation through linear least squares (LS) techniques. It is further assumed, that a feedback loop is available inside the transmitter for the purpose of extracting the complex envelope of the PA or the I/Q modulator output signal, which is needed in estimating the predistorter parameters. Due to the adaptive nature, the term adaptive digital predistortion is often used to describe such processing. During the estimation stage, no specially designed training data or specific modulation format is required, but the estimators can basically utilize the regular transmitted data for training, promoting flexible and standard-independent operation.

5.1 Background and Prior Art

Related work in the literature focusing on digital transmitter I/Q calibration is now briefly reviewed. The works in [21], [32], [57], [86], and [167] address the I/Q calibration task in an ordinary single-channel DCT, while a low-IF type single-channel DCT is assumed in [159]. The basic assumption in all the previous studies is that I/Q imbalance is frequency-independent within the signal band. The studies in [30], [70], [140], in turn, are more general in the sense that frequency-dependent I/Q imbalance is assumed. A multi-channel signal structure is explicitly assumed in [70], and the compensator is operating in a pair-wise manner for each symmetric mirror-channel pair. However, within any individual channel, the I/Q imbalance is assumed constant. Moreover, the mirror signal band is assumed vacant during

the calibration, meaning that a specific training period is needed. In [140], the modulator imbalances are not considered, but the treatment is limited to the mismatches between the analog reconstruction filters. Thus, the feedback signal is measured from the *input* of the modulator. The approach in [31] is based on inverse modeling of the imbalance filters with real-valued signals, utilizing linear least squares parameter estimation. This work, along with [P1], represent the state-of-the-art in TX I/Q imbalance mitigation, because these techniques are the only techniques in the literature that can handle frequency-selective imbalances, require no special training data or period, and are applicable in any direct I/Q upconversion based TX, independent of modulation format.

Regarding studies related to the scope of [P3] and [P4], the magnitude of research that has been done on PA digital predistortion during the past 20 years is too big to be summarized here. The reader is referred to [44], [59], [98], [121] for reviews and references on PA predistortion and behavioral modeling, which are intimately linked. Instead, we focus on the studies that consider the digital predistortion of both PA nonlinearity and I/Q modulator impairments.

In Section 2.5, it was shown that the I/Q modulator impairments (I/Q imbalance and LO leakage) are interacting with the PA nonlinearity. Despite the parameters of PA and I/Q modulator impairments being nonlinearly coupled, it is possible to estimate these impairments (or the corresponding predistorters) individually with the help of extra RF hardware. This is an underlying assumption in [P1], as well as in [31], which assume that a second coupler is implemented (at the IQM output), along with an RF switch to choose between the couplers at the IQM output and the PA output (see Figure 5-1). In [23] and [33] a second, envelope detector based, feedback loop is needed for the purpose of IQM impairment estimation. Purely algorithmic methods for decoupling the PA and IQM predistorter estimates using a single observation of the PA output only do not exist at the moment, at least to the best of the author's knowledge.

Joint predistorters, needing no extra RF hardware for their training, were developed in [53] and [72]. However, these techniques only considered frequency-independent (memoryless) impairments, limiting their applicability in modern broadband systems. The purpose of [P3] and [P4] is to introduce a practical and effective joint PA and IQM predistorter structure for *frequency-dependent* impairments, as well as to propose procedures for its training.

5.2 Transmitter Front-End With Feedback Receiver and Adaptive Digital Predistortion

The general I/Q transmitter structure assumed in the studies [P1], [P3] and [P4], including the internal feedback loop and the adaptive digital predistorter (in serial configuration), is shown in Figure 5-1. The feedback loop involves downconversion to a low IF by a single mixer

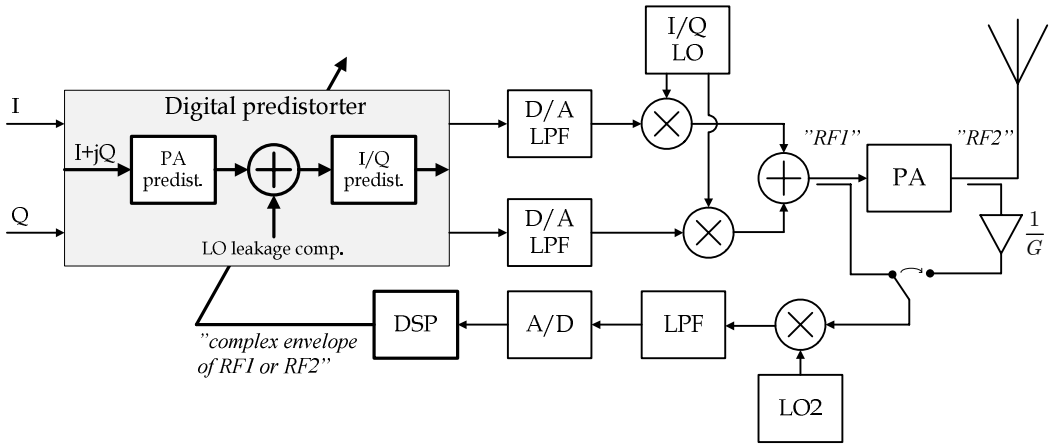

Figure 5-1: General transmitter structure based on direct I/Q upconversion, including the feedback loop and principle digital predistorter in serial configuration.

(complex mixing is not required because the mirror band is empty), lowpass filtering, A/D conversion, followed by downconversion to baseband and lowpass filtering in the digital domain. A similar feedback structure was also used in [31] and [159]. Compared to using I/Q demodulation in the feedback loop, the single-mixer low-IF structure avoids any demodulator I/Q imbalances or DC offsets from corrupting the signal, while also halving the component count. Thus, a high precision observation of the PA or IQM output signal can be obtained, which is crucial for accurate estimation of the predistorter parameters. The price paid for using the low-IF structure is the doubling of the sampling rate for the sole ADC. In half duplexing systems, it may be possible to utilize the receiver part of the transceiver as the feedback receiver, while in full duplexing systems the feedback loop receiver needs to be separately built.

The serial predistorter structure seen in Figure 5-1 is the conventional structure, assumed in principle in [P1]. It compensates for the impairments in the reversed order of appearance, and is a conceptually feasible structure. However, compared to a transmitter housing only pure adaptive PA predistortion, a second coupler and an RF switch are needed to guarantee the identifiability of the constituent predistorters. This raises material and design costs, as well as requires extra space. This observation was the initial motivation for the joint predistortion studies [P3] and [P4], which introduced a *parallel* predistortion structure, which is *guaranteed to be identifiable* using only a single observation of the PA output signal (switch always in position "*RF2*").

5.3 Digital Transmitter I/Q Imbalance Calibration

The contributions related to digital calibration of TX I/Q imbalance from [P1] are reviewed. The techniques utilize the WL compensation structure given in (2.48) and shown in Figure 2-10. In [P1], two alternative principles for predistorter parameter estimation are proposed, utilizing the internal feedback signal introduced above. The first estimation approach stems

from the second-order statistics of complex communication signals, while the second technique is based on widely-linear least-squares (WL-LS) model fitting.

The baseband feedback signal, after A/D conversion, translation to baseband, and lowpass filtering is given as

$$\begin{aligned} y_{fb}(n) &= G_{fb}e^{j\theta_{fb}}h_{fb}(n) \star z_{TX}(n - \tau_{fb}/T_s) \\ &= G_{fb}e^{j\theta_{fb}}h_{fb}(n) \star [g_{1,TX}(n) \star z(n - \tau_{fb}/T_s) + g_{2,TX}(n) \star z^*(n - \tau_{fb}/T_s)] \\ &= \tilde{g}_{1,TX}(n) \star z(n - \tau_{fb}/T_s) + \tilde{g}_{2,TX}(n) \star z^*(n - \tau_{fb}/T_s) \end{aligned} \quad (5.1)$$

where G_{fb}, θ_{fb}, $h_{fb}(n)$ and τ_{fb} denote the gain, phase, impulse response and delay of the feedback path, respectively, relative to the actual complex envelope of the I/Q modulator output signal $z_{TX}(n)$ [P1], [8], and T_s is the sample interval. In (5.1), $\tilde{g}_{1,TX}(n) = G_{fb}e^{j\theta_{fb}}h_{fb}(n) \star g_{1,TX}(n)$ and $\tilde{g}_{2,TX}(n) = G_{fb}e^{j\theta_{fb}}h_{fb}(t) \star g_{2,TX}(n)$ denote the *observable imbalance filters* which contain also the feedback loop response.

The techniques in [P1] aim to estimate the observable imbalance filters, and then calculate the compensator filter $w_{TX}(n)$ through solving the relation $\tilde{g}_{2,TX}(n) + \tilde{g}_{1,TX}(n) \star w_{TX}(n) = 0 \ \forall n$, which is the necessary condition for mitigating the conjugate signal term [P1]. Doing this, the effects of the feedback loop gain, phase and impulse response are in fact seen to *cancel out*, assuming that the time support of the model filters $\tilde{g}_{1,TX}(n)$ and $\tilde{g}_{2,TX}(n)$ is equal to (or greater than) the time support of the true system $h_{fb}(n) \star g_{1,TX}(n)$ [P1], [93]. Notice that the possible feedback delay τ_{fb} can also be merged into the formal feedback loop filter $h_{fb}(t)$, because delay corresponds to an LTI filter. Thus overall, by having sufficiently long model filters in the estimation, the techniques presented in [P1] can tolerate any residual delay error[9]. This issue was discussed and verified with simulations in [93].

5.3.1 Second-Order Statistics –Based Estimation

Now, as described in [P1], the ordinary and complementary cross-correlations between the feedback signal $y_{fb}(n)$ and the ideal transmit data $z(n)$ can be used directly for identifying the observable imbalance filters $\tilde{g}_{1,TX}(n)$ and $\tilde{g}_{2,TX}(n)$. Assuming that the feedback signal $y_{fb}(n)$ and the original transmit data signal $z(n)$ are time-aligned, these cross-correlations can be expressed with vector-matrix algebra as

$$\begin{aligned} \boldsymbol{\gamma}_{zy} &\triangleq \mathrm{E}[\mathbf{z}^*(n)y_{fb}(n)] = \boldsymbol{\Gamma}_z^*\tilde{\mathbf{g}}_{1,TX} \\ \mathbf{c}_{zy} &\triangleq \mathrm{E}[\mathbf{z}(n)y_{fb}(n)] = \boldsymbol{\Gamma}_z\tilde{\mathbf{g}}_{2,TX} \end{aligned} \quad (5.2)$$

[9] On the other hand, it is advantageous to estimate and remove the delay as accurately as possible, in order to keep the model filters reasonably short.

where $\mathbf{z}(n) = [z(n), z(n-1), ..., z(n-N_g+1)]^{\mathrm{T}}$, $\tilde{\mathbf{g}}_i = [\tilde{g}_{i,1}\ \tilde{g}_{i,2} \cdots \tilde{g}_{i,N_g}]^{\mathrm{T}}$, $i = 1,2$, N_g is the length of the model filters, and $\mathbf{\Gamma}_z = \mathrm{E}[\mathbf{z}(n)\mathbf{z}^{\mathrm{H}}(n)]$ is the autocorrelation matrix of the transmit signal. Further, in deriving (5.2), it has been assumed that the transmit signal $z(n)$ is *proper*, i.e., $\mathrm{E}[z(n+\tau)z(n)] = 0, \forall\tau$. The observable imbalance filters can then be calculated as

$$\begin{aligned} \tilde{\mathbf{g}}_{1,TX} &= \mathbf{\Gamma}_z^{*-1}\boldsymbol{\gamma}_{zy} \\ \tilde{\mathbf{g}}_{2,TX} &= \mathbf{\Gamma}_z^{-1}\mathbf{c}_{zy} \end{aligned} \tag{5.3}$$

The cross-correlations in (5.2) that are needed in evaluating (5.3) are in practice estimated from a finite sample of data through the natural sample estimates (in a similar manner as in (3.19) and (3.20)). The autocorrelation matrix has a specific structure, dependent on modulation format and pulse shape, hence it can be assumed to be known. Alternatively, it can also be estimated via the sample estimates. The estimates of $\tilde{\mathbf{g}}_{1,TX}$ and $\tilde{\mathbf{g}}_{2,TX}$ are subsequently used to calculate the predistorter filter as outlined above.

5.3.2 Widely-Linear Least-Squares Estimation

Another way to utilize the feedback signal in (5.1) for parameter estimation is to do least-squares (LS) type model fitting, as described in [P1] or in [31]. First, for a measured data block of L samples, the feedback signal in (5.1) can be written in vector-matrix notations as [P1]

$$\mathbf{y}_{fb}(n) = \mathbf{Z}(n)\tilde{\mathbf{g}}_{1,TX} + \mathbf{Z}^*(n)\tilde{\mathbf{g}}_{2,TX} = \begin{bmatrix}\mathbf{Z}(n) & \mathbf{Z}^*(n)\end{bmatrix}\begin{bmatrix}\tilde{\mathbf{g}}_{1,TX} \\ \tilde{\mathbf{g}}_{2,TX}\end{bmatrix} = \mathbf{Z}_b(n)\begin{bmatrix}\tilde{\mathbf{g}}_{1,TX} \\ \tilde{\mathbf{g}}_{2,TX}\end{bmatrix} \tag{5.4}$$

where $\tilde{\mathbf{g}}_{1,TX}$ and $\tilde{\mathbf{g}}_{2,TX}$ are the $N_g \times 1$ vector representations of the (unknown) observable imbalance filters, $\mathbf{Z}(n)$ is the convolution matrix formed from the transmit data samples (samples of $z(n)$), $\mathbf{y}_{fb}(n) \triangleq [y_{fb}(n), y_{fb}(n-1), \ldots, y_{fb}(n-L+1)]^{\mathrm{T}}$. A linear LS solution for $\tilde{\mathbf{g}}_{1,TX}$ and $\tilde{\mathbf{g}}_{2,TX}$ can then be obtained as

$$\begin{bmatrix}\hat{\tilde{\mathbf{g}}}_{1,TX} \\ \hat{\tilde{\mathbf{g}}}_{2,TX}\end{bmatrix} = \mathbf{Z}_b^{+}(n)\mathbf{y}_{fb}(n), \tag{5.5}$$

where $\mathbf{Z}_b^{+}(n)$ represents the pseudo-inverse of $\mathbf{Z}_b(n)$ [51]. The convolution matrix of the input data $\mathbf{Z}(n)$, assuming covariance windowing, has the following form [8], [51]

$$\mathbf{Z}(n) = \begin{bmatrix} z(n-N_g+1) & z(n-N_g+2) & \ldots & z(n) \\ z(n-N_g) & z(n-N_g+1) & \ldots & z(n-1) \\ \vdots & \vdots & \ddots & \vdots \\ z(n-L+1) & z(n-L) & \cdots & z(n-L-N_g) \end{bmatrix} \tag{5.6}$$

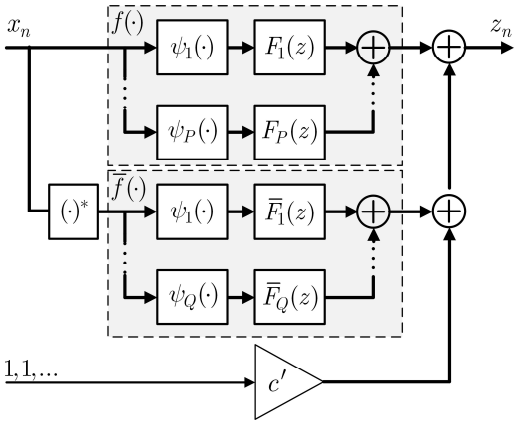

Figure 5-2. The proposed parallel structure for the joint predistortion of PA nonlinearity, I/Q imbalance, and LO leakage.

The predistortion filter can then be solved using $\hat{\tilde{\mathbf{g}}}_{1,TX}$ and $\hat{\tilde{\mathbf{g}}}_{2,TX}$ as described above and in [P1].

Measurement-based studies in [68] and [93], focusing on the WL-LS solution, have verified that the technique is effective, yielding image rejections of at least 55-60 dB with commercial I/Q modulator chips. Recursive LS based implementations of the WL-LS estimator were also formulated and simulated in [93], along with measurements with the USRP/GNU-radio combo (see www.ettus.com and www.gnuradio.org for details on the USRP and GNU radio software).

5.4 Joint Predistortion of Power Amplifier and I/Q Modulator Impairments

The work in [P3] introduced a joint predistorter for PA nonlinearity, LO leakage, and I/Q mismatch. The serial PD structure seen in Figure 5-1 was used as the starting point, assuming the PA predistorter to be parallel Hammerstein (PH), and the I/Q predistorter a symmetric WL filter. An equivalent parallel structure was then derived that is fully linear with respect to its parameters, thus lending itself well to linear LS estimation. In [P3] a basic block LS solution to the estimation problem was derived, utilizing the indirect learning architecture (ILA). Adaptive estimation of the predistorter, based on recursive LS (RLS) estimation and the ILA, was proposed in [P4], along with different efficient training procedures.

5.4.1 Predistorter Structure and Signal Model

The final parallel predistorter structure derived in [P3] is shown in Figure 5-2. The input signal is processed with one PH nonlinearity, while the conjugate of the input signal is processed with another PH nonlinearity. The output of the predistorter is formally written as

$$z_n = f(x_n) + \overline{f}(x_n^*) + c' \tag{5.7}$$

where the PH nonlinearities are defined as (see (2.61))

$$f(x_n) = \sum_{p \in I_P} f_{p,n} \star \psi_p(x_n)$$
$$\overline{f}(x_n^*) = \sum_{q \in I_Q} \overline{f}_{q,n} \star \psi_q(x_n^*) \tag{5.8}$$

and c' is the LO leakage compensator coefficient. In (5.8), $f_{p,n}$ and $\overline{f}_{q,n}$ are the (complex-valued) impulse responses of $F_p(z)$ and $\overline{F}_q(z)$, respectively, $\psi_p(x_n)$ are the static nonlinearities of the model, which in this thesis are polynomial nonlinearities defined in (2.61), and I_P and I_Q are the sets of used polynomial orders for the non-conjugate and conjugate PD, respectively (defined similarly as after (2.61)). The polynomial weights in (2.61) are generally fixed, so estimating the predistorter boils down to estimating the filter tap values $f_{p,n}$ and $\overline{f}_{q,n}$.

5.4.2 Predistorter Estimation

The estimation of the predistorter coefficients is performed with the indirect learning architecture (ILA), shown in Figure 5-4, combined with LS estimation. The ILA enables direct estimation of the predistorter parameters without PA model identification and, when a suitable PD structure such as PH is utilized, doing so with completely linear estimation techniques.

First, we define an *ILA iteration* as a single cycle of the following operations:

1) transmitting a predistorted signal block of length N (in the first ILA iteration the predistorter is turned off),
2) measuring the signal in the feedback loop and identifying the post-inverse of the PA, and
3) plugging the post-inverse parameter estimates into the predistorter.

The postdistorter coefficients in the identification step 2) are found as a solution to a selected optimization criterion, such as minimizing the least-squares error or mean-square error between the postdistorter output and the reference signal. For more information on the ILA, the interested reader is referred to [30], [32], [62], [92], [107], [151].

With reference to Figure 5-3, we denote the postdistorter input signal (the complex envelope of the scaled PA output) by s_n, the postdistorter output signal by $\hat{z}_n$, and the training signal length by N. Assuming finite time spans for the filters $f_{p,n}$ and $\overline{f}_{q,n}$, denoted respectively by L_p and $\overline{L}_q$, we can write the postdistorter output signal (5.7) in vector-matrix notation as

$$\hat{z}_n = \sum_{p \in I_P} \boldsymbol{\psi}_{p,n}^{\mathrm{T}} \mathbf{f}_p + \sum_{q \in I_Q} \overline{\boldsymbol{\psi}}_{q,n}^{\mathrm{T}} \overline{\mathbf{f}}_q + c' . \tag{5.9}$$

Above, the filter impulse response vectors are given as

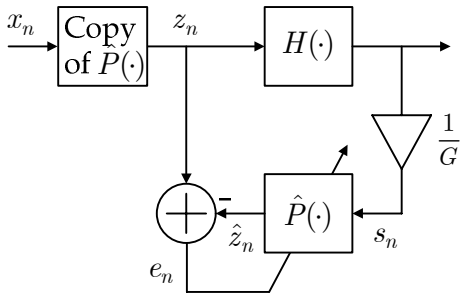

Figure 5-3. The indirect learning architecture. $H(\cdot)$ denotes the PA nonlinear function, $\hat{P}(\cdot)$ is the estimate of the post-inverse of the PA, and e_n is the error signal that is to be minimized in estimation.

$$\begin{aligned} \mathbf{f}_p &= [f_{p,0} \;\; f_{p,1} \cdots f_{p,L_p-1}]^{\mathrm{T}},\ p \in I_P \\ \overline{\mathbf{f}}_q &= [\overline{f}_{q,0} \;\; \overline{f}_{q,1} \cdots \overline{f}_{q,\overline{L}_q-1}]^{\mathrm{T}},\ q \in I_Q \end{aligned} \tag{5.10}$$

and the input vectors to the filters are given as

$$\begin{aligned} \boldsymbol{\psi}_{p,n} &\triangleq [\psi_p(s_n) \;\; \psi_p(s_{n-1}) \cdots \psi_p(s_{n-L_p+1})]^{\mathrm{T}},\ p \in I_P \\ \overline{\boldsymbol{\psi}}_{q,n} &\triangleq [\psi_q(s_n^*) \;\; \psi_q(s_{n-1}^*) \cdots \psi_q(s_{n-\overline{L}_q+1}^*)]^{\mathrm{T}},\ q \in I_Q \end{aligned} \tag{5.11}$$

Notice that $\mathbf{f}_1$ and $\overline{\mathbf{f}}_1$ are the *linear filters* of the predistorter, with respective lengths L_1 and $\overline{L}_1$, while $\mathbf{f}_p$ and $\overline{\mathbf{f}}_p$, $p > 1$ are the *polynomial filters*.

Now, a block of N_B samples of the observed signal s_n is collected, starting from sample index *n*=0 for notational convenience. The loop delay is also assumed to be estimated and removed from s_n. The output vectors of the *p*th non-conjugate and *q*th conjugate predistorter branches can then be written as

$$\begin{aligned} \mathbf{z}_p &= \boldsymbol{\Psi}_p \mathbf{f}_p \\ \overline{\mathbf{z}}_q &= \overline{\boldsymbol{\Psi}}_q \overline{\mathbf{f}}_q \end{aligned} \tag{5.12}$$

Here $\boldsymbol{\Psi}_p$ and $\overline{\boldsymbol{\Psi}}_q$ are the non-conjugate and conjugate polynomial basis matrices of orders *p* and *q*, constructed as convolution matrices of the filter input vectors (5.11) (see [P3], [51], [151]).

Then, zero rows are added to the bottom of all $\boldsymbol{\Psi}_p$ and $\overline{\boldsymbol{\Psi}}_q$ to make them of equal height. By collecting all the polynomial basis matrices into a single block matrix, and appending it with a vector of all-ones (denoted $\mathbf{1}$) to account for the LO leakage compensator, we obtain the complete data matrix

$$\boldsymbol{\Psi} = [\boldsymbol{\Psi}_1 \;\; \boldsymbol{\Psi}_2 \cdots \boldsymbol{\Psi}_P \;\; \overline{\boldsymbol{\Psi}}_1 \;\; \overline{\boldsymbol{\Psi}}_2 \cdots \overline{\boldsymbol{\Psi}}_Q \;\; \mathbf{1}]. \tag{5.13}$$

Finally, stacking the filter impulse responses in (5.10) and the LO leakage compensator coefficient into a single vector as

$$\mathbf{f} = \left[\mathbf{f}_1^{\mathrm{T}}\ \mathbf{f}_2^{\mathrm{T}}\ \cdots\ \mathbf{f}_P^{\mathrm{T}}\ \overline{\mathbf{f}}_1^{\mathrm{T}}\ \overline{\mathbf{f}}_2^{\mathrm{T}}\ \cdots\ \overline{\mathbf{f}}_Q^{\mathrm{T}}\ c'\right]^{\mathrm{T}}, \tag{5.14}$$

we can write the complete postdistorter output vector as

$$\hat{\mathbf{z}} = \boldsymbol{\Psi}\mathbf{f}\,. \tag{5.15}$$

Using (5.9)-(5.15), and denoting the corresponding reference signal vector by $\mathbf{z} = [z_1, z_2, ..., z_{N_B}, 0, ..., 0]^{\mathrm{T}}$ (appended with $\max(L_p, \overline{L}_q)$ zeros), the LS estimation problem is constructed as finding that parameter vector $\hat{\mathbf{f}}$ which minimizes the cost function $J(\mathbf{f}) = \|\mathbf{z} - \hat{\mathbf{z}}\|^2$, yielding the well-known LS solution [51]

$$\hat{\mathbf{f}}_{LS} = (\boldsymbol{\Psi}^{\mathrm{H}}\boldsymbol{\Psi})^{-1}\boldsymbol{\Psi}^{\mathrm{H}}\mathbf{z}. \tag{5.16}$$

In practical implementations, numerical methods like QR decomposition or singular value decomposition (SVD) can be used to implement the pseudo-inverse ($(\boldsymbol{\Psi}^{\mathrm{H}}\boldsymbol{\Psi})^{-1}\boldsymbol{\Psi}^{\mathrm{H}}$) calculations.

Alternatively to the block LS solution, a recursive LS estimator can be used, as was proposed in [P4]. There, the RLS estimation rule corresponding to the previous LS solution was formulated, and different training schemes were proposed to effectively combine the RLS learning rule and indirect learning. The RLS algorithm and its variants are much more amenable to practical implementation on an FPGA or ASIC compared to block solutions, due to them avoiding any matrix inverse or pseudo-inverse calculations. Denoting the RLS iteration index by $i = 1, 2, ..., N_B$, a single update cycle of the recursive learning rule can be formulated as [P4]

$$\begin{aligned}
\mathbf{k}(i) &= \frac{\mathbf{M}(i-1)\mathbf{v}^*(i)}{\lambda + \mathbf{v}^T(i)\mathbf{M}(i-1)\mathbf{v}^*(i)} \\
e(i) &= d(i) - \mathbf{f}^T(i-1)\mathbf{v}(i) \\
\mathbf{f}(i) &= \mathbf{f}(i-1) + \mathbf{k}(i)e(i) \\
\mathbf{M}(i) &= \lambda^{-1}[\mathbf{M}(i-1) - \mathbf{k}(i)\mathbf{v}^T(i)\mathbf{M}(i-1)].
\end{aligned} \tag{5.17}$$

Here $\mathbf{v}(i) = \boldsymbol{\Psi}(i,:)$ denotes the i-th row of the previous data matrix $\boldsymbol{\Psi}$ in (5.13), $\mathbf{f}(i)$ denotes the pre-distortion parameter vector estimate at iteration i, $d(i) = z_i$ denotes the reference signal value at iteration i, and λ is the internal memory of the algorithm, often called the forgetting factor. For more details on the recursive training procedure, please refer to [P4], and on recursive learning rules in general, see, e.g., [51].

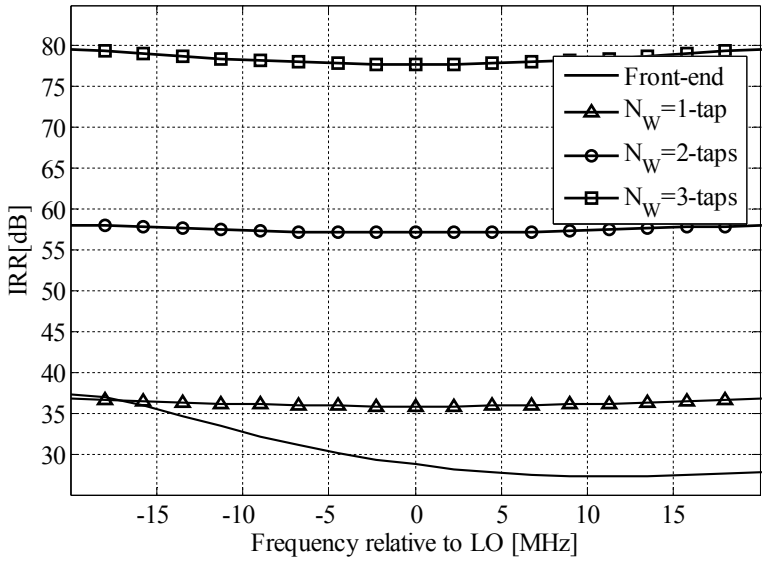

Figure 5-4. Simulated IRR vs. frequency curves for the direct-conversion transmitter case with different pre-distortion filters using the widely-linear least-squares model fitting approach.

5.5 Simulation and Measurement Examples

5.5.1 Digital Transmitter I/Q Calibration

The performance of the WL-LS compensation algorithm is demonstrated with computer simulations and with laboratory RF signal measurements. Both zero-IF and low-IF input signals are considered. In all the simulations and measurements, the imbalance estimator filter length N_g is fixed to 3-taps, and the pre-distortion filter length (N_W) is either 1, 2, or 3 taps.

The simulation example corresponds to a zero-IF transmitter with 64-QAM single-carrier signal with 9 MHz bandwidth and 40 MHz sample rate in the digital front-end. The I/Q mixer imbalance values used in the simulations are $g = 1.03$ and $\phi = 3^\circ$, and the impulse responses of frequency selective I and Q branches are $\mathbf{h}_I = [0.99, \ -0.1]^T$ and $\mathbf{h}_Q = [0.98, \ -0.07]^T$, respectively. This represents a practical case and corresponds to an overall IRR of approximately 25-35 dB without compensation, as shown in Figure 5-4 ('Front-end'). The achieved IRR including pre-distortion is also plotted in the figure as a function of frequency after averaging 100 independent simulation runs. In this simulation, in the feedback loop, we use 10,000 samples of the original and imbalanced signals to calculate the predistortion filter coefficients using the WL-LS method described earlier. The simulation results indicate a clear improvement in the obtained mirror frequency attenuation for a pre-distortion filter of 3-taps, reaching and IRR level in the order of 75-80dB, which is surely enough for any practical transmitter deployment.

In the measurement example, we use standard state-of-the-art signal generation and analysis devices in a radio signal laboratory environment. The transmitter topology used is low-IF transmitter with 7.5 MHz waveform bandwidth and 4.5 MHz transmitter IF.

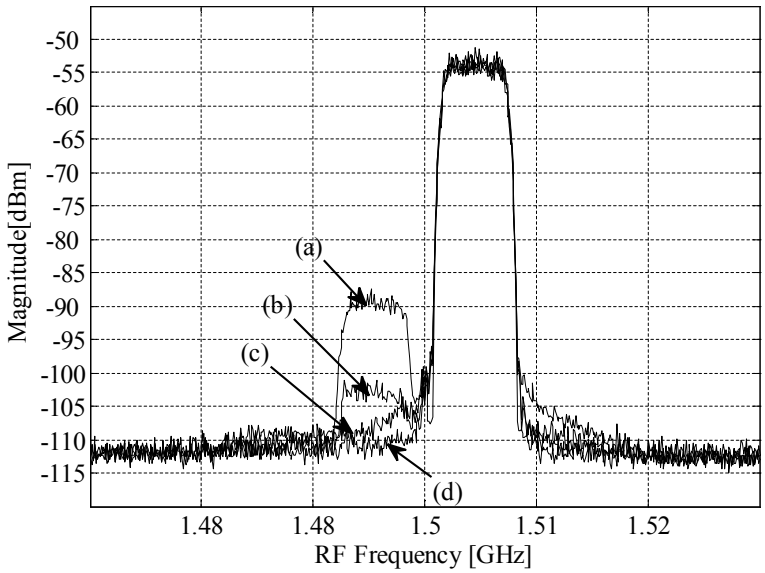

Figure 5-5. Measured I/Q modulator output without and with I/Q pre-distortion, (a) without pre-distortion (b) with 1-tap pre-distortion filter, (c) with 2-tap pre-distortion filter, (d) with 3-tap pre-distortion filter.

The modulation method used is again 64-QAM with root-raised cosine pulse-shaping. The basic sample rate in the transmitter digital front-end is 72 MHz. The actual RF frequency range is 1.5 GHz. 20,000 samples of the original and feedback data are used for pre-distortion coefficient estimation. The obtained transmitter RF spectrum is depicted in Figure 5-5. Clearly, the mirror-frequency component is well-attenuated, reaching 55-60 dB measured IRR level with the 3-tap predistorter.

5.5.2 Joint Predistortion of PA Nonlinearity, LO Leakage, and I/Q Mismatch

The first simulation example tests the RLS algorithm on the single-carrier frequency division multiple access (SC-FDMA) waveforms of LTE uplink 10 MHz mode [1], [2]. The signal is occupying subcarriers +101 through to +300, thus having a bandwidth of about 3 MHz around an IF of 3 MHz. The amplifier model is the Rapp solid-state amplifier model with smoothness parameter p=1.5, while input back-off from the 1-dB compression point is about 1 dB. The PD is 9th/5th order with filter lengths $L_p = 4,4,4,3,3$ and $\overline{L}_q = 4,3,3$, and it is trained with 500 RLS recursions within each ILA iteration. Figure 5-6 shows the PSD of the PA output without and with PD, plotted after the 10th ILA iteration, averaged over 100 realizations. The operation of the I/Q imbalance and LO leakage compensators are seen clearly since the MFI and LO leakage signal both fall outside the desired signal band. The proposed PD is able to push the spectral regrowth, mirror frequency interference and LO leakage considerably down, in a way that practically no distortion is visible in the PSD. The memoryless joint PD is able to mitigate the spectral regrowth due to the (memoryless) PA nonlinearity successfully, as well as the LO leakage, but cannot mitigate the MFI fully. The plain PH PD can also mitigate the LO leakage and part of the spectral regrowth, but naturally fails to do anything to the MFI.

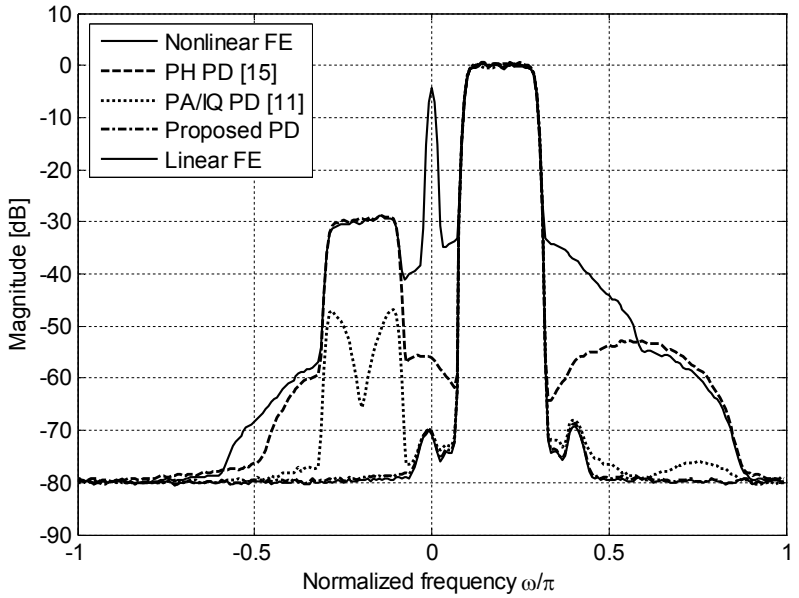

*Figure 5-6. Output spectra of the power amplifier with ideal linear amplification, the Rapp PA model (*p*=1.5, IBO=1dB) without predistortion and with the proposed joint PA and I/Q predistorter. Compared with the plain parallel Hammerstein PD [30] ([15] in figure legend) and the memoryless joint PA/IQ PD from [72] ([11] in figure legend). SC-FDMA 16-QAM signal with pulse shaping, and feedback SNR=60 dB. 500 samples used for coefficient estimation at each ILA iteration.*

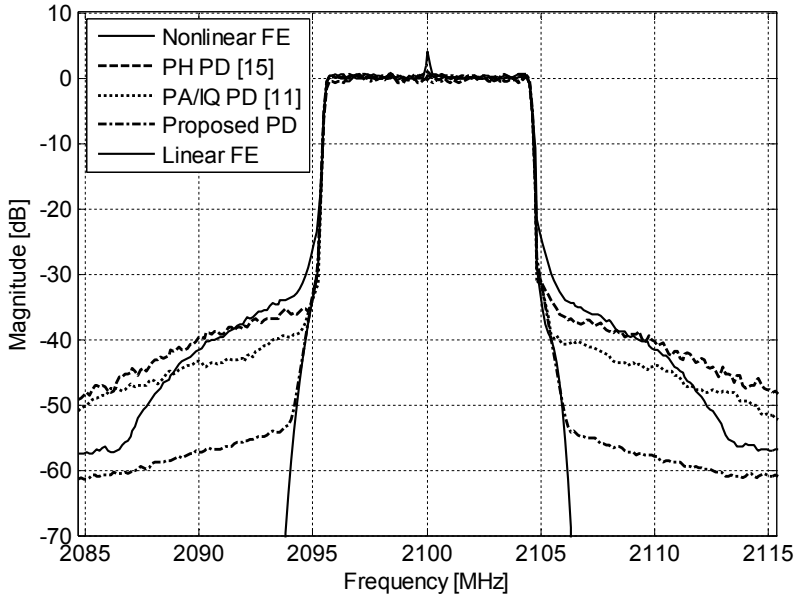

Figure 5-7. Spectra of measured amplifier output signals, averaged over 10 independent measurements. OFDM signals according to LTE downlink specifications, with 600 active subcarriers out of 1024 and 15 kHz subcarrier spacing. PD orders are 9th/5th. In the figure legend, [15] corresponds to [30], and [11] to [72] in the current manuscript.

The measurement example consists of an OFDM signal with 600 active subcarriers (out of 1024), with a spacing of 15 kHz, thus corresponding to a fully loaded 3GPP LTE downlink signal in 10 MHz mode [2]. The signal is oversampled by 4 and then filtered before upconverting to 2.1 GHz carrier frequency. Predistorter is 9th/5th order with filter lengths of

$L_p = 5,4,3,2,2$ and $\overline{L_q} = 5,3,3$, and it is trained with 1,500 RLS recursions in each ILA iteration. Figure 5-7 shows the PSD of the PA output without PD, with the reference techniques, and with the proposed PD structure after the 10th iteration (10 ILA cycles), averaged over 10 independent measurements. Clear performance improvement over the uncompensated case and the reference techniques can be obtained with the proposed method. The new joint PA/IQ PD yields 15-20 dB improvement in ACPR compared to the "Nonlinear front-end" case, and 10-15 dB better results than the reference predistorters.

Chapter 6

Summary

This thesis deals with modeling and digital compensation of the effects of analog circuit impairments in direct-conversion receivers and transmitters. Specifically, the modeling and mitigation of transmitter and receiver I/Q imbalances at the source, and the joint modeling and predistortion of transmitter I/Q imbalance, LO leakage, and PA nonlinearity, are addressed. The modeling and compensation developments rely heavily on the use of widely-linear signal models, which are augmented linear-conjugate-linear models that take into account the complex conjugate of the signal as well. Such signal models arise naturally in the presence of I/Q imbalance, and are paramount for the understanding of I/Q imbalance and its interactions with the other impairments, and also lend themselves for constructing intuitive and effective compensator structures. The compensation of these impairments is performed in the *digital front-end* of the transmitter or receiver, as a last processing step before the DAC or the first step after the ADC, respectively.

The main findings and results of this thesis are summarized in the following. In [P2], [P5]-[P7], several novel algorithms for compensating both frequency-selective and frequency-independent I/Q mismatches in direct-conversion receivers were developed (as summarized in Chapter 4 of this manuscript). The second-order statistics of receiver front-end signals under impairments related to the circuit implementation and the radio channel, and their relevance in terms of receiver I/Q mismatch compensation, were analyzed in [P2], [P8] (reviewed in Chapter 3). The concept of *time-average properness*, which is essential for analyzing and fully understanding the second-order statistics of cyclostationary signals under I/Q imbalances, was established in Chapter 3 (Definition 3-1), followed by a very intuitive frequency-domain interpretation of time-average properness. A method and algorithm was developed for the estimation and predistortion of frequency-selective I/Q mismatch in DCTs [P1] (summarized in Chapter 5). The first ever predistortion structure for the joint compensation of frequency-selective power amplifier nonlinearity, I/Q mismatch, and LO leakage in direct-conversion transmitters was developed in [P3]. Such a joint structure is needed to simplify the hardware that is required for its estimation, and to guarantee the identifiability of the predistorter. Furthermore, estimation algorithms and procedures for

training the previous predistorter structure were derived in [P3], [P4], as summarized in Chapter 5.

All the compensation techniques introduced in this thesis, and outlined above, are in principle applicable with almost *any* type of communication signals, whether they are single-carrier or multi-carrier signals, single-user or multi-user signals, or sums of such signals. They are practically independent of modulation format, and can also be applied in multi-antenna systems to each antenna subsystem separately. None of the proposed algorithms requires dedicated training data, but they utilize the regular transmitted/received signals for their learning. Furthermore, the receiver-based algorithms are robust against most of the other system impairments, and are in fact benefiting from some of them. The techniques are therefore very generally applicable, and waveform and standard independent. Due to their nature, they can in principle be applied in any type of wireless transceiver that employs the direct-conversion principle, provided of course that the application at hand benefits from the extra processing in terms of improved performance, lower production costs, and/or lower power consumption. Notable example application platforms are basestation and mobile transceivers for cellular networks, broadcast transmitters, and future software-defined, flexible, multi-standard radio terminals, targeted for example for cognitive radio.

The functionality and performance of the algorithms was verified with extensive simulations and laboratory radio signal measurements, exhibiting very good performance under variable signals and system conditions. Altogether, the results demonstrate that the proposed techniques provide efficient and robust DSP based solutions for the analog implementation impairments in question, thus facilitating the implementation of wideband, multi-standard, flexible, yet low-cost radio devices for current as well as emerging wireless systems.

Several potential avenues for further research in the area have emerged as a result of the thesis work. The role of cyclic statistics in analysis and compensation of I/Q imbalances, as well as other RF impairments, is worth investigating in more detail. Exploring the possibilities of using higher order statistics and higher order circularity in analyzing and compensating for I/Q imbalances is another potentially fruitful research direction. The possibilities of utilizing circularity for combating other impairments, such as dynamic DC offset, should also be explored. Further development of the circularity-based receiver algorithms, as well as their analytical performance evaluation, are also interesting topics for future work. Developing the transmitter predistortion algorithms further, as well as looking into a joint PAPR reduction and digital predistortion solution, are other possible future study items. Finally, the emergence of cognitive radio represents a huge challenge for the overall transceiver design. There, the need for digitally-enhanced or assisted RF front-ends is obvious and almost inevitable, and will open up many possibilities for innovative solutions on both sides of the A/D interface.

Epilogue

This thesis was concerned with digitally-enhanced transmitters and receivers for wireless communications applications. The general goal was to develop practical and computationally efficient digital algorithms for compensating the deleterious effects of certain circuit impairments that are related to the implementation of direct-conversion receivers and transmitters. The direct-conversion radio, while simple in structure and integrable on a single chip, suffers from several performance degrading circuit impairments, such as I/Q imbalance, DC offsets, LO leakage, nonlinearities, and interactions between these impairments.

The *potential* of DSP in solving these issues has been demonstrated in the last 10-15 years time and again, by researchers in our group as well as by many others. However, it is only through interaction and cooperation *between* traditional RF design and digital front-end signal processing, that the *true value and benefit* of digital signal processing in combating radio front-end impairments can be fully realized. This cooperation should exist in many levels, from academic research to the actual design and implementation of digitally-enhanced radio front-ends. A simple analogue from optimization theory states, that solving two interrelated optimization problems separately generally leads to a suboptimum solution. A joint optimization procedure is needed to find the optimum solution. This is exactly what designing a radio front-end is – a highly complex and nonlinear optimization problem, involving optimizing both the analog and digital circuits. But because of the complexity of the design rules, technologies, and interactions between the physical and the digital world, this has not been attempted.

For the above to realize, we must bridge the gap between the two R&D communities, in a way that the people working on the "dirty" side of the analog-to-digital (A/D) interface also understand and grasp the potential of DSP in solving real circuit implementation related problems. On the other hand, we (the digital guys) need to have a better understanding of analog electronics and its possibilities, and to realize that not everything can be post-corrected in the digital domain.

Cognitive radio devices will be the ultimate test to transceiver design and implementation, especially in terms of the linearity of the receiver. There, due to the extremely wide bandwidths in the order of several GHz seen by the radio front-end, the presence of powerful blocking signals will be more the rule than the exception, and extreme linearity would be required from the radio front-end. On the other hand, purely digital techniques for impairment

mitigation, especially for the receiver nonlinearities, are not realistic in the foreseeable future due to limitations of A/D converters and the needed processing power. Therefore, so-called hybrid techniques, or digitally-assisted calibration of the RF modules, will likely play a significant role in cognitive radio, and research in that direction is currently ongoing. This line of work, again, requires good understanding of both analog circuits and digital signal processing.

Bibliography

[1] 3GPP Technical Specification Group Radio Access Network, "Evolved Universal Terrestrial Radio Access (E-UTRA) and Evolved Universal Terrestrial Radio Access (E-UTRAN); Overall description; Stage 2," Technical Specification TS 36.300, V8.12.0, March 2010.

[2] 3GPP Technical Specification Group Radio Access Network, "Evolved Universal Terrestrial Radio Access (E-UTRA); Physical Channels and Modulation" Technical Specification TS 36.211, V9.1.0, March 2010.

[3] 3GPP Technical Specification Group Radio Access Network, "Requirements for further advancements for Evolved Universal Terrestrial Radio Access (E-UTRA) (LTE-Advanced)" Technical Report TR 36.913, V10.0.0, March 2011.

[4] A. A. Abidi, "Direct conversion radio transceivers for digital communications," *IEEE Journal of Solid-State Circuits*, vol. 30, pp. 1399-1410, Dec. 1995.

[5] A. A. Abidi, "CMOS wireless transceiver: The new wave," *IEEE Communications Magazine*, vol. 37, pp. 119-124, Aug. 1999.

[6] L. Anttila, M. Valkama, and M. Renfors, "3.9G radio reception with SC-FDMA waveforms under I/Q imbalance," in *Proc. IEEE International Symposium on Circuits and Systems (ISCAS '07)*, New Orleans, LA, USA, May 2007.

[7] L. Anttila, M. Valkama, and M. Renfors, "Efficient mitigation of frequency-selective I/Q imbalance in OFDM receivers," in *Proc. IEEE Vehicular Technology Conference (VTC-F '08)*, Calgary, Canada, September 2008.

[8] L. Anttila, Y. Zou, and M. Valkama, "Digital compensation and calibration of I/Q gain and phase imbalances," Chapter 16 in *Digital Front-End in Wireless Communications and Broadcasting*, Cambridge, UK: Cambridge University Press, 2011 (to appear).

[9] E. Aschbacher, *Digital Pre-distortion of Microwave Power Amplifiers*, Dr. Tech. thesis, Technischen Universität Wien, Vienna, Austria, 2005.

[10] R. Bagheri, A. Mirzaei, M. E. Heidari, S. Chehrazi, M. L. Lee, W. K. Tang, and A. A. Abidi, "Software-defined radio receiver: Dream to reality," *IEEE Communications Magazine*, vol. 44, pp. 111–118, Aug. 2006.

[11] A. Baier, "Quadrature mixer imbalances in digital TDMA mobile radio receivers," in Proc. International Zurich Seminar on Digital Communications, Electronic Circuits and Systems for Communications, pp. 147–162, Zurich, Switzerland, March 1990.

[12] R. J. Baxley and G. Tong Zhou, "Power savings analysis of peak-to-average power ratio in OFDM," *IEEE Transactions on Consumer Electronics*, vol. 50, 2004.

[13] E. Biglieri, S. Barberis, and M. Catena, "Analysis and compensation of nonlinearities in digital transmission systems," *IEEE Journal on Selected Areas in Communications*, vol. 6, Jan. 1988, pp. 42-51.

[14] D. Brady and J. Feigin, "Joint transmitter/receiver I/Q imbalance compensation for direct conversion OFDM in packet-switched multipath environments," *IEEE Transactions on Signal Processing*, vol. 57, Nov. 2009, pp. 4588-4593.

[15] M. Brandolini *et al.*, "Toward multistandard mobile terminals - fully integrated receivers requirements and architectures," *IEEE Transactions on Microware Theory and Techniques*, vol. 53, March 2005, pp. 1026-1038.

[16] W. M. Brown and R. B. Crane, "Conjugate linear filtering," *IEEE Transactions on Information Theory*, vol. 15, July 1969, pp. 462-465.

[17] S. Burglechner, A. Shahed Hagh Ghadam, A. Springer, M. Valkama, and G. Hueber, "DSP oriented implementation of a feedforward power amplifier linearizer," in *Proc. IEEE International Symposium on Circuits and Systems (ISCAS'09)*, Taipei, Taiwan, May 2009, pp. 1755-1758.

[18] H. Cao, A. S. Tehrani, C. Fager, T. Eriksson, and H. Zirath, "I/Q imbalance compensation using a nonlinear modeling approach," *IEEE Transactions on Microwave Theory and Techniques*, vol. 57, 2009, pp. 513-518.

[19] A. B. Carlson, *Communication Systems*, 3rd ed., New York, USA: McGraw-Hill, 1986.

[20] N. B. Carvalho and J. C. Pedro, A comprehensive explanation of distortion sideband asymmetries," *IEEE Transactions on Microwave Theory and Techniques*, vol. 50, September 2002, pp. 2090-2101.

[21] J. K. Cavers and M. W. Liao, "Adaptive compensation for imbalance and offset losses in direct conversion transceivers," *IEEE Transactions on Vehicular Technology*, vol. 42, Nov. 1993, pp. 581-588.

[22] J. K. Cavers, "The effect of quadrature modulator and demodulator errors on adaptive digital predistorters for amplifier linearization," *IEEE Transactions on Vehicular Technology*, vol. 46, May 1997, pp. 456-466.

[23] J. K. Cavers, "New methods for adaptation of quadrature modulators and demodulators in amplifier linearization circuits," *IEEE Transactions on Vehicular Technology*, vol. 46, Aug. 1997, pp. 707-716.

[24] R. Chandrasekaran, "Model-based feedforward linearization of amplifiers," U.S Patent no. 6,765,440, June 2004.

[25] Y.-H. Chung and S.-M. Phoong, "Joint estimation of I/Q imbalance, CFO and channel response for MIMO OFDM systems," *IEEE Transactions on Communications*, vol. 58, May 2010, pp. 1485 –1492.

[26] S. Cripps, *RF Power Amplifiers for Wireless Communications*, Norwood, MA: Artech House, 1999.

[27] J. Crols and M. S. J. Steyaert, *CMOS Wireless Transceiver Design*, Dordrecht, The Netherlands: Kluwer, 1997.

[28] K. David, S. Dixit, and N. Jefferies, "2020 vision. The Wireless World Research Forum looks to the future," *IEEE Vehicular Technology Magazine*, Sept. 2010.

[29] S. De Rore, E. Lopez-Estraviz, F. Horlin, and L. Van der Perre, "Joint estimation of carrier frequency offset and IQ imbalance for 4G mobile wireless systems," in *Proc. IEEE International Conference on Communications (ICC'06)*, 2006.

[30] L. Ding, G. Tong Zhou, D. R. Morgan, Z. Ma, J. S. Kenney, J. Kim, and C. R. Giardina, "A robust digital baseband predistorter constructed using memory polynomials," *IEEE Transactions on Communications*, vol. 52, 2004, pp. 159–165.

[31] L. Ding, Z. Ma, D. R. Morgan, M. Zierdt, and G. Tong Zhou, "Compensation of frequency-dependent gain/phase imbalance in predistortion linearization systems," *IEEE Transactions on Circuits and Systems*, vol. 55, Feb. 2008, pp. 390-397.

[32] C. Eun, E. J. Powers, "A new Volterra predistorter based on the indirect learning architecture," *IEEE Transactions on Signal Processing* vol. 45, 1997, pp. 223-227.

[33] M. Faulkner, T. Mattsson, W. Yates, "Automatic adjustment of quadrature modulators," *Electronics Letters* vol. 27, 1991, pp. 214-216.

[34] M. Faulkner and T. Mattsson, "Spectral sensitivity of power amplifiers to quadrature modulator misalignment," *IEEE Transactions on Vehicular Technology*, vol. 41, 1992, pp. 516-525.

[35] M. Faulkner, "DC offset and IM2 removal in direct conversion receivers," *IEE Proceedings in Communications*, vol. 149, June 2002, pp. 179-184.

[36] J. Feigin and D. Brady, "Joint transmitter/receiver I/Q imbalance compensation for direct conversion OFDM in packet-switched multipath environments," IEEE Transactions on Signal Processing, vol. 57, Nov. 2009, pp. 4588-4593.

[37] G. Fettweis, M. Löhning, D. Petrovic, M. Windisch, P. Zillmann, and W. Rave, "Dirty RF: A new paradigm," *Springer International Journal of Wireless Information Networks*, vol. 14, June 2007, pp. 133-148.

[38] S. Fouladifard and H. Shafiee, "Frequency offset estimation in OFDM systems in presence of IQ imbalance," in *Proc. IEEE International Conference on Communications (ICC'03)*, Anchorage, AK, May 2003, pp. 2071-2075.

[39] W. A. Gardner and L. E. Franks, "Characterization of cyclostationary random signal processes," *IEEE Transactions on Information Theory*, vol. IT-21, Jan. 1975, pp. 4-14.

[40] W. A. Gardner, *Introduction to Random Processes: With Applications to Signals and Systems*, 2nd ed., New York, USA: McGraw-Hill, 1989.

[41] W. A. Gardner, "Cyclic Wiener filtering: Theory and method," *IEEE Transactions on Communications*, vol. 41, Jan. 1993, pp. 151-163.

[42] W. A. Gardner, A. Napolitano, and L. Paura, "Cyclostationarity: Half a century of research," *Signal Processing*, vol. 86, Sept. 2005, pp. 639-697.

[43] W. H. Gerstacker, R. Schober, and A. Lampe, "Receivers with widely linear processing for frequency-selective channels," *IEEE Transactions on Communications*, vol. 51, Sept. 2003, pp. 1512-1523.

[44] F. M. Ghannouchi and O. Hammi, "Behavioral modeling and predistortion," *IEEE Microwave Magazine*, Dec. 2009, pp. 52-64.

[45] G.-T. Gil, Y. D. Kim, and Y. H. Lee, "Non-data-aided approach to I/Q mismatch compensation in low-IF receivers," *IEEE Transactions on Signal Processing*, vol. 55, pp. 3360–3365, July 2007.

[46] G.-T. Gil, "Nondata-aided I/Q mismatch and DC offset compensation for direct-conversion receivers," *IEEE Transactions on Signal Processing*, vol. 56, pp. 2662-2668, July 2008.

[47] S. J. Grant, J. K. Cavers, and P. A. Goud, "A DSP controlled adaptive feedforward amplifier linearizer", in *Proc 5th IEEE International Conference on Universal Personal Communications (ICUPC'96)*, Cambridge, MA, USA, Sept. 29-Oct. 2, 1996.

[48] O. Hammi, S. Boumaiza, and F. M. Ghannouchi, "On the robustness of digital predistortion function synthesis and average power tracking for highly nonlinear power amplifiers," *IEEE Transactions on Microwave Theory and Techniques*, vol. 55, June 2007, pp. 1382-1389.

[49] L. Hanzo, M. El-Hajjar, and O. Alamri, "Near-Capacity Wireless Transceivers and Cooperative Communications in the MIMO Era: Evolution of Standards, Waveform Design, and Future Perspective," *Proceedings of the IEEE*, vol. 99, 2011.

[50] F. Harris, "Digital filter equalization of analog gain and phase mismatch in I-Q receivers," in *Proc. 5th IEEE International Conference on Universal Personal Communications (ICUPC'96)*, Cambridge, MA, USA, Sept. 29-Oct. 2, 1996, pp. 793-796.

[51] S. Haykin, *Adaptive Filter Theory*, 4th ed., Upper Saddle River, NJ, USA: Prentice Hall, 2002.

[52] T. Hentschel, M. Henker, and G. Fettweis, "The digital front-end of software radio terminals," *IEEE Personal Communications*, vol. 6, Aug. 1999.

[53] D. S. Hilborn, S. P. Stapleton, and J. K. Cavers, "An adaptive direct conversion transmitter," *IEEE Transactions on Vehicular Technology* vol. 43, 1994, pp. 223-233.

[54] C.-J. Hsu and W.-H. Sheen, "Joint estimation and compensation of transmitter and receiver radio impairments in MIMO-OFDM receivers," in *Proc. International Symposium on Personal, Indoor and Mobile Radio Communications (PIMRC'09),* Tokyo, Japan, Sept. 2009.

[55] C.-J. Hsu, R. Cheng, and W.-H. Sheen, "Joint least squares estimation of frequency, DC Offset, I-Q imbalance, and channel in MIMO receivers," *IEEE Transactions on Vehicular Technology*, vol. 58, Jun 2009, pp. 2201–2213.

[56] C.-J. Hsu and W.-H. Sheen, "Compensation of cascaded radio impairments in MIMO-OFDM systems with direct-conversion architecture," in *Proc. Global Mobile Congress (GMC'10)*, 2010.

[57] X. Huang and M. Caron, "Efficient transmitter self-calibration and amplifier linearization techniques," in *Proc. IEEE International Symposium on Circuits and Systems (ISCAS'07)*, New Orleans, LA, May 2007, pp. 265-268.

[58] J. Huettner, S. Reinhardt, and M. Huemer, "Low complex IQ-imbalance compensation for low-IF receivers," in *Proc. IEEE Radio and Wireless Symposium*, San Diego, CA, Jan. 2006, pp. 303-306.

[59] M. Isaksson, D. Wisell, and D. Rönnow, "A comparative analysis of behavioral models for RF power amplifiers," *IEEE Transactions on Microwave Theory and Techniques*, vol. 54, 2006, pp. 348-359.

[60] M. Isaksson and D. Rönnow, "A parameter-reduced Volterra model for dynamic RF power amplifier modeling based on orthonormal basis functions," *International Journal of RF and Microwave Computer-Aided Engineering*, vol. 17, 2007, pp. 542-551.

[61] ITU-R Rep. M.2134, "Requirements Related to Technical Performance for IMT-Advanced Radio Interface(s)," 2008.

[62] H. Jiang and P. A. Wilford, "Digital predistortion for power amplifiers using separable functions," *IEEE Transactions on Signal Processing*, vol. 58, Aug. 2008, pp. 4121-4130.

[63] T. Jiang and Y. Wu, "An overview: Peak-to-average power ratio reduction techniques for OFDM signals," *IEEE Transactions on Broadcasting*, vol. 54, June 2008, pp. 257-268.

[64] Y. Jin, J. Kwon, Y. Lee, J. Ahn, W. Choi, and D. Lee, "Additional diversity gain in OFDM receivers under the influence of IQ imbalances," in *Proc. IEEE International Conference on Communications (ICC'07)*, Glasgow, Scotland, June 2007, pp. 5915-5920.

[65] A. Katz, "Linearization: reducing distortion in power amplifiers," *IEEE Microwave Magazine*, Dec. 2001, pp. 37-49.

[66] A. Katz, R. Gray, and R. Dorval, "Truly wideband linearization," *IEEE Microwave Magazine*, Dec. 2009.

[67] P. B. Kenington, *High-linearity RF amplifier design*, Norwood, MA, USA: Artech House, 2000.

[68] A. Kiayani, L. Anttila, O. Mylläri, and M. Valkama, "Prototype implementation and RF performance measurements of DSP based transmitter I/Q imbalance calibration,"

in *Proc. IEEE, IET International Symposium on Communication Systems, Networks, and Digital Signal Processing (CSNDSP-2010)*, Newcastle, UK, July 2010.

[69] A. Kiayani, L. Anttila, Y. Zou, and M. Valkama, "Hybrid time/frequency domain compensator for RF impairments in OFDM systems," in *Proc. International Symposium on Personal, Indoor and Mobile Radio Communications (PIMRC'11)*, Toronto, Canada, Sept. 2011 (to appear).

[70] W.-J. Kim, S. P. Stapleton, J. H. Kim, and C. Edelman, "Digital predistortion linearizes wireless power amplifiers," *IEEE Microwave Magazine*, Sept. 2005, pp. 54-61.

[71] W.-J. Kim, K.-J. Cho, S. P. Stapleton, and J.-H. Kim, "Efficiency comparison of a digitally predistorted and a feed-forward linearized Doherty amplifier with crest factor reduction," *Microwave Journal*, vol. 50, May 2007.

[72] Y.-D. Kim, E.-R. Jeong, and Y. H. Lee, "Adaptive compensation for power amplifier nonlinearity in the presence of quadrature modulation/demodulation errors," *IEEE Transactions on Signal Processing* vol. 55, 2007, pp. 4717-4721.

[73] E. A. Lee and D. G. Messerschmitt, *Digital Communication*, 2nd ed., Norwell, MA, USA: Kluwer, 1994.

[74] S.A. Leyonhjelm and M. Faulkner, "The effect of reconstruction filters on direct upconversion in a multichannel environment," *IEEE Transactions on Vehicular Technology*, vol. 44, pp. 95-102, Feb. 1995.

[75] X. Li and M. Ismail, *Multi-Standard CMOS Wireless Receivers*. Norwell, MA: Kluwer, 2002.

[76] H. Lin, X. Zhu, and K. Yamashita, "Pilot-aided low-complexity CFO and I/Q imbalance compensation for OFDM systems," in *Proc. IEEE International Conference on Communications (ICC'08)*, Beijing, China, May 2008.

[77] H. Lin, X. Zhu, and K. Yamashita, "Hybrid domain compensation for analog impairments in OFDM systems," in *Proc. IEEE Global Communications Conference (GLOBECOM'08)*, New Orleans, LA, USA, Dec. 2008.

[78] J. Lin and E. Tsui, "Joint adaptive transmitter/receiver IQ imbalance correction for OFDM systems," in *Proc. IEEE International Symposium on Personal, Indoor and Mobile Radio Communications (PIMRC'04)*, Barcelona, Spain, Sept. 2004, pp. 1511-1516.

[79] L. Lanante Jr., M. Kurosaki, and H. Ochi, "Low complexity compensation of frequency dependent I/Q imbalance and carrier frequency offset for direct conversion receivers," in *Proc. IEEE International Symposium on Circuits and Systems (ISCAS'10)*, Paris, France, 2010.

[80] M. Loève, *Probability Theory II*, 4th ed., New York, NY, USA: Springer, 1978.

[81] E. Lopez-Estraviz et al., "Optimal training sequences for joint channel and frequency-dependent IQ imbalance estimation in OFDM-based receivers," in *Proc. IEEE*

International Conference on Communications (ICC'06), Istanbul, Turkey, June 2006, pp. 4595-4600.

[82] E. Lopez-Estraviz and L. Van der Perre, "EM based frequency-dependent transmit/receive IQ imbalance estimation and compensation in OFDM-based transceivers," in *Proc. IEEE Global Telecommunications Conference (Globecom'07)*, Washington DC, Nov. 2007, pp. 4274-4279.

[83] J. Luo, W. Keusgen, and A. Kortke, "Preamble designs for efficient joint channel and frequency-selective I/Q-imbalance compensation in MIMO OFDM systems," in *Proc. Wireless Communications and Networking Conference (WCNC'10)*, 2010.

[84] P.-I. Mak, S.-P. U, and R. P. Martins, "Transceiver Architecture Selection: Review, State-of-the-Art Survey and Case Study," *IEEE Circuits and Systems Magazine*, vol. 7, pp. 6-25, Second Quarter 2007.

[85] D. P. Mandic and V. S. L. Goh, *Complex Valued Nonlinear Adaptive Filters. Noncircularity, Widely Linear and Neural Models*, New York, NY, USA: John Wiley & Sons, 2009.

[86] R. Marchesani, "Digital precompensation of imperfections in quadrature modulators," *IEEE Transactions on Communications*, vol. 48, pp. 552-556, April 2000.

[87] K. W. Martin, "Complex signal processing is not complex," *IEEE Transactions on Circuits and Systems I*, vol. 51, pp. 1823-1836, Sept. 2004.

[88] L. Maurer, R.Stuhlberger, C. Wicpalek, G. Haberpeuntner, and G. Hueber, "Be flexible," *IEEE Microwave Magazine*, April 2008.

[89] H. Meyr, M. Moeneclaey, and S. A. Fechtel, *Digital Communication Receivers: Synchronization, Channel Estimation, and Signal Processing,* New York, NY, USA: John Wiley & Sons, 1997.

[90] S. Mirabbasi and K. Martin, "Classical and modern receiver architectures," *IEEE Communications Magazine*, vol. 38, pp. 132-139, Nov. 2000.

[91] J. Mitola III and G. Q. Maguire Jr., "Cognitive radio: Making software radios more personal," *IEEE Personal Communications*, vol. 6, Aug. 1999.

[92] D. R. Morgan, M. Zhengxiang, K. Jaehyeong, M. G. Zierdt, and J. Pastalan, "A generalized memory polynomial model for digital predistortion of RF power amplifiers," *IEEE Transactions on Signal Processing*, vol. 54, 2006, pp. 3852-3860.

[93] O. Mylläri, L. Anttila, and M. Valkama, "Digital transmitter I/Q imbalance calibration: Real-time prototype implementation and performance measurement," in *Proc. EURASIP European Signal Processing Conference (EUSIPCO-2010)*, Aalborg, Denmark, August 2010.

[94] B. Narasimhan, D. Wang, S. Narayanan, H. Minn, and N. Al-Dhahir, "Digital compensation of frequency-dependent joint Tx/Rx I/Q imbalance in OFDM systems under high mobility," *IEEE Journal of Selected Topics in Signal Processing*, vol. 3, pp. 405-417, June 2009.

[95] F. D. Neeser and J. L. Massey, "Proper complex random processes with applications to information theory," *IEEE Transactions on Information Theory*, vol. 39, pp. 1293-1302, July 1993.

[96] E. Ollila and V. Koivunen, "Generalized complex elliptical distributions," in Proc. IEEE Sensor Array and Multichannel Signal processing Workshop, July 2004, pp. 460-464.

[97] A. E. Parker and J. G. Rathmel, "Broad-band characterization of FET self-heating," *IEEE Transactions on Microwave Theory and Techniques*, vol. 53, July 2005, pp. 2424-2429.

[98] J. C. Pedro and S. A. Maas, "A comparative overview of microwave and wireless power amplifier behavioral modeling approaches," *IEEE Transactions on Microwave Theory and Techniques*, vol. 53, Apr. 2005, pp. 1150-1163.

[99] B. Picinbono, "On circularity," *IEEE Transactions on Signal Processing*, vol. 42, Dec. 1994, pp. 3473-3482.

[100] B. Picinbono and P. Chevalier, "Widely linear estimation with complex data," *IEEE Transactions on Signal Processing*, vol. 43, pp. 2030-2033, Aug. 1995.

[101] B. Picinbono and P. Bondon, "Second-order statistics of complex signals," *IEEE Transactions on Signal Processing*, vol. 45, pp. 411-420, Feb. 1997.

[102] J. G. Proakis, *Digital communications*, 4th ed., New York, USA: McGraw-Hill, 2000.

[103] K. P. Pun, J. E. Franca, C. Azeredo-Leme, C. F. Chan, and C. S. Choy "Correction of frequency-dependent I/Q mismatches in quadrature receivers," *Electronics Letters*, vol. 37, pp. 1415-1417, Nov. 2001.

[104] F. H. Raab et al., "Power amplifiers and transmitters for RF and microwave," *IEEE Transactions on Microwave Theory and Techniques*, vol. 50, Mar. 2002.

[105] F. H. Raab et al., "RF and microwave power amplifier and transmitter technologies," Parts 1-4, *High Frequency Electronics*, May-Aug. 2003.

[106] R. Raich, H. Qian, and G. Tong Zhou, "Orthogonal polynomials for power amplifier modeling and predistorter design," *IEEE Transactions on Vehicular Technology*, vol. 53, 2004, pp. 1468–1479.

[107] R. Raich and G. Tong Zhou, "Orthogonal polynomials for complex Gaussian processes," *IEEE Transactions on Signal Processing*, vol. 52, 2004, pp. 2788-2797.

[108] R. M. Rao and B. Daneshrad, "Analog impairments in MIMO-OFDM systems," *IEEE Transactions on Wireless Communications*, vol. 5, pp. 3382-3387, Dec. 2006.

[109] C. Rapp, "Effects of HPA-nonlinearity on a 4-DPSK/OFDM-signal for a digital sound broadcasting system," in *Proc. of the Second European Conference on Satellite Communications*, Liege, Belgium, Oct. 22-24, 1991, pp. 179-184.

[110] B. Razavi, "Design considerations for direct-conversion receivers," *IEEE Transactions on Circuits and Systems II*, vol. 44, pp. 428–435, June 1997.

[111] B. Razavi, *RF Microelectronics*, Upper Saddle River, NJ, USA: Prentice Hall, 1998.

[112] B. Razavi, "Cognitive radio design challenges and techniques," *IEEE Journal of Solid-State Circuits*, vol. 45, Aug. 2010, pp. 1542-1553.

[113] S. J. Roome, "Analysis of quadrature detectors using complex envelope notation," *IEE Proceedings*, vol. 136, Apr. 1989, pp. 95-100.

[114] P. Rykaczewski, V. Blaschke, and F. Jondral, "I/Q imbalance compensation for software defined radio OFDM based direct conversion receivers," in *Proc. 8th IEEE International OFDM Workshop (InOWo'03)*, Hamburg, Germany, Sept. 2003, pp. 279–283.

[115] P. Rykaczewski, M. Valkama, and M. Renfors, "On the connection of I/Q imbalance and channel equalization in direct-conversion transceivers," *IEEE Transactions on Vehicular Technology*, vol. 57, May 2008, pp. 1630-1636.

[116] T.C.W. Schenk, P.F.M. Smulders, and E.R.Fledderus, "Estimation and compensation of frequency selective TX/RX IQ imbalance in MIMO OFDM systems," in *Proc. IEEE International Conference on Communications (ICC'06)*, Istanbul, Turkey, June 2006, pp. 251-256.

[117] T.C.W. Schenk, *RF Impairments in Multiple Antenna OFDM - Influence and Mitigation*, Ph.D. thesis, TU Eindhoven, The Netherlands, Nov. 2006.

[118] M. Schetzen, "Theory of *p*th-order inverses of nonlinear systems," *IEEE Transactions on Circuits and Systems* CAS-23, 1976, pp. 285-291.

[119] P.J. Schreier and L.L. Scharf, "Second-order analysis of improper complex random vectors and processes," *IEEE Transactions on Signal Processing*, vol. 51, pp. 714-725, March 2003.

[120] P. J. Schreier and L. L. Scharf, *Statistical Signal Processing of Complex-Valued Data*, Cambridge, UK: Cambridge University Press, 2010.

[121] D. Schreurs, M. O'Droma, A. A. Goacher, and M. Gadringer, *RF Power Amplifier Behavioral Modeling*, Cambridge, UK, Cambridge University Press, 2009.

[122] A. Schuchert, R. Hasholzner, and P. Antoine, "A novel IQ imbalance compensation scheme for the reception of OFDM signals," *IEEE Transactions on Consumer Electronics*, vol. 47, pp. 313-318, Aug. 2001.

[123] J. F. Sevic, K. L. Burger, and M.B. Steer, "A Novel Envelope-Termination Load-Pull Method for ACPR Optimization of RF/Microwave Power Amplifiers," *in IEEE MTT-S International Microwave Symposium Digest*, June 1998, pp. 273-276.

[124] S. Simoens, M. de Courville, F. Bourzeix, and P. de Champs, "New I/Q imbalance modeling and compensation in OFDM systems with frequency offset," in *Proc. IEEE International Symposium on Personal, Indoor and Mobile Radio Communications (PIMRC'02)*, Lisboa, Portugal, Sept. 2002, pp. 561-566.

[125] I.-H. Sohn, E.-R. Jeong, and Y.H. Lee, "Data-aided approach to I/Q mismatch and DC-offset compensation in communication receivers," *IEEE Communications Letters*, vol. 6, pp. 547-549, Dec. 2002.

[126] H. Starck and J. W. Woods, *Probability and Random Processes with Applications to Signal Processing*, 3rd ed., Upper Saddle River, NJ, USA: Prentice Hall, 2001.

[127] R. Svitek and S. Raman, "DC offsets in direct-conversion receivers: Characterization and implications," *IEEE Microwave Magazine*, Sept. 2005, pp. 76-86.

[128] T. B. Sørensen, P. E. Mogensen, and F. Frederiksen, "Extension of the ITU channel models for wideband (OFDM) systems," in *Proc. IEEE Vehicular Technology Conference (VTC'05)*, Dallas, TX, Sept. 2005, pp. 392-396.

[129] D. Tandur and M. Moonen, "Joint adaptive compensation of transmitter and receiver IQ imbalance under carrier frequency offset in OFDM-based systems," *IEEE Transactions on Signal Processing*, vol. 55, pp. 5246 – 5252, Nov. 2007.

[130] D. Tandur and M. Moonen, "Joint compensation of OFDM frequency-selective transmitter and receiver IQ imbalance," *EURASIP Journal on Wireless Communications and Networking*, 2007.

[131] D. Tandur and M. Moonen, "Compensation of RF impairments in MIMO OFDM systems," in *Proc. International Conference on Acoustics, Speech, and Signal Processing (ICASSP'08)*, Washington, USA, 2008.

[132] A. Tarighat, R. Bagheri, and A.H. Sayed, "Compensation schemes and performance analysis of IQ imbalances in OFDM receivers," *IEEE Transactions on Signal Processing*, vol. 53, pp. 3257-3268, Aug. 2005.

[133] A. Tarighat and A.H. Sayed, "MIMO OFDM receivers for systems with IQ imbalances," *IEEE Transactions on Signal Processing*, vol. 53, pp. 3583-3596, Sept. 2005.

[134] A. Tarighat and A.H. Sayed, "Joint compensation of transmitter and receiver impairments in OFDM systems," *IEEE Transactions on Wireless Communications*, vol. 6, pp. 240-247, Jan. 2007.

[135] G. Tong Zhou, H. Qian, L. Ding, R. Raich, "On the baseband representation of a bandpass nonlinearity," *IEEE Transactions on Signal Processing*, vol. 53, 2005, pp. 2953-2957.

[136] E. Tsui and J. Lin, "Adaptive IQ imbalance correctionfor OFDM systems with frequency and time offsets," in *Proc. IEEE Global Telecommunications Conference (Globecom'04)*, Dallas, TX, Nov. 2004, pp. 4004-4010.

[137] J. Tubbax, B. Come, L. Van der Perre, L. Deneire, S. Donnay, M. Engels, "Compensation of IQ imbalance in OFDM systems," in *Proc. IEEE International Conference on Communications (ICC'03)*, Anchorage, AK, May 2003, pp. 3403-3407.

[138] J. Tubbax, B. Come, L. Van der Perre, S. Donnay, M. Engels, M. Moonen, H. De Man, "Joint compensation of IQ imbalance and frequency offset in OFDM systems," in

Proc. IEEE Radio Wireless Conference (RAWCON'03), Boston, MA, Aug. 2003, pp. 39-42.

[139] J. Tubbax, B. Come, L. Van der Perre, S. Donnay, M. Engels, H. De Man, M. Moonen, "Compensation of IQ imbalance and phase noise in OFDM systems," *IEEE Transactions on Wireless Communications*, vol. 4, pp. 872-877, May 2005.

[140] J. Tuthill and A. Cantoni, "Efficient compensation for frequency-dependent errors in analog reconstruction filters used in IQ modulators," *IEEE Transactions on Communications*, vol. 53, pp. 489-496, March 2005.

[141] W. Tuttlebee, Ed., *Software Defined Radio: Enabling Technologies*, Chichester, UK: Wiley, 2002.

[142] M. Valkama and M. Renfors, "Advanced DSP for I/Q imbalance compensation in a low-IF receiver," in *Proc. IEEE International Conference on Communications (ICC'00)*, New Orleans, LA, June 2000, pp. 768-772.

[143] M. Valkama, M. Renfors, and V. Koivunen, "Compensation of frequency-selective I/Q imbalances in wideband receivers: Models and algorithms," in *Proc. 3rd IEEE Workshop on Signal Processing Advances in Wireless Communications (SPAWC'01)*, Taoyuan, Taiwan, R.O.C., Mar. 2001, pp. 42-45.

[144] M. Valkama, M. Renfors, and V. Koivunen, "Advanced methods for I/Q imbalance compensation in communications receivers," *IEEE Transactions on Signal Processing*, vol. 49, pp. 2335-2344, Oct. 2001.

[145] M. Valkama, L. Anttila, and M. Renfors, "Digital image signal rejection in WCDMA receivers based on adaptive interference cancellation," in *Proc. IEEE Vehicular Technology Conference (VTC-F '05)*, Stockholm, Sweden, May 2005.

[146] M. Valkama, M. Renfors, and V. Koivunen, "Blind I/Q imbalance compensation in OFDM receivers based on adaptive I/Q signal decorrelation," in *Proc. IEEE International Symposium on Circuits and Systems (ISCAS'05)*, Kobe, Japan, May 2005, pp. 2611-2614.

[147] M. Valkama, M. Renfors, and V. Koivunen, "Blind I/Q signal separation based solutions for receiver signal processing," *EURASIP Journal on Applied Signal Processing - Special Issue on DSP Enabled Radios*, vol. 2005, no. 16, pp. 2708-2718, Sept. 2005.

[148] M. Valkama, M. Renfors, and V. Koivunen, "Blind signal estimation in conjugate signal models with application to I/Q imbalance compensation" *IEEE Signal Processing Letters*, vol. 12, pp. 733-736, Nov. 2005.

[149] M. Valkama, L. Anttila, M. Renfors, "Some radio implementation challenges in 3G-LTE context," in *Proc. IEEE 8th Workshop on Signal Processing Advances in Wireless Communications (SPAWC '07)*, Helsinki, Finland, June 2007.

[150] M. Valkama, A. Springer, and G. Hueber, "Digital signal processing for reducing the effects of RF imperfections in radio devices – An overview," in *Proc. IEEE*

International Symposium on Circuits and Systems (ISCAS'10), Paris, France, May-June 2010, pp. 813-816.

[151] M. Valkama and L. Anttila, "Joint digital predistortion of I/Q modulator and power amplifier impairments," Chapter 17 in *Digital Front-End in Wireless Communications and Broadcasting*, Cambridge, UK: Cambridge University Press, 2011 (to appear).

[152] A. van den Bos, "The multivariate complex normal distribution – A generalization," *IEEE Transactions on Information Theory*, vol. 41, Mar.1995, pp. 537-539.

[153] S. Verdu, *Multiuser Detection*, Cambridge, UK: Cambridge University Press, 1998.

[154] J. H. K. Vuolevi, T. Rahkonen, J. P. A. Manninen, "Measurement Technique for Characterizing Memory Effects in RF Power Amplifiers," *IEEE Transactions on Microwave Theory and Techniques*, vol. 49, Aug. 2001, pp. 1383-1389.

[155] J. R. Wilkerson, K. G. Gard, A. G. Schuchinsky, and M. B. Steer, "Electro-Thermal Theory of Intermodulation Distortion in Lossy Microwave Components," *IEEE Transactions on Microwave Theory and Techniques*, vol. 56, December 2008, pp. 2717-2725.

[156] D. J. Williams, J. Leckey, and P. J. Tasker, "A Study of the Effect of Envelope Impedance on Intermodulation Asymmetry using a Two-tone Time Domain Measurement System," *IEEE MTT-S International Microwave Symposium Digest*, pp. 1841-44, June 2002.

[157] M. Windisch and G. Fettweis, "Blind I/Q imbalance parameter estimation and compensation in low-IF receivers," in *Proc. First International Symposiun on Control, Communications, and Signal Processing (ISCCSP'04)*, Hammamet, Tunisia, March 2004, pp. 75-78.

[158] M. Windisch and G. Fettweis, "Standard-independent I/Q imbalance compensation in OFDM direct-conversion receivers," in *Proc. International OFDM Workshop (InOWo'04)*, Dresden, Germany, Sept. 2004.

[159] M. Windisch and G. Fettweis, "Adaptive I/Q imbalance compensation in low-IF transmitter architectures," in *Proc. IEEE Vehicular Technology Conference (VTC2004-Fall)*, Los Angeles, CA, Sept. 2004, pp. 2096-2100.

[160] M. Windisch, *Estimation and compensation of I/Q imbalance in broadband communications receivers*, Dr. Tech. thesis, Techn. Univ. Dresden, 2007.

[161] G. Xing, M. Shen, and H. Liu, "Frequency offset and I/Q imbalance compensation for OFDM direct-conversion receivers," in *Proc. International Conference on Acoustics, Speech, and Signal Processing (ICASSP'03)*, Hong Kong, China, April 2003.

[162] G. Xing, M. Shen, and H. Liu, "Frequency offset and I/Q imbalance compensation for direct-conversion receivers," *IEEE Transactions on Wireless Communications*, vol. 4, pp. 673-680, March 2005.

[163] Y. Yoshida, K. Hayashi, H. Sakai, and W. Bocquet, "Analysis and compensation of transmitter IQ imbalances in OFDMA and SC-FDMA systems," *IEEE Transactions on Signal Processing*, vol. 57, Aug. 2009, pp. 3119-3129.

[164] L. Yu and W.M. Snelgrove, "A novel adaptive mismatch cancellation system for quadrature IF radio receivers," *IEEE Transactions on Circuits and Systems II*, vol. 46, pp. 789-801, June 1999.

[165] D. Zhou and V. E. DeBrunner, "Novel adaptive nonlinear predistorters based on the direct learning algorithm," *IEEE Transactions on Signal Processing*, vol. 55, Jan. 2007, pp. 120-133.

[166] A. Zhu, J. C. Pedro, and T .R. Cunha, "Pruning the Volterra series for behavioral modeling of power amplifiers using physical knowledge," *IEEE Transactions on Microwave Theory and Techniques*, vol. 55, May 2007, pp. 813-821.

[167] Z. Zhu and X. Huang, "Theoretical analysis of timing error in a direct transmitter self-calibration system," in *Proc. IEEE International Conference on Acoustics, Speech, and Signal Processing (ICASSP'06)*, Toulouse, France, May 2006, pp. 417-420.

[168] Q. Zou, A. Tarighat, and A. H. Sayed, "On the joint compensation of IQ imbalances and phase noise in MIMO-OFDM systems," in *Proc. International Symposium on Circuits and Systems (ISCAS'07)*, New Orleans, LA, May 2007.

[169] Y. Zou, M. Valkama, and M. Renfors, "Digital compensation of I/Q imbalance effects in space-time coded transmit diversity systems," *IEEE Transactions on Signal Processing*, vol. 56, pp. 2496-2508, June 2008.

[170] Y. Zou, M. Valkama, and M. Renfors, "Analysis and compensation of transmitter and receiver I/Q imbalances in space-time coded multiantenna OFDM systems," *EURASIP Journal on Wireless Communications Networks (Special Issue on Multicarrier Techniques)*, vol. 2008, Article ID 391025, 2008.

[171] Y. Zou, M. Valkama, and M. Renfors, "Pilot-based compensation of frequency-selective I/Q imbalances in direct-conversion OFDM transmitters," in *Proc. IEEE Vehicular Technology Conference (VTC2008-Fall)*, Calgary, Canada, Sept. 2008.

[172] Y. Zou, *Analysis and Mitigation of I/Q Imbalances in Multi-Antenna Transmission Systems*, Dr. Tech. thesis, Tampere University of Technology, Finland, 2009.

[173] C.-P. Yen, Y. Tsai, G. Zhang, and R. Olesen, "Blind estimation and compensation of frequency-flat I/Q imbalance using cyclostationarity," in *Proc. IEEE Vehicular Technology Conference (VTC2008-Fall)*, Calgary, Canada, Sept. 2008.

Publications

Tampereen teknillinen yliopisto
PL 527
33101 Tampere

Tampere University of Technology
P.O.B. 527
FI-33101 Tampere, Finland

ISBN 978-952-15-2651-0
ISSN 1459-2045